

MICHELLE KYLE DEAKIN

MÉTALLOGÉNIE DU GÎTE À PB–ZN–AG DE NICHOLAS-DENYS, NOUVEAU-BRUNSWICK

Mémoire présenté
à la Faculté des études supérieures de l'Université Laval
dans le cadre du programme de Maîtrise interuniversitaire en sciences de la Terre
pour l'obtention du grade de maître ès sciences (M.Sc)

DÉPARTEMENT DE GÉOLOGIE ET GÉNIE GÉOLOGIQUE
FACULTÉ DES SCIENCES ET GÉNIE
UNIVERSITÉ LAVAL
QUÉBEC

2011

Résumé

Le gîte à Pb–Zn–Ag de Nicholas-Denys, dans le camp minier de Bathurst (Nouveau-Brunswick), est constitué de plusieurs lentilles à pyrrhotite–sphalérite–galène, encaissées par le mudstone de la Formation de Millstream du Groupe de Fournier, déposé dans un bassin d’arrière-arc ordovicien. Les lentilles de sulfures sont concordantes avec la foliation régional S_1 , et sont boudinées parallèlement à la faille de Rocky-Brook Millstream, indiquant que les sulfures prédatent la déformation décrochante dévonienne. Le soufre provient de la réduction bactérienne de l’eau de mer ordovicienne dans un système ouvert aux sulphates, dans une colonne d’eau dysoxique à anoxique, avec mélange de soufre magmatique lessivé des roches mafiques sous-jacentes. Le plomb a été lessivé des sédiments du mudstone de la Formation de Millstream du bassin d’arrière-arc ainsi que des gabbros sous-jacents. Le fluide minéralisateur était réduit et acide, favorable à une minéralisation riche en pyrrhotite. Le gîte Nicholas-Denys se compare bien aux gîtes de type SEDEX.

Abstract

The Nicholas-Denys Pb–Zn–Ag deposit, located in the Bathurst Mining Camp (New Brunswick), consists of several pyrrhotite–sphalerite–galena sulphide lenses hosted by black mudstone of the Millstream Formation of the Fournier Group, deposited in an Ordovician backarc basin. The Nicholas-Denys sulphide lenses are conformable to the bedding-parallel S_1 regional foliation, and are sheared parallel to the Rocky Brook-Millstream shear zone, indicating a pre-Devonian deformation timing for mineralization. Reduced sulphur for Nicholas-Denys sulphides comes from bacterial reduction of Ordovician seawater sulphates in a system open to sulphates under dysoxic to anoxic bottomwater conditions, with addition of magmatic sulphur from underlying mafic volcanic rocks. Lead was leached from the backarc basin sediments of the Millstream Formation mudstone and from underlying synvolcanic gabbros. The mineralizing fluid for Nicholas-Denys sulphides was reduced and acidic, favourable for precipitation of a pyrrhotite-rich mineralization. Characteristics of the Nicholas-Denys deposit are compatible with a SEDEX-type classification.

Avant-propos

Tous les chapitres de ce mémoire ont été écrits en totalité par l'auteure de ce mémoire, y compris l'article du dixième chapitre. Les co-auteurs de l'article sont Georges Beaudoin (Université Laval) et Michel Malo (INRS-ETE). Georges Beaudoin et Michel Malo sont également directeur et co-directeur, respectivement, du projet de maîtrise de l'auteure. Alain Hupé est présentement responsable du projet Nicholas-Denys de la compagnie Exploration Puma (Rimouski).

Ce projet a bénéficié du support et de la collaboration de plusieurs personnes. J'aimerais tout d'abord remercier mon directeur de maîtrise, Georges Beaudoin. Son expertise en métallogénie, sa grande disponibilité, son souci du détail et son intérêt pour le projet ont contribué de manière inéquivoque à la qualité de ce mémoire. Je tiens aussi à remercier mon co-directeur, Michel Malo, pour avoir contribué son expertise en géologie structurale aussi bien sur le terrain qu'à la rédaction du mémoire.

Le projet s'est réalisé avec le soutien financier et logistique de la compagnie Exploration Puma (Rimouski, Québec), en particulier avec la collaboration de Marcel Robillard (antérieurement de Exploration Puma), ainsi qu'avec le soutien financier du CRSNG et de la SEG. Mon travail de terrain au gîte Nicholas-Denys a bénéficié de l'aide et de la bonne compagnie de Mona Baker (antérieurement de Exploration Puma) et Dominique Gagné. Les conseils de Daniel Brisebois en géologie sédimentaire et structurale sont également très appréciés, ainsi que son expertise culinaire. Jim Walker et de Steve McCutcheon du Département des Ressources Naturelles du Nouveau-Brunswick à Bathurst ont grandement contribué au projet avec leurs connaissances approfondies sur la géologie régionale du camp minier de Bathurst.

Je remercie mes amis, mes béquilles par les moments plus pénibles. À mes Françaises favorites, Stéphanie, Julie, Rachel – qu'auraient été ces années de maîtrise sans vous? Aussi, à Mérouane, les trois Émilie, Anno, Sophie, Véronique et Alex pour leur bonne humeur qui rend le couloir du troisième étage un endroit bien agréable!

À Jessy, Jul, et Pez, ma famille à Québec. Je leur suis reconnaissante de m'avoir si bien accueillie.

À ma vraie famille, pour m'avoir appuyé dans tous mes projets, et ce avec enthousiasme.

Et finalement, je remercie Kevin, mon amoureux, qui se mérite le titre de champion en soutien moral.

Table des matières

| | |
|--|--------------------------------------|
| RÉSUMÉ | II |
| ABSTRACT..... | III |
| AVANT-PROPOS..... | IV |
| TABLE DES MATIÈRES..... | V |
| LISTE DES TABLES | VI |
| LISTE DES FIGURES | VII |
| CHAPITRE 1 - INTRODUCTION | 1 |
| 1.1 CADRE GÉNÉRAL..... | 1 |
| 1.2 PROBLÉMATIQUE ET OBJECTIFS | 2 |
| 1.3 PRÉSENTATION DE L'ARTICLE | 3 |
| CHAPITRE 2 - METALLOGENY OF THE NICHOLAS-DENYS PB-ZN-AG DEPOSIT, CANADA | 4 |
| 2.1 INTRODUCTION | 4 |
| 2.2 GEOLOGICAL FRAMEWORK | 5 |
| 2.2.1 <i>Tectonic history</i> | 5 |
| 2.2.2 <i>Geology of the Bathurst Mining Camp</i> | 6 |
| 2.2.3 <i>Metallogeny of the BMC</i> | 9 |
| 2.3 ANALYTICAL METHODS | 10 |
| 2.4 DEPOSIT GEOLOGY | 11 |
| 2.4.1 <i>Host rock lithogeochemistry</i> | 16 |
| 2.4.2 <i>Hydrothermal alteration</i> | 17 |
| 2.4.3 <i>Mineralization</i> | 25 |
| 2.4.4 <i>Sulphur isotopes</i> | 36 |
| 2.4.5 <i>Lead isotopes</i> | 38 |
| 2.5 DISCUSSION | 39 |
| 2.5.1 <i>Provenance of sediments</i> | 41 |
| 2.5.2 <i>Physiochemical properties of the ambient environment and mineralizing fluid</i> | 44 |
| 2.5.3 <i>Source of sulphur</i> | 47 |
| 2.5.4 <i>Source of lead</i> | 48 |
| 2.5.5 <i>Implications for genetic classification</i> | 49 |
| 2.5.5.1 <i>SEDEX mineralization</i> | 50 |
| 2.5.5.2 <i>Comparison of the Nicholas-Denys deposit to similar deposits</i> | 51 |
| 2.6 CONCLUSION..... | 52 |
| CHAPITRE 3 - CONCLUSION | 54 |
| BIBLIOGRAPHIE..... | 56 |
| ANNEXE A..... | 61 |
| ANNEXE B..... | 65 |
| ANNEXE C..... | 67 |
| ANNEXE D..... | 71 |
| ANNEXE E..... | 76 |
| ANNEXE F..... | 79 |
| ANNEXE G | ERREUR ! SIGNET NON DEFINI.85 |

Liste des tableaux

| | |
|--|-----------|
| TABLE 1. BULK LITHOGEOCHEMICAL COMPOSITIONS OF UNALTERED MILLSTREAM FORMATION MUDSTONE. | 18 |
| TABLE 2. BULK LITHOGEOCHEMICAL COMPOSITIONS OF UNALTERED MILLSTREAM FORMATION SANDSTONE. | 19 |
| TABLE 3. BULK LITHOGEOCHEMICAL COMPOSITIONS OF ALTERED MILLSTREAM FORMATION MUDSTONE. | 21 |
| TABLE 4. ELECTRON MICROPROBE ANALYSES OF SULPHIDES. | 31 |
| TABLE 4.1 MAJOR AND TRACE ELEMENTS IN ARSENOPYRITE. | 31 |
| TABLE 4.2 MAJOR AND TRACE ELEMENTS IN GALENA. | 31 |
| TABLE 4.3 MAJOR AND TRACE ELEMENTS IN PYRRHOTITE. | 32 |
| TABLE 4.4 MAJOR AND TRACE ELEMENTS IN SPHALERITE. | 33 |
| TABLE 4.5 MAJOR AND TRACE ELEMENTS IN FREIBERGITE. | 34 |
| TABLE 4.6 MAJOR AND TRACE ELEMENTS IN STANNITE. | 35 |
| TABLE 5. SULPHUR ISOTOPE COMPOSITIONS AND TEMPERATURE ESTIMATES FOR SULPHIDES OF THE FOURNIER AND CHALEURS GROUPS. | 37 |
| TABLE 6. LEAD ISOTOPE RATIOS FOR GALENAS OF THE FOURNIER AND CHALEURS GROUPS. | 39 |

Liste des figures

| | |
|---|-----------|
| FIGURE 1. GENERALIZED GEOLOGICAL MAP OF THE BATHURST MINING CAMP..... | 7 |
| FIGURE 2. GEOLOGICAL MAP OF THE NICHOLAS-DENYS DEPOSIT AREA..... | 8 |
| FIGURE 3. DETAILED GEOLOGICAL MAP OF THE HACHÉ SHOWING | 13 |
| FIGURE 4. PHOTOGRAPHS OF UNALTERED MILLSTREAM FORMATION DRILLCORE..... | 14 |
| FIGURE 5. CROSS SECTION OF THE HACHÉ SULPHIDE LENSES..... | 15 |
| FIGURE 6. PHOTOMICROGRAPHS OF UNALTERED MILLSTREAM FORMATION..... | 16 |
| FIGURE 7. BIVARIATE PLOTS OF SELECTED MAJOR AND TRACE ELEMENTS FOR UNALTERED MILLSTREAM FORMATION SAMPLES..... | 17 |
| FIGURE 8. PHOTOMICROGRAPHS AND ISOCON MASS BALANCE PLOTS OF ALTERED MUDSTONE | 24 |
| FIGURE 9. PHOTOMICROGRAPHS OF LATE ALTERATION PHASES | 25 |
| FIGURE 10. PHOTOGRAPHS OF NICHOLAS-DENYS SULPHIDES IN DRILL CORE..... | 27 |
| FIGURE 11. PHOTOMICROGRAPHS OF NICHOLAS-DENYS SULPHIDE TEXTURES..... | 29 |
| FIGURE 12. PARAGENETIC SEQUENCE FOR THE NICHOLAS-DENYS DEPOSIT..... | 36 |
| FIGURE 13. BAR PLOTS OF SULPHUR ISOTOPE COMPOSITIONS | 38 |
| FIGURE 14. LEAD ISOTOPE RATIO PLOTS | 40 |
| FIGURE 15. SEDIMENTARY ROCK TECTONIC SETTING DISCRIMINANT PLOT | 41 |
| FIGURE 16. SEDIMENT PROVENANCE DISCRIMINANT PLOTS | 43 |
| FIGURE 17. FE- AND MN-BASED PALEOENVIRONMENT DISCRIMINANT DIAGRAMS..... | 45 |
| FIGURE 18. REDOX CONDITIONS DISCRIMINANT PLOT..... | 46 |

Chapitre 1 - Introduction

1.1 Cadre général

Le gîte de Nicholas-Denys est situé dans la partie nord du Nouveau-Brunswick, dans le Camp minier de Bathurst (CMB). Le CMB est un des plus importants districts de sulfures massifs volcanogènes (SMV) au monde. Le camp compte quelques quarante-cinq gîtes de SMV et en 2001, représentait 53%, 30% et 17% des ressources en plomb, zinc et argent du Canada, respectivement, en plus d'engendrer deux milles emplois directs (Goodfellow and McCutcheon 2003). La découverte de nouveaux gisements dans le CMB, comme le gîte de Nicholas-Denys, est donc de première importance pour assurer la santé économique de la région.

Les travaux sur le gîte de Nicholas-Denys remontent aux années 1880 avec la découverte de l'indice Shaft par le professeur Edward Jack de Fredericton. Jusqu'à la fin du 19^e siècle, les « veines » de l'indice Shaft font l'objet de plusieurs études métallogéniques, dont une en 1892 par la Commission géologique du Canada qui révèle des teneurs élevées en argent et en or (Department of Natural Resources New Brunswick 2006). Au courant des trente années suivantes, des prospecteurs creusent des tranchées et des puits, et entreprennent des études additionnelles qui confirment les teneurs intéressantes en argent, ainsi qu'en plomb et en zinc. En 1937, la compagnie Consolidated Mining and Smelting Co. fore deux trous à l'indice Shaft, suivis de vingt-six trous additionnels par le Gloucester Mining Syndicate dont dix à l'indice de Pine Tree et deux à l'indice Henry. Quebec Sturgeon River Mines fait l'acquisition de la propriété et, en 1956, réalise un puits de 552 pieds de profondeur, avec des galeries souterraines à 200 et 500 pieds, après quoi les travaux cessèrent (Department of Natural Resources New Brunswick 2006). Par la suite, la cartographie des indices Haché, Shaft et Pine Tree est réalisée par Davies et al. (1969). En 2005, la compagnie Exploration Puma fait l'acquisition des droits miniers sur le site de l'indice Shaft, ainsi que des propriétés adjacentes comportant d'autres indices à Pb-Zn-Ag sur une superficie totale de 69 km², pour constituer la propriété de Nicholas-Denys. Les efforts d'exploration sont concentrés dans la partie sud de la propriété, dans les roches ordoviciennes du Groupe de Fournier.

Ce projet de maîtrise s'inscrit dans le cadre des travaux d'exploration présentement en cours au gîte de Nicholas-Denys sous la direction de la compagnie Exploration Puma. Bien que le gîte comporte plusieurs indices Pb-Zn-Ag, l'étude porte principalement sur l'indice Haché. Des campagnes de forages en 2006, 2007 et 2008 ainsi qu'un décapage de 100m x 50m en 2007 ont rendu ce secteur

propice à une étude métallogénique approfondie. Les carottes des forages effectués en 2005 à l'indice Pine Tree et en 2006 et 2007 aux indices Henry et Shaft, aussi décrites en détail, démontrent plusieurs similitudes à la minéralisation de la lentille Haché, ce qui mène à proposer une métallogénèse commune pour l'ensemble des indices Pb–Zn–Ag de la propriété de Nicholas-Denys.

1.2 Problématique et objectifs

La classification gîtologique de Nicholas-Denys est ambiguë. Historiquement, les indices Haché, Shaft et Pine Tree étaient considérées comme des veines à pyrite-pyrrhotite-sphalérite-galène (Davies et al. 1969). D'autre part, (1) la localisation du gîte de Nicholas-Denys dans des roches sédimentaires déposées dans un bassin d'arrière-arc, (2) la granulométrie fine des sulfures et (3) la relation concordante des sulfures avec le litage ont mené à considérer une hypothèse de minéralisation syngénétique pour les sulfures de Nicholas-Denys. Le gîte de Nicholas-Denys démontre toutefois des différences marquées avec les SMV du CMB. Les SMV du CMB se caractérisent par un assemblage pyrite–sphalérite–galène encaissé par des roches volcano-sédimentaires d'âge Ordovicien moyen, alors que le gîte de Nicholas-Denys se caractérise par un assemblage pyrrhotite–sphalérite–galène, encaissé par des roches sédimentaires plus jeunes d'âge Ordovicien moyen à tardif. De plus, le gîte de Nicholas-Denys se situe à proximité d'une faille de décrochement majeure, et la déformation dévonienne le long de cette faille affecte les sulfures de Nicholas-Denys ce qui complique l'interprétation de la relation temporelle des sulfures par rapport à leur encaissant ordovicien.

Cette étude vise donc à établir un modèle métallogénique du gîte de Nicholas-Denys et à proposer une classification gîtologique. Les quatre objectifs principaux de cette étude et les méthodes spécifiques pour chaque objectif sont de :

1) Placer le gîte de Nicholas-Denys dans son contexte géologique avec :

- La cartographie détaillée de la minéralisation et de l'altération hydrothermale aux indices de Haché et Shaft
- La description et mise en section de forages pour déterminer la relation stratigraphique et structurale des sulfures de Nicholas-Denys par rapport à leur encaissant

2) Caractériser la minéralisation à Pb–Zn–Ag et l'altération hydrothermale par :

- La pétrographie de l'altération hydrothermale et de la minéralisation
- La lithogéochimie de l'altération hydrothermale

- L'analyse à la microsonde des sulfures et des minéraux d'altération
- L'analyse isotopique des sulfures pour déterminer les sources du soufre et du plomb

3) Interpréter le paléoenvironnement grâce à :

- Une étude littéraire du contexte géodynamique et du style de minéralisation dans le CMB
- La lithogéochimie des roches encaissantes non-altérées pour déterminer la provenance des sédiments et les conditions d'oxydo-réduction ambiantes dans la colonne d'eau

4) Proposer un modèle métallogénique avec :

- La classification du gîte de Nicholas-Denys
- La comparaison aux gîtes SMV dans le CMB, aux veines polymétalliques Nigadoo et Cullinan et à d'autres gîtes à Pb-Zn-Ag semblables dans le monde

1.3 Présentation de l'article

Le deuxième chapitre de ce mémoire est constitué de l'article « Metallogeny of the Nicholas-Denys Pb-Zn-Ag deposit, Canada », qui sera soumis pour publication à la revue scientifique *Mineralium Deposita*.

L'article débute en abordant les caractéristiques principales du gîte de Nicholas-Denys par rapport à celles des SMV du CMB, et introduisant la problématique de classification du gîte de Nicholas-Denys. Le contexte géologique régional permet de synthétiser l'histoire géodynamique, les divisions tectono-stratigraphiques et la métallogénie du CMB. Une brève description des méthodes analytiques employées s'ensuit. La géologie du gîte détaille en premier lieu les caractéristiques macroscopiques des indices à Pb-Zn-Ag et la cartographie détaillée de l'indice Haché, puis présente en deuxième lieu des descriptions pétrographiques et géochimiques de l'encaissant sédimentaire, de l'altération hydrothermale et de la minéralisation. S'enchaîne une discussion sur la relation temporelle entre la minéralisation et la déformation, sur les conditions paléoenvironnementales, et sur les sources du soufre et du plomb pour les sulfures de Nicholas-Denys. La discussion aborde ensuite l'hypothèse d'une minéralisation syngénétique de type SEDEX pour le gîte de Nicholas-Denys, suivie d'une comparaison avec des gîtes semblables dans le CMB et avec le gîte marocain de Draa Sfar. L'article conclut en énumérant les caractéristiques du gîte de Nicholas-Denys compatibles avec une minéralisation SEDEX, mettant l'accent sur la différence avec les attributs des gîtes SMV du CMB.

Chapitre 2 - Metallogeny of the Nicholas-Denys Pb–Zn–Ag deposit, Canada

2.1 Introduction

The Nicholas-Denys deposit is located in the Appalachian orogen, approximately 25 km northwest of the city of Bathurst, New Brunswick, Canada (Fig. 1). The deposit is composed of several Pb–Zn–Ag sulphide lenses, and is within the Bathurst Mining Camp (BMC) which hosts several Pb–Zn–Cu–Ag volcanogenic massive sulphide (VMS) deposits.

The majority of deposits in the BMC are Paleozoic in age (478–465Ma) (Goodfellow 2007), and coincide with a global peak in formation of VMS, as well as sedimentary-exhalative (SEDEX)-type deposits (Meyer 1985). Periods of ocean anoxia coupled with increased hydrothermal activity during Paleozoic continent reassembly are believed to have provided optimal conditions for precipitation and preservation of VMS and SEDEX deposits (Goodfellow 1987; Franklin et al. 2005).

Deposit type classification for several BMC massive sulphides is problematic as they share characteristics with both VMS and SEDEX deposits. Many authors refer to BMC deposits as volcanic-sediment-hosted massive sulphides (VSHMS), although Franklin et al. (2005) emphasize the difference between VSHMS and VMS, and warn against using these terms interchangeably, as ‘VSHMS’ specifies host rock whereas ‘VMS’ implies a volcanic genetic relationship. Accordingly, Franklin et al. (2005) assigned BMC deposits to the ‘siliciclastic-felsic’ group of VMS deposits, along with massive sulphides of the Iberian Pyrite Belt (Spain and Portugal), the Lachlan Fold Belt (Australia) and the Jebilet (Morocco), acknowledging the sedimentary and felsic volcanic host rocks and the volcanogenic origin of these deposits. This paper will herein refer to BMC massive sulphides hosted by felsic volcanic and volcanoclastic rocks as siliciclastic-felsic VMS deposits.

The Nicholas-Denys deposit occurs in slightly younger rocks of the BMC (~460–455 Ma; van Staal and Fyffe 1991) than neighbouring BMC massive sulphides, and mirrors several features characterizing some siliciclastic-felsic VMS deposits of the BMC thought to have formed in vent-distal, stable depositional environments, such as (1) abundant sedimentary clastic rocks in the host sequence, (2) absence of a Cu-rich vent complex, (3) absence of a sulphide stringer zone, (4) Pb–Zn–Ag sulphide lenses with a sheet-like morphology and (5) lack of vertical and lateral metal

zoning (Goodfellow and McCutcheon 2003; Goodfellow 2007). However, bedded sulphides, a key criterion for recognition of syngenetic mineralization and a feature common to several siliciclastic-felsic VMS deposits of the BMC, are not observed at the Nicholas-Denys deposit. The Nicholas-Denys deposit also contrasts with siliciclastic-felsic VMS deposit of the BMC by (1) the dominance of pyrrhotite over pyrite in the Pb-Zn-Ag sulphide assemblage and (2) the absence of felsic volcanic rocks in the footwall of the host rock sequence.

Despite similarities with vent-distal siliciclastic-felsic VMS deposits of the BMC, marked differences in the sulphide textures, mineralogy and host lithology make classification of the Nicholas-Denys deposit problematic. Furthermore, the proximity of the Nicholas-Denys deposit to a regional shear zone has imposed substantial deformation to Nicholas-Denys sulphides, obliterating primary features of the deposit. The objectives of this contribution are therefore to characterize mineralization and alteration, identify the sources of sulphur and lead, and determine the paleoenvironment conditions prevailing during sulphide precipitation and sedimentation in order to establish the metallogensis of the Nicholas-Denys deposit and place the deposit in its context within the regional geological framework of the BMC.

2.2 Geological framework

2.2.1 Tectonic history

The BMC (Fig. 1) is comprised of Ordovician rocks deposited in a continental backarc rift developed on the passive margin of Ganderia, a peri-Gondwanan microcontinent (van Staal 2007). Progressive Ordovician rifting of the Ganderian continental crust, from a continental backarc rift basin to a marginal sea, is recorded by transition from felsic volcanic-dominated sequences to more mafic volcanic and fine-grained sedimentary units higher in the stratigraphic column (van Staal 1987). Rifting is believed to have progressed heterogeneously across the basin, leading to multiple rifting centres and sub-basins, analogous to the complex architecture of the modern-day Sea of Japan (Rogers and van Staal 1997). Late Ordovician to Early Silurian basin closure led to exhumation of backarc sequences, forming the Brunswick subduction complex (van Staal 1994).

At least four relatively continuous phases of deformation affect the Brunswick subduction complex, where strain is heterogeneous on all scales (van Staal and de Roo 1995). Polyphase deformation records the evolving tectonic regime during Laurentian-Ganderian collision, from (1) early

subduction and (2) collision, to later (3) extensional collapse and (4) dextral transpression. Earliest bedding-parallel thrust structures were deformed into tight, upright folds and affected by sinistral transpressive shear zones following Late Ordovician to Early Silurian oblique collision. Recumbent folds and kinks overprint earlier structures as a consequence of vertical coaxial shortening during Early Devonian extensional collapse. Subsequent Devonian dextral transpression accounts for kilometre-scale open folds, as well as development of the regional Rocky-Brook Millstream (RBM) shear zone. The RBM shear zone is a ~225 km-long dextral, subvertical ductile-brittle shear zone with a component of reverse movement (van Staal and de Roo 1995; Fig. 1). Lateral displacement estimates vary greatly, from 12 to 60 km, and heterogeneous strain along the shear zone resulted in a splayed morphology (Dimitrov et al. 2003). At its northeastern extremity, near the Nicholas-Denys deposit, the RBM shear zone has an ENE–WSW orientation and splays into a northern branch, termed the Main Break, and a South Branch (Fig. 2).

2.2.2 Geology of the Bathurst Mining Camp

The current configuration of the BMC consists of four more or less coeval Middle Ordovician tectonic blocks, the Tetagouche, California Lake, Sheephouse Brook and Fournier blocks, which represent separate areas of the backarc rift basin, possibly different sub basins, which were later structurally juxtaposed during Late Ordovician-Silurian basin closure (van Staal et al. 2003; Fig. 1). Each tectonic block comprises a stratigraphic group of the same name. The Tetagouche, California Lake and Sheephouse Brook groups consist of Ordovician volcano–sedimentary rocks underlain by Ganderian Cambro-Ordovician passive margin sediments of the Miramichi Group. The Ordovician volcano–sedimentary sequence comprises bimodal volcanic rocks, composed of porphyric rhyolitic to dacitic flows and pyroclastic rocks, aphyric and crystal tuffs, tuffites, volcanoclastics, transitional alkalic-tholeiitic basaltic pillow lavas and massive flows, intercalated with siliciclastic sedimentary rocks.

The Fournier block, which hosts the Nicholas-Denys deposit, is considered to be a remnant of transitional to oceanic crust marking the opening of the continental backarc rift basin into a marginal sea (van Staal et al. 2003). The Fournier block forms the structural top of the BMC, and is also exposed outside the camp as an inlier (Belledune-Elmtree) within Silurian sedimentary rocks (Fig. 1). In contrast to bimodal volcanic and sedimentary rocks of the Tetagouche, California Lake and Sheephouse Brook groups, the Fournier Group is characterized by mafic volcanic rocks, comprising synvolcanic gabbros, oceanic pillow basalts ranging in composition from island arc

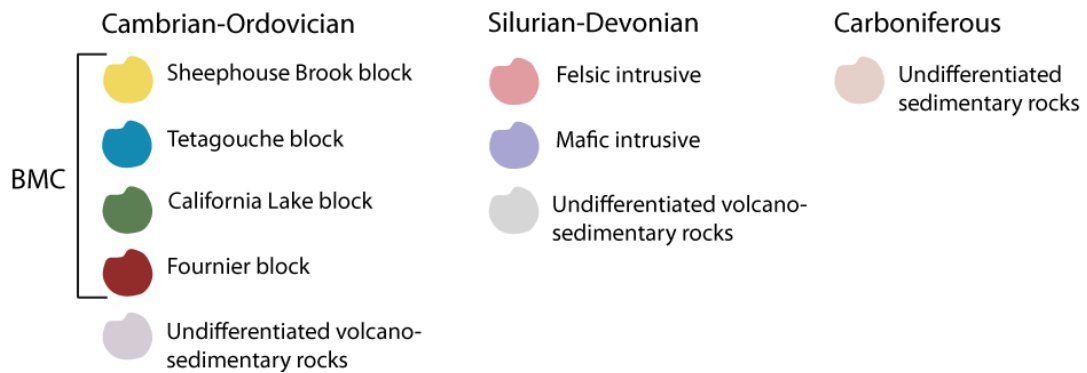
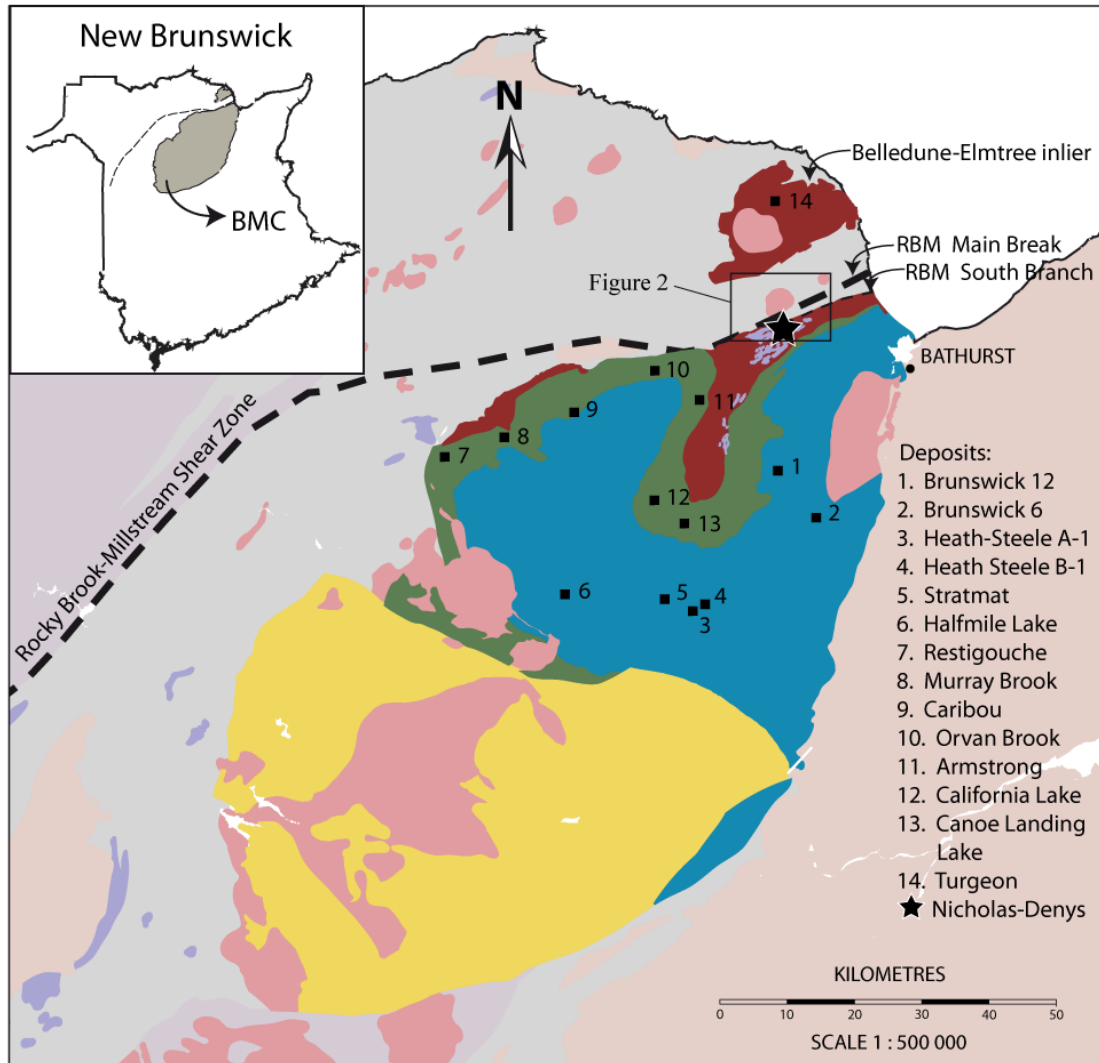


Figure 1. Generalized geological map of the Bathurst Mining Camp (BMC) showing the four tectonic blocks, location of massive sulphide deposits and trace of the Rocky Brook-Millstream (RBM) shear zone (modified after van Staal et al, 2003).

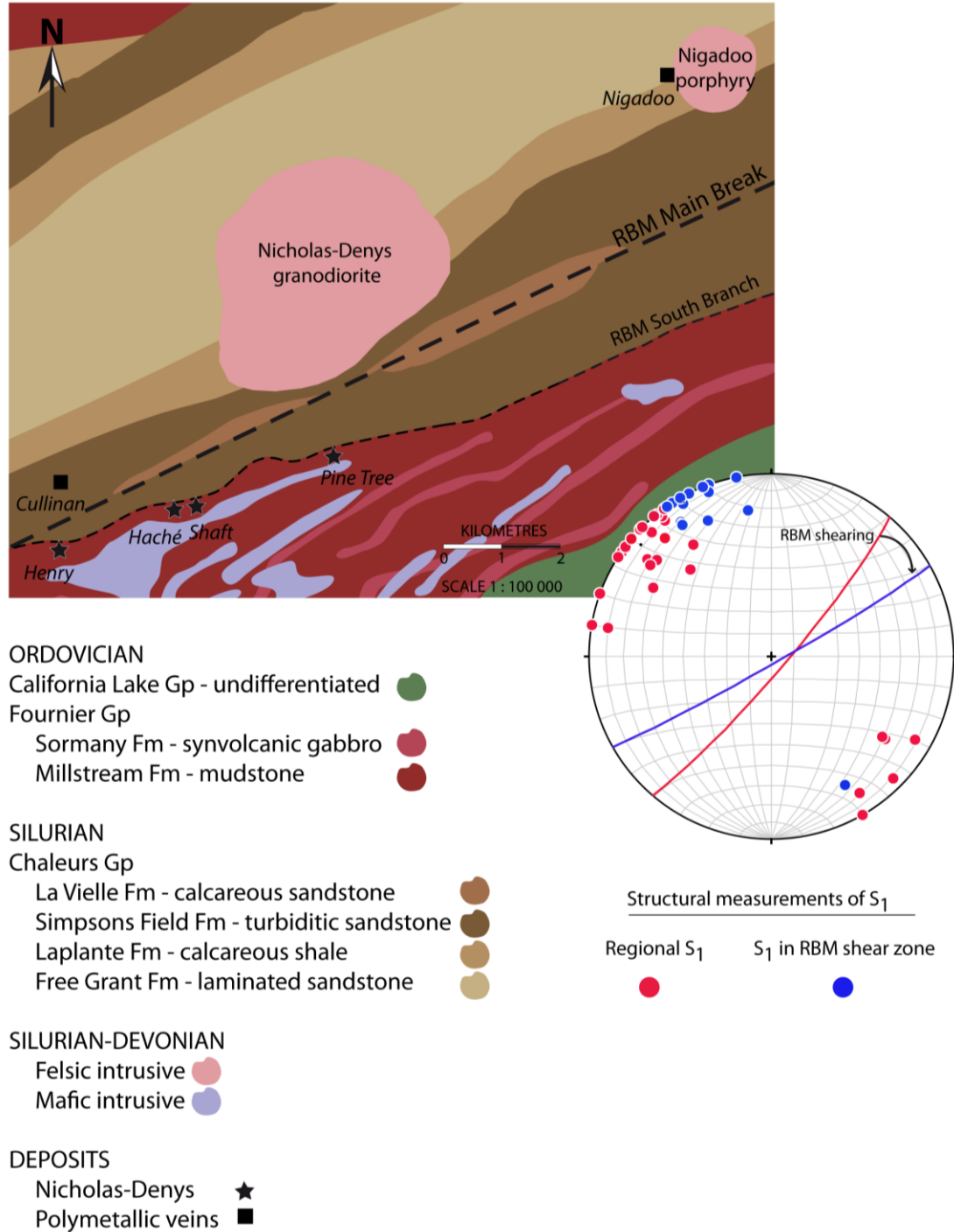


Figure 2. Geological map of the Nicholas-Denys deposit area. Stereonet diagram with foliation (S_1) data from the Millstream and Simpsons Field formations away from (red) and near to the Rocky Brook-Millstream (RBM) shear zone (blue), indicating clockwise rotation of the NE-SW regional S_1 to an ENE-WSW orientation by RBM shearing. Poles to foliation planes are plotted with great circles generated from a cylindrical best-fit analysis.

basalts (IAB) to mid-ocean ridge basalts (MORB) to ocean-island basalts (OIB), and deepwater sedimentary rocks, comprising black shale, sandstone, wacke and minor limestone, as well as a tectonic mélange unit (Belledune mélange). At the northern limit of the BMC, Silurian sedimentary rocks of the Chaleurs Group unconformably overlie Ordovician volcano-sedimentary rocks, locally occurring in fault contact along the RBM shear zone (Figs. 1 and 2). Chaleurs Group sedimentary rocks were deposited in a forearc basin and comprise calcareous sandstone, turbiditic sandstone, calcareous shale and laminated weakly calcareous sandstone of the Lower Silurian La Vieille and Simpsons Field formations and Upper Silurian Laplante and Free Grant formations, respectively (Dimitrov et al. 2004; Dimitrov and McCutcheon 2007). Ordovician and Silurian rocks are intruded by Upper Silurian-Devonian felsic and mafic plutons, including the Nicholas-Denys granodiorite (381 Ma; Walker et al. 1991) and Nigadoo quartz-feldspar porphyry (Fig. 2).

2.2.3 Metallogeny of the BMC

Felsic volcanic and sedimentary rocks of the Lower-Middle Ordovician Tetagouche and California Lake groups host the majority of massive sulphide deposits in the BMC (Fig. 1). Goodfellow (2007) and Goodfellow and McCutcheon (2003) summarize the main attributes of the BMC deposits. The deposits occur within four stratigraphic horizons related to episodes of hydrothermal activity in a backarc rift, dated at 478 Ma, 472–470 Ma, 469–468 Ma, and 467–465 Ma (van Staal et al. 2003). Deposits are intensely deformed, and their morphology varies from pod-like to tabular bodies, to sheet-like lenses. The majority of BMC deposits are tabular and have an internal architecture consisting of a proximal pyrrhotite–magnetite–pyrite–chalcopyrite vent complex and distal bedded pyrite–sphalerite–galena to bedded pyrite. Massive sulphides are vertically and laterally zoned with Cu/(Pb+Zn) decreasing away from the vent complex, and are typically underlain by a sulphide stringer zone. Pod- and sheet-shaped deposits are less common in the BMC. Pods are typically Cu-rich, and represent vent complexes lacking the distal bedded ore facies, whereas sheet-like lenses are marked by the absence of a vent complex and metal zonation, and are considered vent-distal or reworked deposits.

The Turgeon and Nicholas-Denys deposits are the only massive sulphide deposits known in the Fournier Group (Fig. 1). The Turgeon deposit is located in the Belledune-Elmtree inlier and consists of a pyrite–chalcopyrite–sphalerite sulphide lens. The Turgeon deposit occurs in pillow lavas and gabbros of the Devereaux Formation (~464Ma) of the Fournier Group, of slightly younger stratigraphic age than units hosting other VMS deposits in the BMC. The Cu >> Pb metal content

and mafic composition of volcanic host rocks set the Turgeon deposit apart from siliciclastic-felsic VMS deposits, and are similar to “Cyprus-type” mafic-hosted VMS deposits (Thurlow 1993). The Nicholas-Denys deposit consists of pyrrhotite–sphalerite–galena sulphides and is hosted by mudstone of the Millstream Formation (~460–455 Ma) of the Fournier Group (Fig. 1). The Nicholas-Denys host rocks are slightly younger than siliciclastic-felsic rocks that host VMS deposits of the Tetagouche and California Lake Groups, and mafic volcanic rocks of Devereaux Formation that host the Turgeon deposit. The absence of volcanic rocks in the host sequence and abundance of pyrrhotite set Nicholas-Denys apart from siliciclastic-felsic BMC VMS deposits and from the mafic-hosted Turgeon deposit.

Outside the BMC, the Chaleurs Group hosts polymetallic veins (Fig. 2). The Nigadoo deposit consists of a system of N- and NW-striking sphalerite–galena–chalcopyrite–pyrite–pyrrhotite–arsenopyrite–quartz–calcite veins, which are approximately 1 m-thick and extend down to a depth of 650 m, with a strike length of 1 km. The polymetallic Nigadoo veins cut sedimentary rocks of the Chaleurs Group and the Nigadoo Devonian quartz-feldspar porphyritic intrusion (Davies et al. 1969), indicating the Nigadoo deposit is Devonian in age or younger. The narrower Cullinan vein system cuts turbiditic sandstone of the Lower Silurian Simpsons Field Formation ~500 m north of the RBM main break, and consists of NW-striking arsenopyrite–pyrite–galena–sphalerite veins up to 0.6 m-thick, with one vein having a strike length of 240 m. Rocks of the Lower Silurian Simpsons Field Formation are estimated to have formed during the Ludlow Age (Dimitrov et al. 2004), indicating the Cullinan vein system is Late Silurian-Early Devonian in age or younger. Both the Nigadoo and Cullinan veins are steeply-dipping and characterized by underformed, coarse-grained sulphides in sharp contact with foliated host rocks, indicating that the veins post-date Devonian deformation associated with the Acadian orogeny.

2.3 Analytical methods

Twenty-three unaltered and altered samples of sedimentary rocks from the Nicholas-Denys deposit were selected for whole rock analysis at Activation Laboratories Ltd., Ancaster, Ontario. Major elements and trace elements Ba, Be, Sr, V and Y were analysed by Inductively Coupled Plasma - Optical Emission Spectrometry (ICP-OES) and lithium metaborate/tetraborate fusion. Trace elements Bi, Cs, Ga, Ge, Hf, In, Mo, Nb, Rb, Sn, Ta, Th, Tl, U and Zr and elements of the lanthanide series were analysed by Inductively Coupled Plasma - Mass Spectrometry (ICP-MS) and lithium metaborate/tetraborate fusion. Trace elements Au, As, Br, Co, Cr, Hg, In, Sb, Sc, Se and W

were analysed by Instrumental Neutron Activation Analysis (INAA). Trace elements Cd, Cu, Ni, Pb and S were analysed by ICP-OES and four acid digestion. A combination of the INAA and ICP-OES methods with a four acid digestion were used to analyse for Ag and Zn. Organic carbon content was determined by combustion of the samples at 1370°C followed by infrared detection of released CO₂ gas.

Silicate and sulphide mineral compositions were determined using the CAMECA SX-100 electron microprobe equipped with 5 wavelength dispersive spectrometers at Université Laval, Québec. Analytical conditions for major elements were 15kV and 20nA, with counting times of 20s on peak and 10s on background. Analytical conditions for trace elements in sulphide minerals were 15kV and 100nA, with counting times of 40s on peak, and 20s on background. Natural standards from Astimex Scientific LTD were used.

Sixty-two sulphide separates from Nicholas-Denys, two sulphide separates from Nigadoo, two sulphide separates from Turgeon and one pyrite aggregate from the Belledune mélange unit were hand-picked under a binocular lens and the sulphur isotope composition was determined at the G.G Hatch Isotope Laboratories at the University of Ottawa. Samples were loaded in an elemental analyser (EA) and were flash combusted at 1800°C. The SO₂ gas was introduced into the DeltaPlus isotope ratio mass spectrometer (IRMS) for analysis. Sulphur isotope ratios are reported as δ³⁴S values relative to V-CDT (Vienna Canyon Diablo Troilite) with a precision of 0.2 per mil.

Fourteen grains of galena (~1 mm) from the Nicholas-Denys deposit, as well as one galena grain from the Nigadoo deposit and three galena grains from the Cullinan deposit, were selected for lead isotope ratio analysis. Samples were analysed at the GEOTOP laboratory, Université du Québec à Montréal (UQAM). Lead isotope ratios are normalized to NBS981 with a precision (2s) of 0.003% (²⁰⁶Pb/²⁰⁴Pb, ²⁰⁷Pb/²⁰⁴Pb) and 0.011% (²⁰⁸Pb/²⁰⁴Pb).

2.4 Deposit geology

The Nicholas-Denys deposit occurs in black mudstone of the Middle Ordovician Millstream Formation of the Fournier Group (Fig. 2), approximately 90 m south of the RBM South Branch. Sandstone of the Lower Silurian Simpsons Field Formation immediately north of the RBM South Branch is altered to hornfel by contact metamorphism due to intrusion of the Nicholas-Denys granodiorite. The contact metamorphic aureole surrounding the Nicholas-Denys granodiorite is

truncated by the RBM shear zone, such that mudstone of the Millstream Formation south of the RBM South Branch does not show the same indurated hornfel texture as the Simpsons Field Formation north of the RBM South Branch. Along the RBM main break, lenses of calcareous sandstone crop out, which are thought to be contemporaneous with the Late Llandovery-Wenlock La Vieille Formation (Dimitrov, 2004). North of the RBM Main Break, the Devonian Nicholas-Denys granodiorite and Nigadoo porphyry intrude the Chaleurs Group. Approximately 200 m south of the Nicholas-Denys deposit, Upper Silurian-Devonian gabbros intrude black mudstone of the Middle Ordovician Millstream and synvolcanic gabbros of the Middle Ordovician Sormany Formation of the Fournier Group.

Rocks of the Silurian Simpsons Field and Ordovician Millstream formations are affected by a NE-striking, subvertical, bedding-parallel foliation (S_1) (Fig. 2), that is thought to be associated with regional Devonian Acadian deformation. The S_1 foliation is penetrative in unaltered to weakly altered mudstone of the Millstream Formation, whereas S_1 is spaced in altered and mineralized mudstone. Two joint systems dominate the structural style of the altered and mineralized mudstone: (1) NW–SE and NNE–SSW conjugate joints, and (2) ENE–WSW joints, parallel to the RBM shear zone (Fig. 3). The conjugate joints are also present in Lower Silurian rocks of the Simpsons Field Formation and elsewhere in the Millstream Formation. At the Haché showing, ENE–WSW shear zones are present at the northern and southern contacts of altered and mineralized mudstone with unaltered mudstone (Fig. 3). The shear zones are characterized by clockwise rotation of the NE-striking regional S_1 fabric to an ENE–WSW orientation (Fig. 2), and asymmetric folding of S_1 into “z”-shaped folds, indicating a dextral sense of shear, compatible with Devonian dextral transpressive deformation along the RBM shear zone (van Staal and de Roo 1995).

The Millstream Formation mudstone consists of alternating dark grey and black beds and laminae interlayered with medium grey siltstone laminae and 1–5% diagenetic pyrite (Fig. 4a). A *mélange*-type rock occurs locally in the drill core and at the Haché showing, and consists of subrounded to subangular siltstone clasts in a dark grey to black mudstone matrix (Fig. 4b). Coarse-grained quartz is abundant in the Haché drill core (5–10 vol%), particularly north of the sulphide lenses and increases in abundance with proximity to mineralization (up to 30 vol%). Quartz occurs as : (1) patches of irregular grains with embayed margins, (2) undeformed veins in sharp contact with host rock, (3) *ptygmatically* folded veins (Fig. 4b) and (4) vein fragments wrapped by S_1 . South of the sulphide lenses, a ~20 m-thick sandstone bed within the Millstream Formation is in sharp contact with mudstone (Fig. 4c) and defines the locally sub-vertical, NE-striking S_0 for the Millstream

Formation (Fig. 5). The sandstone bed has a bimodal grain size distribution, characterized by 2–20% subangular quartz grains (1–5 mm) and 50–70% subrounded quartz grains (≤ 1 mm) in a fine-grained micaceous matrix (Fig. 4d). Sedimentary structures are generally absent, except for a few graded beds and load casts which yield contrasting directions for stratigraphic polarity, indicating folding of the host rock sequence.

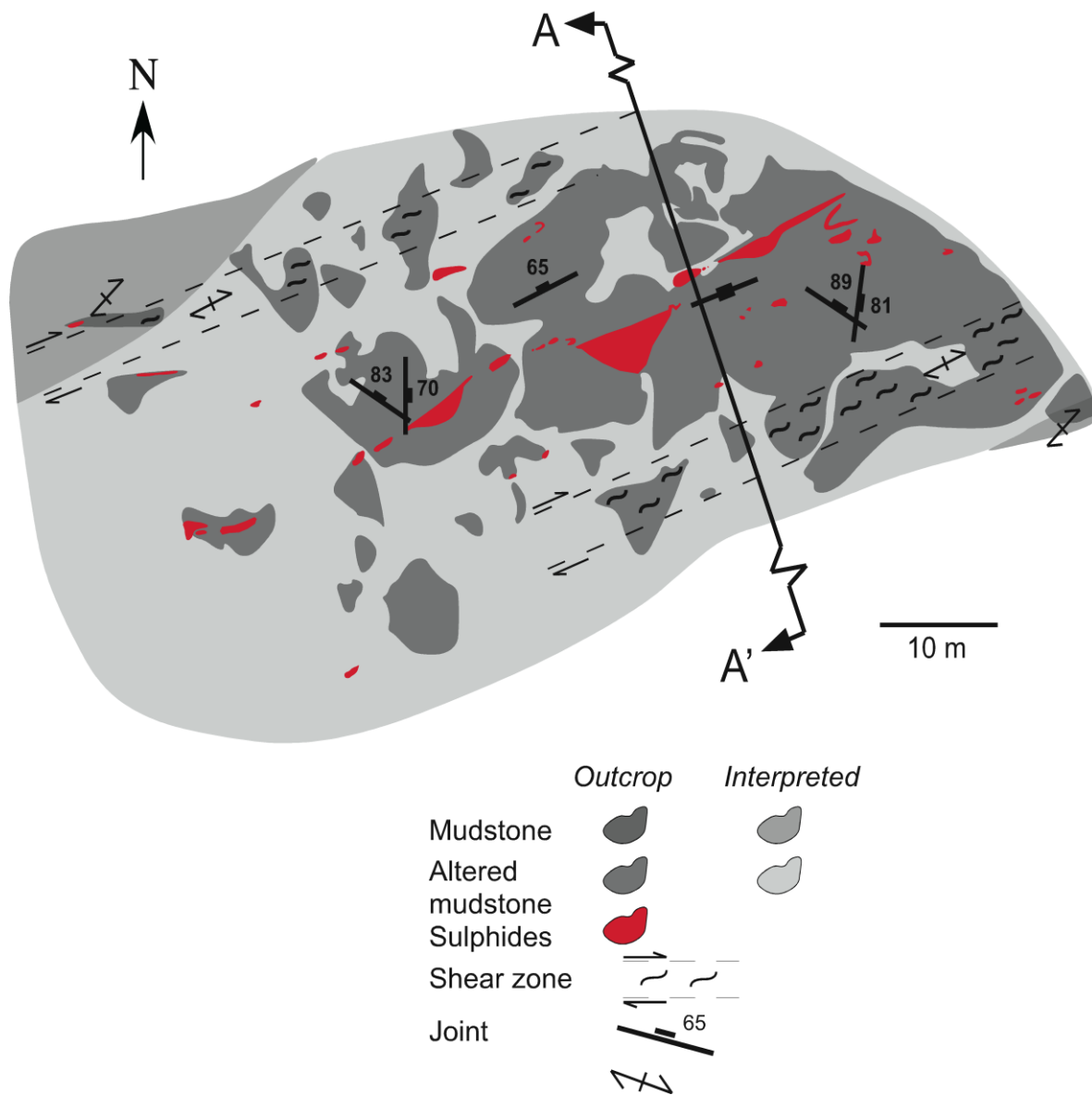


Figure 3. Detailed geological map of the Haché showing. Cross-section A-A' is shown in Figure 5.

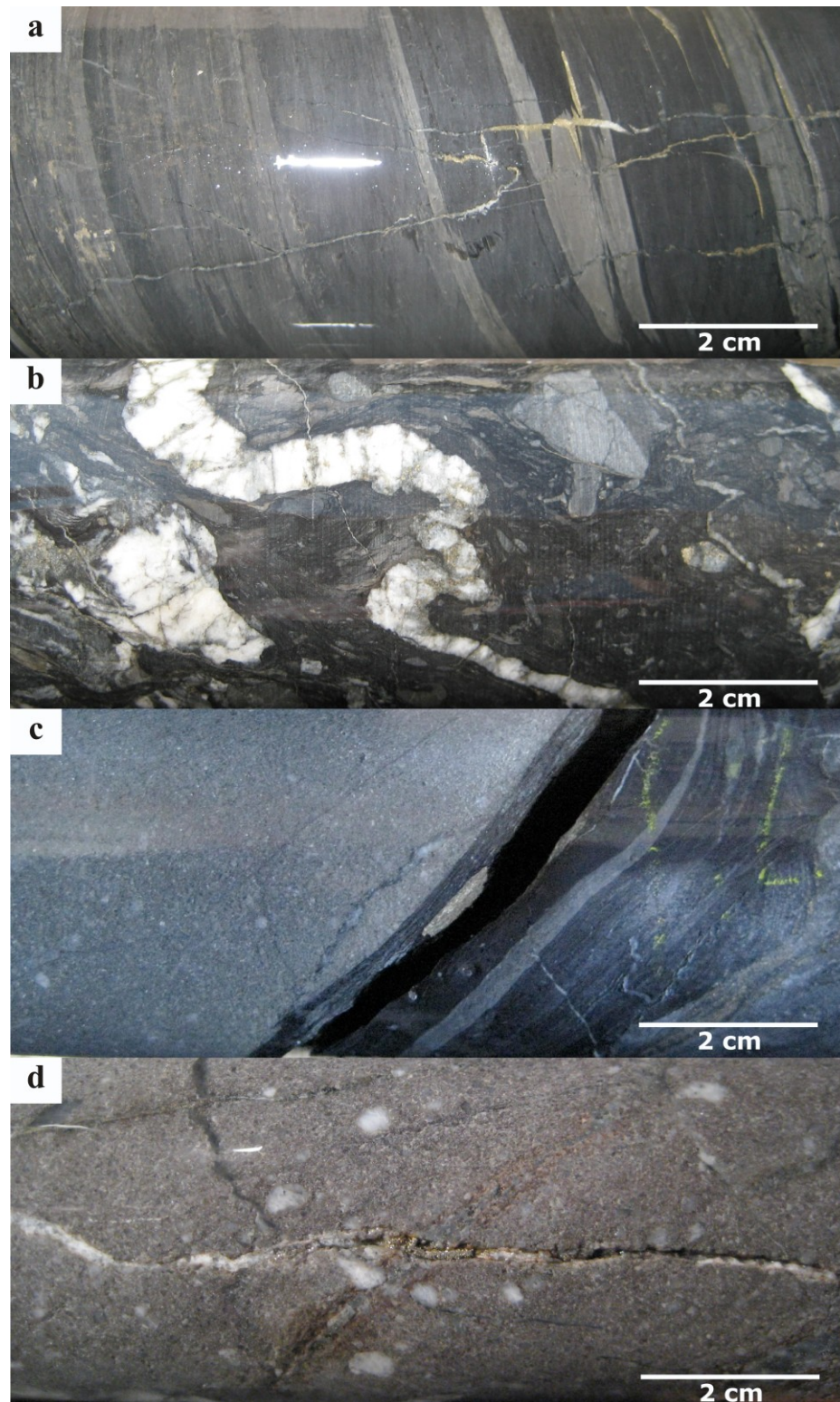


Figure 4. Photographs of unaltered Millstream Formation drillcore. a) Mudstone interlayered with siltstone laminae and diagenetic pyrite. b) Subangular siltstone clasts, ptygmatic quartz veins and vein fragments in mélangé unit. c) Sharp bedding plane between sandstone and mudstone, conformable to S_1 in mudstone. d) Sandstone cut by late calcite-quartz-pyrite vein.

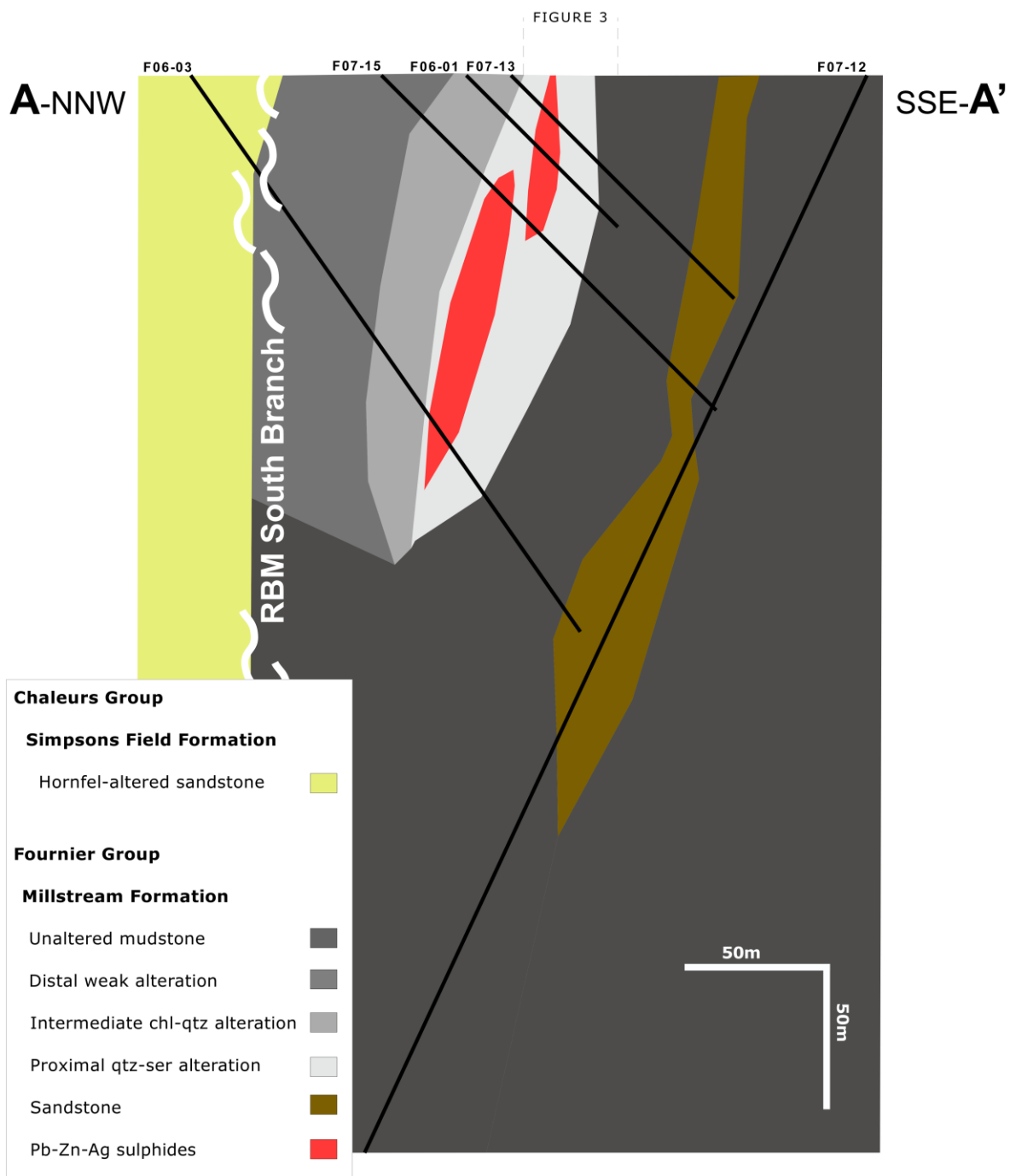


Figure 5. Cross section of the Haché sulphide lenses (surface map of the Haché showing in Figure 3). From north to south, DDH intersect hornfel-altered sandstone of the Simpsons Field Formation, the RBM South Branch, three facies of altered mudstone and sulphide lenses conformable to local subvertical bedding, as defined by the sandstone bed intercalated within unaltered mudstone of the Millstream Formation, south of the sulphide lenses.

Deformation textures in the Millstream Formation are heterogeneous. Mudstone beds are characterized by a penetrative S_1 foliation, a crenulation foliation (S_2), millimetre- to decimetre-scale disharmonic folds, and micro-faults. Siltstone laminae are deformed into bedding-parallel boudins. The S_1 foliation is discrete within the laminae/boudins, and the crenulation foliation (S_2) is absent (Fig. 6a). The crenulation foliation (S_2) is also absent in the bimodal sandstone. However, the fine-grained micaceous matrix of the sandstone shows a penetrative S_1 foliation, with coarse quartz grains subtly aligned with the S_1 foliation (Fig. 6b).

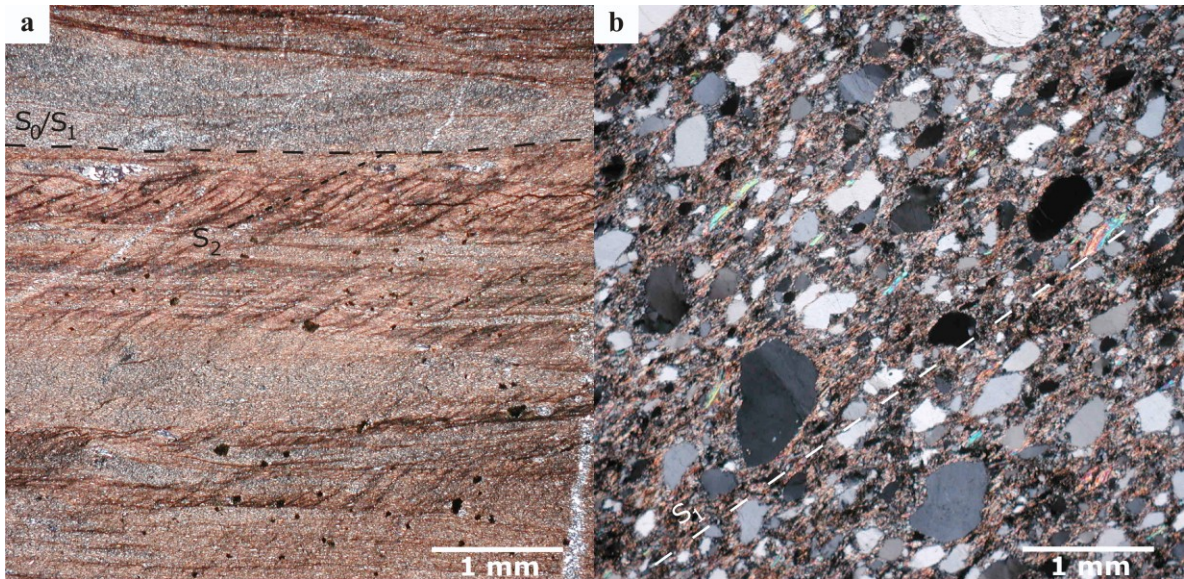


Figure 6. Photomicrographs of unaltered Millstream Formation in polarized light. a) Mudstone interlayered with siltstone laminae. b) Bimodal grain size sandstone consisting of subtly aligned subangular quartz fragments in a fine-grained foliated micaceous matrix.

2.4.1 Host rock lithogeochemistry

Unaltered Millstream Formation mudstone ($n=6$) and sandstone ($n=4$) were sampled south of the Nicholas-Denys sulphide lenses for lithogeochemical analyses (Tables 1 and 2). Mudstone samples show a linear covariation for several major, trace and REE elements plotted against Al_2O_3 , whereas sandstone samples show a clustered distribution (Fig. 7). The negative covariation between SiO_2 and Al_2O_3 in mudstone samples is thought to reflect the inversely varying proportions of quartz and clay making up the unit, and the large range in SiO_2 and Al_2O_3 contents is consistent with various proportions of siltstone laminae interlayered within mudstone beds. The large variation of TiO_2 , La and Th concentrations in the mudstone samples and their positive covariation with Al_2O_3 indicate that Ti, La and Th are preferentially bound in the clay fraction of the mudstone. Contents of TiO_2 ,

La and Th in the sandstone samples are tightly clustered, suggesting the overall chemical composition of the sandstone bed is much more uniform than that of the mudstone.

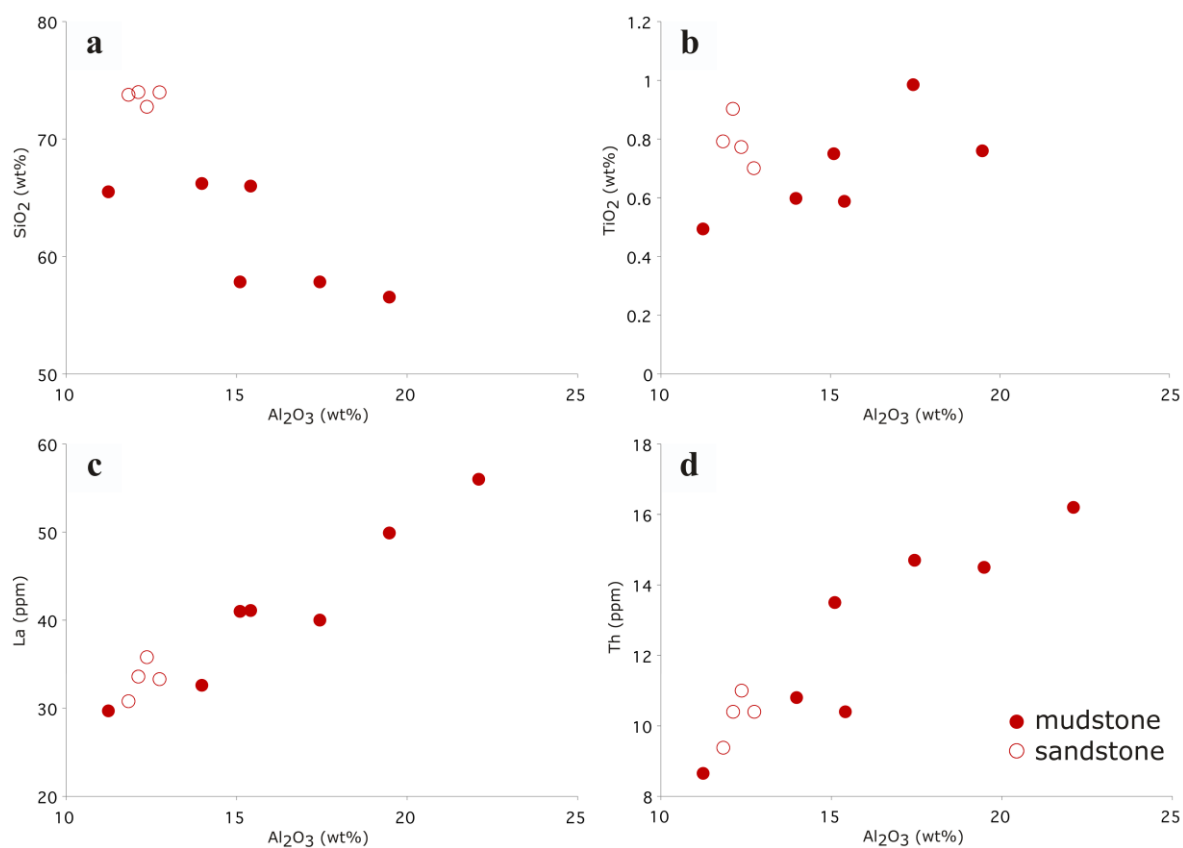


Figure 7. Bivariate plots of selected major and trace elements for unaltered Millstream Formation samples.

2.4.2 Hydrothermal alteration

North of the sulphide lenses, diamond drill holes intersect a gradational asymmetric alteration envelope consisting of three conformable alteration zones (Fig. 5; Table 3): (1) proximal pervasive quartz–sericite alteration, (2) intermediate chlorite–quartz alteration and (3) distal weak alteration. To the north, the distal weak alteration is juxtaposed with hornfel of the Simpsons Field Formation along the RBM South Branch fault contact. South of the sulphide lenses, the pervasive quartz–sericite alteration grades to unaltered black mudstone (Figs. 4a and 6a).

Table 1. Bulk lithochemical compositions of unaltered Millstream Formation mudstone.

| Sample No. | 451667 | 422857 | 422855 | 451670 | 422858 | 422851 |
|----------------------------------|--------|--------|--------|---------|--------|--------|
| wt% | | | | | | |
| SiO ₂ | 66.00 | 56.54 | 57.84 | 57.84 | 66.22 | 65.51 |
| TiO ₂ | 0.59 | 0.76 | 0.99 | 0.75 | 0.60 | 0.49 |
| Al ₂ O ₃ | 15.41 | 19.48 | 17.44 | 15.10 | 13.98 | 11.24 |
| Fe ₂ O ₃ T | 4.46 | 8.32 | 9.38 | 8.74 | 4.71 | 6.87 |
| MnO | 0.08 | 0.16 | 0.39 | 0.29 | 0.10 | 0.15 |
| MgO | 2.19 | 2.97 | 3.50 | 2.35 | 3.20 | 5.07 |
| CaO | 1.60 | 0.40 | 0.78 | 2.46 | 4.38 | 0.76 |
| Na ₂ O | 0.10 | 0.80 | 0.12 | 0.16 | 0.82 | 0.05 |
| K ₂ O | 4.86 | 4.52 | 4.11 | 4.17 | 2.28 | 2.68 |
| P ₂ O ₅ | 0.12 | 0.10 | 0.12 | 0.10 | 0.10 | 0.06 |
| LOI | 5.31 | 4.64 | 5.33 | 6.87 | 3.01 | 6.03 |
| Total | 100.70 | 98.68 | 100.00 | 98.83 | 99.40 | 98.92 |
| S | 0.92 | 0.38 | 0.95 | 2.33 | 0.31 | 1.28 |
| TOC | < 0.05 | 0.05 | 0.06 | < 0.05 | < 0.05 | < 0.05 |
| ppm | | | | | | |
| Ag | 1.00 | 0.50 | 0.60 | 7.70 | < 0.5 | 3.30 |
| As | 58.00 | 20.00 | 30.00 | 223.00 | 5.00 | 42.00 |
| Ba | 583.00 | 603.00 | 563.00 | 800.00 | 224.00 | 261.00 |
| Be | 3.00 | 3.00 | 2.00 | 3.00 | 3.00 | 3.00 |
| Bi | < 0.1 | 0.30 | 0.30 | 1.90 | < 0.1 | < 0.1 |
| Br | < 0.5 | < 0.5 | < 0.5 | < 0.5 | 1.80 | 1.70 |
| Cd | 1.40 | 0.50 | 0.60 | 25.20 | < 0.5 | 1.10 |
| Co | 29.00 | 25.60 | 27.90 | 41.70 | 9.50 | 17.20 |
| Cr | 105.00 | 119.00 | 93.90 | 112.00 | 139.00 | 127.00 |
| Cs | 8.00 | 5.90 | 5.60 | 6.20 | 7.00 | 7.90 |
| Cu | 50.00 | 43.00 | 52.00 | 101.00 | 18.00 | 95.00 |
| Ga | 26.00 | 27.00 | 26.00 | 23.00 | 19.00 | 18.00 |
| Ge | 1.80 | 2.30 | 2.40 | 2.00 | 1.60 | 1.40 |
| Hf | 2.30 | 3.00 | 4.10 | 3.60 | 2.90 | 2.30 |
| Hg | < 1 | < 1 | < 1 | < 1 | < 1 | < 1 |
| In | < 0.1 | < 0.1 | < 0.1 | 0.20 | < 0.1 | < 0.1 |
| Mo | 29.00 | < 2 | < 2 | < 2 | 12.00 | 8.00 |
| Nb | 11.40 | 15.70 | 18.90 | 15.90 | 11.10 | 9.30 |
| Ni | 59.00 | 53.00 | 61.00 | 70.00 | 46.00 | 59.00 |
| Pb | 45.00 | 23.00 | 12.00 | 2690.00 | 14.00 | 99.00 |
| Rb | 195.00 | 158.00 | 136.00 | 145.00 | 105.00 | 110.00 |
| Sb | 7.80 | 4.70 | 5.50 | 10.80 | 4.20 | 27.60 |
| Sc | 14.30 | 19.90 | 20.30 | 20.60 | 16.60 | 14.30 |
| Se | < 0.5 | < 0.5 | < 0.5 | < 0.5 | < 0.5 | < 0.5 |
| Sn | 6.00 | 3.00 | 8.00 | 11.00 | 2.00 | 17.00 |
| Sr | 45.00 | 51.00 | 30.00 | 31.00 | 145.00 | 25.00 |
| Ta | 0.60 | 1.10 | 1.40 | 1.20 | 0.70 | 0.60 |
| Th | 10.40 | 14.50 | 14.70 | 13.50 | 10.80 | 8.65 |

Table 1 continued

| | | | | | | |
|-----|--------|--------|--------|---------|--------|--------|
| U | 6.92 | 2.35 | 2.64 | 2.10 | 11.30 | 7.30 |
| V | 109.00 | 116.00 | 122.00 | 107.00 | 244.00 | 256.00 |
| W | 5.00 | < 1 | 2.00 | 3.00 | < 1 | 2.00 |
| Y | 13.00 | 26.00 | 30.00 | 26.00 | 19.00 | 23.00 |
| Zn | 498.00 | 114.00 | 99.00 | 1380.00 | 63.00 | 109.00 |
| Zr | 105.00 | 130.00 | 179.00 | 159.00 | 130.00 | 106.00 |
| La | 41.10 | 49.90 | 40.00 | 41.00 | 32.60 | 29.70 |
| Ce | 76.50 | 96.50 | 85.20 | 87.60 | 62.50 | 54.80 |
| Pr | 9.25 | 11.80 | 9.98 | 10.20 | 7.69 | 6.88 |
| Nd | 28.90 | 38.30 | 33.40 | 34.20 | 25.40 | 22.10 |
| Sm | 5.04 | 7.34 | 6.67 | 6.98 | 4.89 | 4.13 |
| Eu | 1.20 | 1.53 | 1.06 | 1.37 | 1.20 | 0.91 |
| Gd | 3.91 | 5.83 | 5.81 | 5.79 | 4.23 | 3.61 |
| Tb | 0.59 | 0.90 | 0.98 | 0.94 | 0.69 | 0.65 |
| Dy | 3.08 | 4.98 | 5.85 | 5.30 | 3.90 | 4.05 |
| Ho | 0.57 | 0.96 | 1.17 | 1.03 | 0.77 | 0.86 |
| Er | 1.65 | 2.81 | 3.45 | 3.01 | 2.29 | 2.57 |
| Tl | 2.08 | 1.19 | 1.19 | 1.53 | 1.11 | 1.16 |
| Tm | 0.24 | 0.41 | 0.52 | 0.45 | 0.35 | 0.40 |
| Yb | 1.50 | 2.59 | 3.33 | 2.79 | 2.36 | 2.56 |
| Lu | 0.22 | 0.38 | 0.48 | 0.40 | 0.36 | 0.38 |
| ppb | | | | | | |
| Au | 12 | < 1 | < 1 | 8 | < 1 | < 1 |
| Ir | < 1 | < 1 | < 1 | < 1 | < 1 | < 1 |

Table 2. Bulk lithochemical compositions of unaltered Millstream Formation sandstone.

| Sample No. | 451640 | 451639 | 451860 | 451856 |
|----------------------------------|--------|--------|--------|--------|
| wt% | | | | |
| SiO ₂ | 73.77 | 74.00 | 73.98 | 72.75 |
| TiO ₂ | 0.79 | 0.90 | 0.70 | 0.77 |
| Al ₂ O ₃ | 11.83 | 12.12 | 12.74 | 12.37 |
| Fe ₂ O ₃ T | 4.14 | 4.68 | 3.37 | 4.52 |
| MnO | 0.12 | 0.04 | 0.10 | 0.08 |
| MgO | 1.31 | 1.26 | 1.21 | 1.18 |
| CaO | 1.81 | 0.25 | 0.40 | 0.58 |
| Na ₂ O | 2.18 | 2.09 | 0.23 | 1.16 |
| K ₂ O | 2.59 | 2.31 | 4.10 | 3.07 |
| P ₂ O ₅ | 0.14 | 0.14 | 0.15 | 0.11 |
| LOI | 1.68 | 2.34 | 3.08 | 3.24 |
| Total | 100.40 | 100.10 | 100.10 | 99.84 |
| S | 0.18 | 0.04 | 0.07 | 0.48 |
| TOC | < 0.05 | < 0.05 | < 0.05 | < 0.05 |

Table 2 continued

| | | | | |
|-----|--------|--------|--------|--------|
| ppm | | | | |
| Ag | < 0.5 | < 0.5 | < 0.5 | 1.20 |
| As | 7.00 | 4.00 | 9.00 | 70.00 |
| Ba | 339.00 | 285.00 | 517.00 | 545.00 |
| Be | 1.00 | 1.00 | 2.00 | 2.00 |
| Bi | < 0.1 | 0.10 | < 0.1 | 0.20 |
| Br | < 0.5 | < 0.5 | < 0.5 | < 0.5 |
| Cd | < 0.5 | < 0.5 | < 0.5 | 5.60 |
| Co | 9.40 | 9.20 | 9.40 | 12.10 |
| Cr | 76.80 | 74.40 | 67.20 | 93.00 |
| Cs | 5.50 | 2.70 | 6.60 | 3.80 |
| Cu | 14.00 | 14.00 | 18.00 | 45.00 |
| Ga | 17.00 | 16.00 | 17.00 | 18.00 |
| Ge | 1.60 | 1.50 | 1.40 | 1.70 |
| Hf | 9.60 | 10.90 | 8.20 | 9.50 |
| Hg | < 1 | < 1 | < 1 | < 1 |
| In | < 0.1 | < 0.1 | < 0.1 | < 0.1 |
| Mo | < 2 | < 2 | < 2 | < 2 |
| Nb | 14.30 | 14.90 | 11.10 | 13.90 |
| Ni | 25.00 | 23.00 | 31.00 | 30.00 |
| Pb | 12.00 | 7.00 | 19.00 | 325.00 |
| Rb | 89.00 | 71.00 | 133.00 | 98.00 |
| Sb | 3.10 | 1.10 | 2.20 | 5.00 |
| Sc | 6.18 | 7.68 | 7.32 | 8.58 |
| Se | < 0.5 | < 0.5 | < 0.5 | < 0.5 |
| Sn | 4.00 | 2.00 | 3.00 | 5.00 |
| Sr | 119.00 | 28.00 | 29.00 | 39.00 |
| Ta | 0.80 | 0.90 | 0.70 | 0.90 |
| Th | 9.38 | 10.40 | 10.40 | 11.00 |
| U | 1.76 | 1.89 | 1.89 | 2.12 |
| V | 60.00 | 64.00 | 57.00 | 63.00 |
| W | < 1 | < 1 | < 1 | < 1 |
| Y | 20.00 | 26.00 | 20.00 | 17.00 |
| Zn | 41.00 | 68.00 | 63.00 | 374.00 |
| Zr | 476.00 | 536.00 | 396.00 | 456.00 |
| La | 30.80 | 33.60 | 33.30 | 35.80 |
| Ce | 66.30 | 71.30 | 70.30 | 75.10 |
| Pr | 7.95 | 8.71 | 8.61 | 9.02 |
| Nd | 27.10 | 29.80 | 28.50 | 30.10 |
| Sm | 5.27 | 5.92 | 5.80 | 5.65 |
| Eu | 1.12 | 1.37 | 1.25 | 1.35 |
| Gd | 4.42 | 5.23 | 4.98 | 4.44 |
| Tb | 0.71 | 0.87 | 0.78 | 0.69 |
| Dy | 4.04 | 4.97 | 4.32 | 3.91 |
| Ho | 0.79 | 0.95 | 0.81 | 0.75 |
| Er | 2.34 | 2.73 | 2.34 | 2.22 |

Table 2 continued

| | | | | |
|-----|-------|------|------|------|
| Tl | 0.83 | 0.58 | 1.00 | 0.87 |
| Tm | 0.35 | 0.40 | 0.34 | 0.33 |
| Yb | 2.21 | 2.48 | 2.14 | 2.15 |
| Lu | 0.34 | 0.37 | 0.31 | 0.33 |
| ppb | | | | |
| Au | 25.00 | < 1 | < 1 | < 1 |
| Ir | < 1 | < 1 | < 1 | < 1 |

Table 3. Bulk lithochemical compositions of altered Millstream Formation mudstone.

| <i>Alteration facies</i> | <u>Unaltered</u> | <u>Distal</u> | <u>Intermediate</u> | <u>Proximal unmineralized</u> | <u>Proximal mineralized</u> |
|----------------------------------|------------------|---------------|---------------------|-------------------------------|-----------------------------|
| <i>Sample No.</i> | <i>451855</i> | <i>451748</i> | <i>451608</i> | <i>451730</i> | <i>451703</i> |
| wt% | | | | | |
| SiO ₂ | 57.84 | 53.81 | 61.62 | 60.85 | 67.46 |
| TiO ₂ | 0.99 | 0.85 | 0.57 | 0.61 | 0.27 |
| Al ₂ O ₃ | 17.44 | 22.10 | 12.79 | 14.61 | 7.15 |
| Fe ₂ O ₃ T | 9.38 | 6.63 | 5.69 | 4.79 | 6.54 |
| MnO | 0.39 | 0.05 | 0.23 | 0.16 | 0.40 |
| MgO | 3.50 | 2.50 | 5.98 | 3.64 | 4.53 |
| CaO | 0.78 | 0.34 | 5.33 | 4.58 | 3.88 |
| Na ₂ O | 0.12 | 1.36 | 0.62 | 1.17 | 0.62 |
| K ₂ O | 4.11 | 4.95 | 2.78 | 4.05 | 3.35 |
| P ₂ O ₅ | 0.12 | 0.11 | 0.12 | 0.16 | 0.07 |
| LOI | 5.33 | 5.80 | 3.06 | 4.26 | 5.93 |
| Total | 100.00 | 98.49 | 98.78 | 98.89 | 100.20 |
| S | 0.95 | 1.16 | 0.42 | 1.24 | 3.23 |
| TOC | 0.06 | < 0.05 | < 0.05 | < 0.05 | < 0.05 |
| ppm | | | | | |
| Ag | 0.60 | < 0.5 | < 0.5 | 2.40 | 5.40 |
| As | 30.00 | 33.00 | 30.00 | 186.00 | 20.00 |
| Ba | 563.00 | 817.00 | 772.00 | 673.00 | 332.00 |
| Be | 2.00 | 3.00 | 2.00 | 3.00 | 2.00 |
| Bi | 0.30 | 0.40 | 0.10 | 0.10 | 0.10 |
| Br | < 0.5 | 1.80 | < 0.5 | 1.40 | < 0.5 |
| Cd | 0.60 | 0.80 | < 0.5 | 5.50 | 448.00 |
| Co | 27.90 | 33.40 | 12.60 | 15.90 | 11.30 |
| Cr | 93.90 | 186.00 | 119.00 | 151.00 | 46.80 |
| Cs | 5.60 | 6.50 | 5.20 | 4.80 | 1.20 |
| Cu | 52.00 | 51.00 | 39.00 | 87.00 | 46.00 |
| Ga | 26.00 | 31.00 | 18.00 | 20.00 | 25.00 |
| Ge | 2.40 | 1.90 | 2.60 | 1.60 | < 0.5 |
| Hf | 4.10 | 4.30 | 2.90 | 2.70 | 1.20 |

Table 3 continued

| | | | | | |
|-----|--------|--------|--------|--------|-----------|
| Hg | < 1 | < 1 | < 1 | < 1 | < 1 |
| In | < 0.1 | < 0.1 | < 0.1 | < 0.1 | 2.10 |
| Mo | < 2 | 6.00 | 6.00 | 6.00 | 10.00 |
| Nb | 18.90 | 14.00 | 10.60 | 11.00 | 4.00 |
| Ni | 61.00 | 80.00 | 36.00 | 53.00 | 19.00 |
| Pb | 12.00 | 28.00 | 21.00 | 231.00 | 144.00 |
| Rb | 136.00 | 184.00 | 94.00 | 114.00 | 117.00 |
| Sb | 5.50 | 1.00 | 5.10 | 7.80 | 15.50 |
| Sc | 20.30 | 25.00 | 14.30 | 17.10 | 7.02 |
| Se | < 0.5 | < 0.5 | < 0.5 | < 0.5 | < 0.5 |
| Sn | 8.00 | 3.00 | 14.00 | 23.00 | 33.00 |
| Sr | 30.00 | 90.00 | 157.00 | 186.00 | 48.00 |
| Ta | 1.40 | 1.00 | 0.70 | 0.70 | 0.30 |
| Th | 14.70 | 16.20 | 10.80 | 11.00 | 2.90 |
| U | 2.64 | 6.31 | 7.29 | 6.17 | 2.20 |
| V | 122.00 | 125.00 | 224.00 | 201.00 | 111.00 |
| W | 2.00 | < 1 | < 1 | 4.00 | < 1 |
| Y | 30.00 | 25.00 | 25.00 | 20.00 | 12.00 |
| Zn | 99.00 | 93.00 | 81.00 | 385.00 | 34 300.00 |
| Zr | 179.00 | 159.00 | 130.00 | 123.00 | 56.00 |
| La | 40.00 | 56.00 | 35.10 | 35.40 | 9.55 |
| Ce | 85.20 | 104.00 | 69.80 | 67.80 | 18.60 |
| Pr | 9.98 | 13.00 | 8.57 | 8.33 | 2.34 |
| Nd | 33.40 | 39.00 | 28.00 | 27.50 | 8.30 |
| Sm | 6.67 | 6.78 | 5.67 | 5.19 | 1.90 |
| Eu | 1.06 | 1.48 | 1.53 | 1.24 | 0.75 |
| Gd | 5.81 | 5.43 | 4.93 | 4.27 | 1.90 |
| Tb | 0.98 | 0.87 | 0.81 | 0.67 | 0.34 |
| Dy | 5.85 | 4.82 | 4.64 | 3.71 | 2.06 |
| Ho | 1.17 | 0.93 | 0.90 | 0.72 | 0.42 |
| Er | 3.45 | 2.72 | 2.62 | 2.15 | 1.19 |
| Tl | 1.19 | 1.06 | 1.19 | 0.90 | 1.74 |
| Tm | 0.52 | 0.39 | 0.38 | 0.32 | 0.17 |
| Yb | 3.33 | 2.47 | 2.40 | 2.03 | 1.01 |
| Lu | 0.48 | 0.36 | 0.34 | 0.31 | 0.14 |
| ppb | | | | | |
| Au | < 1 | < 1 | 9.00 | 18.00 | 34.00 |
| Ir | < 1 | < 1 | < 1 | < 1 | < 1 |

Among the six samples of unaltered mudstone collected south of the sulphide lenses, sample 451855 was selected as the mudstone protolith based on small mass gains calculated for all other 'unaltered' samples when compared to it. TiO₂, Zr, Nb, Pr, Sm, Gd, Tb, Dy, Ho, Er, Tm, Yb, Lu and Ta were determined to be the least mobile elements as they consistently form regression lines with correlation coefficients ≥ 0.9 when plotting individual unaltered samples against each other.

Based on this suite of immobile elements, changes in mass and element concentration were calculated for representative samples from each alteration zone against the mudstone protolith 451855 using Gresen's method (Grant 1986; Fig. 8).

The distal weak alteration zone is not distinguished petrographically from unaltered mudstone (Fig. 6a), yet a typical sample from this zone (451748) demonstrates a slight mass gain (18%) compared to the mudstone protolith, enrichments of $\geq 50\%$ in Be, Na₂O, Cr, Ni, Rb, Sr, Ba, La, Pb and U and depletions of $\geq 50\%$ in MnO, Sn and Sb.

The gradual appearance of Mg–chlorite and quartz marks the petrographic transition from the distal weak alteration zone to the intermediate alteration zone. The intermediate chlorite–quartz alteration is preferentially developed in siltstone laminae/boudins, although some quartz alteration in micaceous domains is also found (Fig. 8a). In siltstone domains, equant chlorite and quartz grains are present in approximately equal proportions (Fig. 8b). The quartz and chlorite grains appear undeformed, indicating either (1) low strain deformation of these minerals or (2) a granoblastic texture following recrystallization. A representative sample from the intermediate zone (451608) demonstrates a 38% mass gain compared to the mudstone protolith (Fig. 8c). Similar to distal-altered mudstone, gains in Na₂O, Cr, Sr, Pb and U are noted in addition to significant enrichments in MgO, CaO, V, Sn and Ba. The 137% and 47% increases in MgO and SiO₂, respectively, are consistent with the chlorite and quartz alteration mineralogy.

The proximal quartz–sericite alteration is developed immediately north and south of the sulphide lenses (Fig. 5). Ubiquitous quartz and the disappearance of chlorite mark the transition from the intermediate to proximal alteration facies. Fine-grained quartz with interstitial sericite is pervasive throughout both micaceous and siltstone domains of the mudstone (Fig. 8d). Most quartz grains have irregular, embayed margins and undulose extinction, indicating extensive dissolution and precipitation, although elongate quartz grains defining a discrete foliation are observed locally (Fig. 8e). Based on mapping of the Haché showing, the pervasive quartz–sericite alteration corresponds to the altered mudstone block between the two ENE–WSW shear zones (Figs. 3 and 5). As such, the foliation defined by the quartz grains likely corresponds to the S₁ foliation, indicating quartz alteration predates Devonian deformation along the RBM shear zone. A typical altered sample from the proximal alteration zone (451730) demonstrates a 55% mass gain compared to the mudstone protolith. Element enrichments are similar to those for the intermediate alteration zone (Na₂O, MgO, CaO, V, Cr, Sr, Sn, Ba, Pb and U), in addition to 64% and 53% increases in SiO₂ and K₂O, respectively, and these are compatible with the quartz–sericite alteration mineralogy. A mineralized

sample from the proximal alteration zone (451703) (Table 3) demonstrates a mass gain of 255% relative to the mudstone protolith, and has a comparable geochemical signature to the first unmineralized sample (451730), with additional enrichments in Be, S, MnO, Fe₂O₃, Cu, Zn, Ga, As and Tl (Fig. 8f).

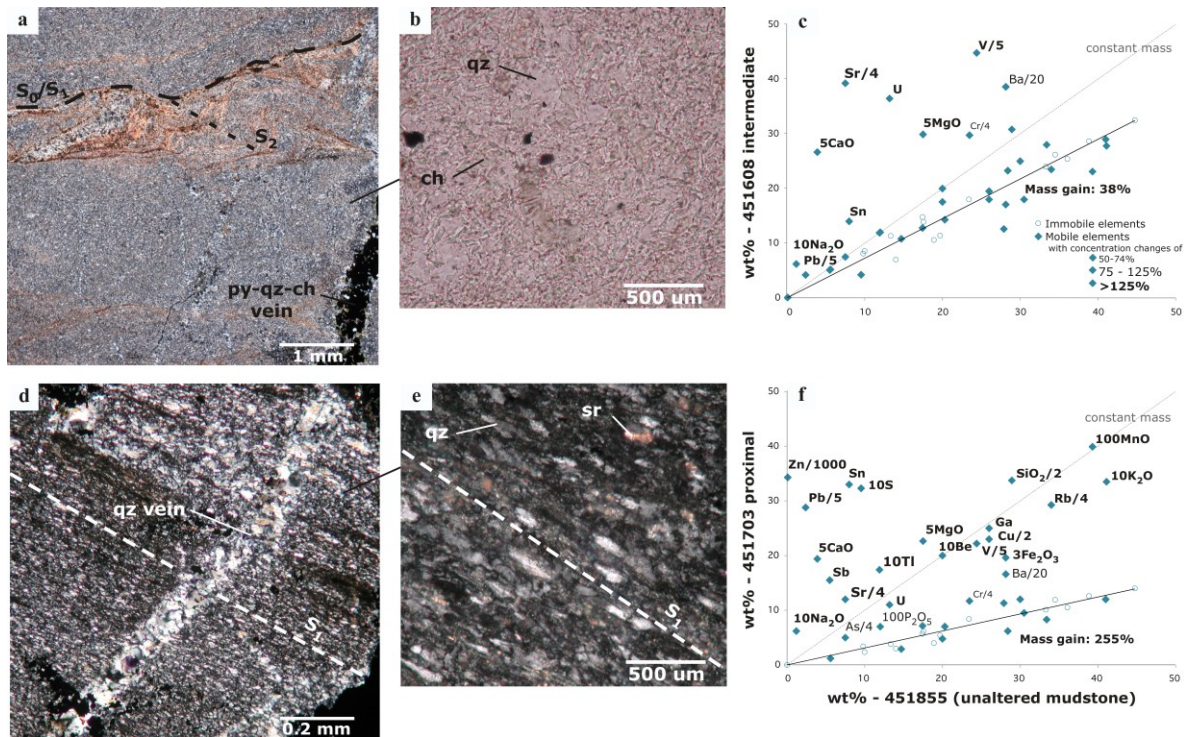


Figure 8. Photomicrographs (a, b, d, and e) and isocon mass balance plots (c and f) of altered mudstone. a) and b) Intermediate chlorite–quartz alteration in polarized (a) and plane (b) light. d) and e) Foliated proximal pervasive quartz–sericite alteration in polarized light. c) and f) Changes in mass and element concentrations (changes > 50% are labelled) for intermediate (c) and proximal (f) alteration.

Three phases of late alteration are documented at the Nicholas-Denys deposit (Fig. 9). Quartz (+/- chlorite, pyrite) veins cut the host Millstream Formation (Figs. 8a and 8d), as well as Simpsons Field Formation hornfels north of the RBM South Branch (Fig. 9a). Quartz (+/- chlorite, pyrite) veins are cut by epidote veins (Fig. 9b). Euhedral epidote crystals occur as (1) veins (+/- quartz, chlorite, calcite) which cut altered mudstone of the Millstream Formation in the proximal alteration zone (Fig. 9b) and hornfels of the Simpsons Field Formation north of the RBM South Branch, and as (2) replacement of altered mudstone in the intermediate and proximal alteration zones (Fig. 9c) as well as of siltstone laminae in the distal alteration zone. Finally, calcite (+/- quartz, pyrite) veins cut epidote (+/- quartz, chlorite, calcite) alteration (Fig. 9d). Calcite veins occasionally carry angular fragments of mudstone, indicating brecciation occurred as late as post-calcite alteration.

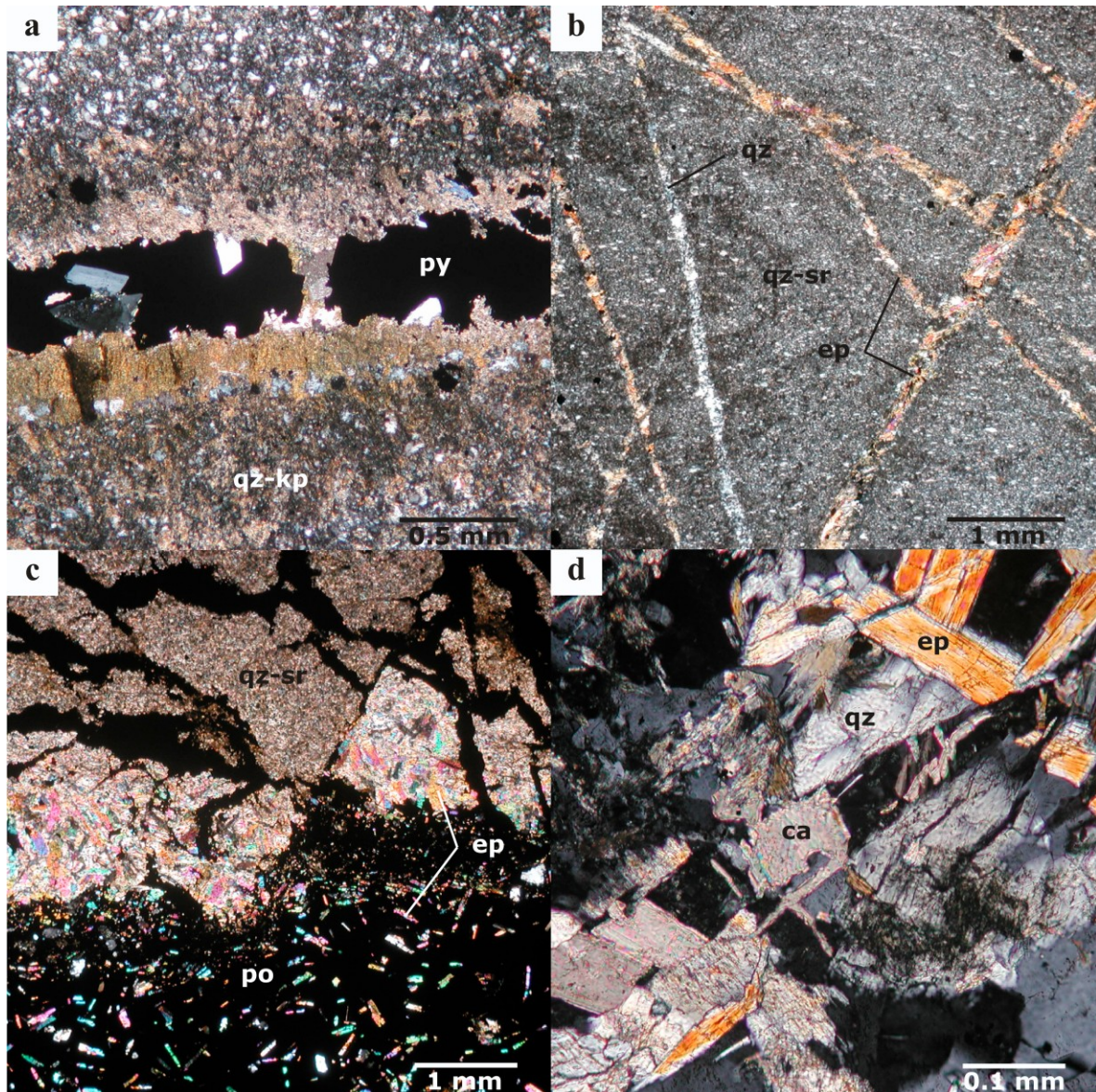


Figure 9. Photomicrographs of late alteration phases in polarized light. a) **Pyrite** (+/- **quartz**, **chlorite**) vein cutting hornfels of the Simpsons Field Formation. b) **Epidote** (+/- **chlorite**, **calcite**, **quartz**) vein cutting **quartz** (+/- **pyrite**, **chlorite**) vein and altered mudstone of the proximal zone. c) **Epidote** replacement of **quartz-sericite** altered mudstone of the proximal zone. d) **Calcite** (+/- **quartz**, **pyrite**) vein cutting **epidote** and **quartz** grains.

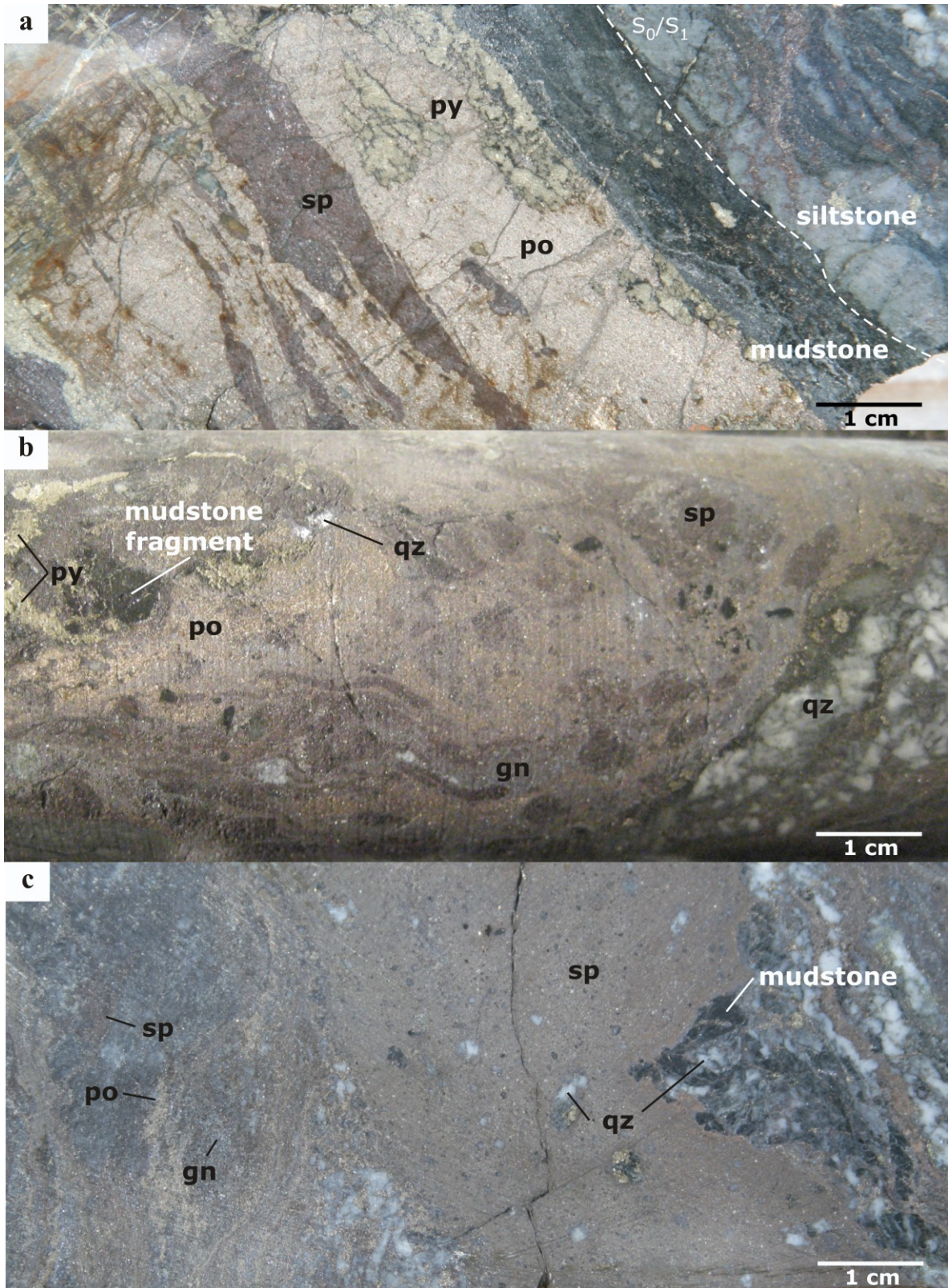
2.4.3 Mineralization

The deposit comprises four Pb–Zn–Ag showings (Henry, Haché, Shaft and Pine Tree; Fig. 2). Mineralization outcrops at the Haché, Shaft and Pine Tree showings as gossans, whereas mineralization at Henry does not crop out. The showings occur over a strike length of 5.4 km along an ENE–WSW orientation, parallel to the S_1 foliation in the RBM shear zone (Fig. 2). Detailed mapping of the Haché showing shows mineralization occurs as several sheared, boudinaged, ENE–WSW-striking, locally folded, and offset sulphide lenses (Fig. 3).

Subvertical, semi-massive to massive sulphide lenses are intersected by diamond drill holes to a depth of 450 m (Fig. 5). Sulphide lenses are 6 to 20 m thick and consist of multiple mineralized intervals 0.1 to 1 m-thick separated by intervals of quartz–sericite altered, weakly mineralized ($\leq 5\%$ disseminated sulphides) mudstone. Mineralized intercepts may represent multiple sulphide-rich intervals (Fig. 5) or intercepts of a single folded sulphide lens.

The sulphide lenses grade on average 1.43% Zn, 0.70% Pb, 95g/t Ag and 0.53g/t Au, with indicated and inferred resources of 0.8 Mt for the Haché showing (Turcotte and Pelletier 2008). Massive sulphides (70–100 vol%) consist of pyrrhotite, sphalerite and galena forming wispy, centimetre-scale, bands conformable to the S_1 foliation in the quartz–sericite-altered host mudstone (Fig. 10a). Breccias of semi-massive to massive sulphides (20–70 vol%) are the most common type of mineralization, and consist of angular fragments of quartz–sericite-altered mudstone, centimetre-scale coarse-grained quartz veins and millimetre-scale subrounded quartz grains in a matrix of fine-grained pyrrhotite–sphalerite–galena (Figs. 10b and 10c). Disseminated mineralization is characterized by interstitial aggregates of pyrrhotite–sphalerite–galena both above and below semi-massive and massive sulphide intervals (Fig. 10d). Veins of pyrrhotite–sphalerite–galena cut and infiltrate along the S_1 foliation in the mudstone in a few places (Fig. 10e). Locally, pyrrhotite–sphalerite–galena occurs as replacement of epidote-altered mudstone (Figs 9c and 10f), suggesting post-depositional sulphide remobilization took place. Arsenopyrite occurs throughout massive and semi-massive zones as individual euhedral crystals (Fig. 11c) or veinlets rimming pyrrhotite–sphalerite–galena massive sulphides. Pyrite occurs as foliated diagenetic pyrite grains interlayered within the S_1 foliation of the mudstone (Fig. 4a), and as coarse-grained aggregates replacing pyrrhotite (Figs. 10a and 10b).

Massive sulphides typically consist of fine-grained anhedral pyrrhotite with interstitial sphalerite which forms irregular, subrounded aggregates with embayed margins, although elongate sphalerite aggregates locally define a ductile foliation parallel to the S_1 foliation (Fig. 11a). In a few places, sphalerite occurs as the main sulphide phase, and hosts irregular, subrounded aggregates of pyrrhotite. Walker et al. (2006) reported rounded, irregular pyrite grains with embayed margins at the deformed Orvan Brook deposit in the California Lake Group of the BMC, and interpreted the texture to result from tectonic dissolution and reprecipitation of the sulphide. The polygonal annealed texture of pyrrhotite (Fig. 11b) suggests pyrrhotite recrystallization has taken place



This page and next page: Figure 10 — caption on p. 29

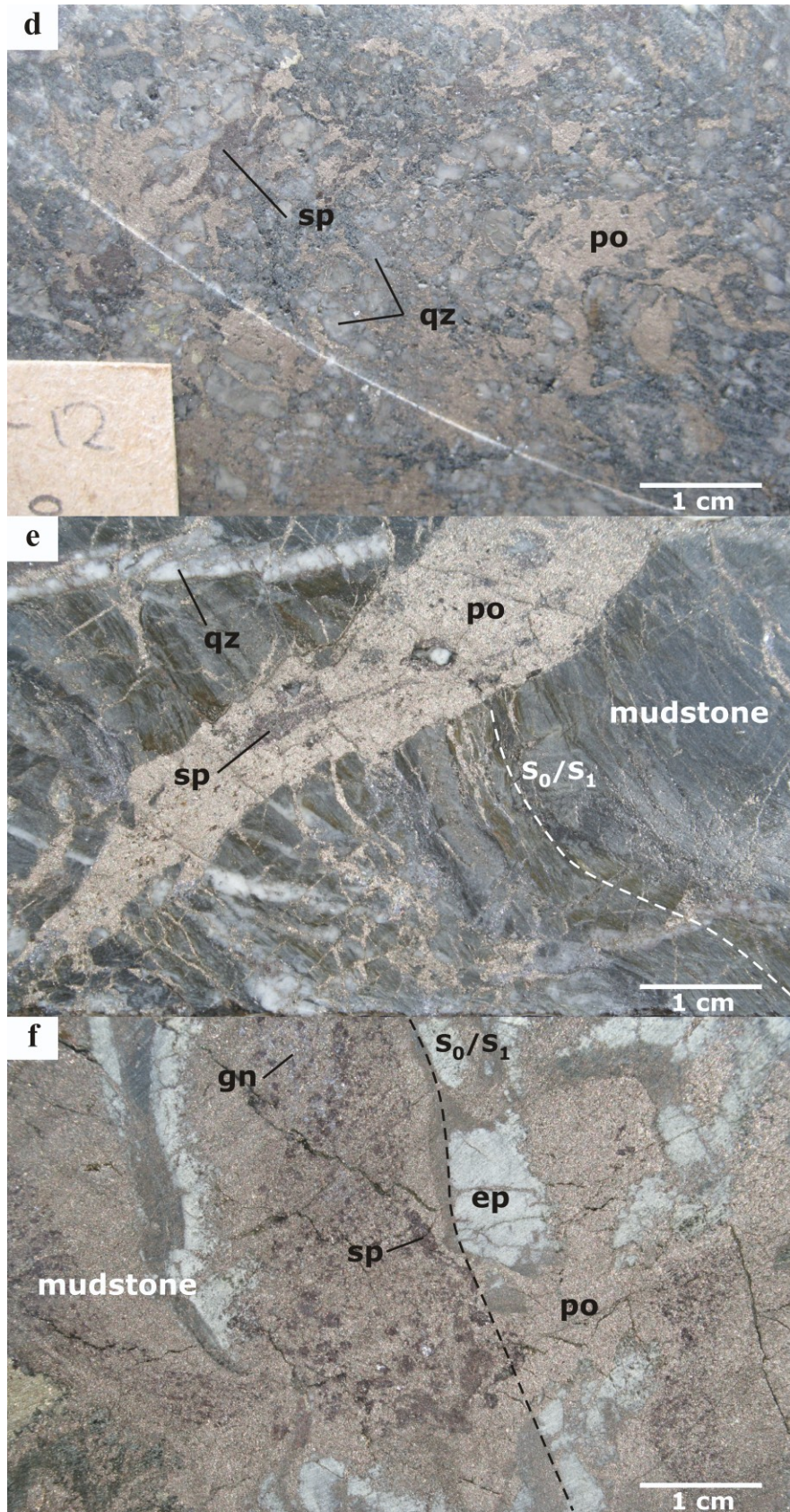


Figure 10 (previous two pages). Photographs of Nicholas-Denys sulphides in drill core. a) Massive banded **pyrrhotite–sphalerite** conformable to S_0/S_1 foliation in host mudstone. b) Wispy bands and irregular aggregates of fine-grained **pyrrhotite–sphalerite–galena** within brecciated, **quartz-altered** mudstone. Late irregular aggregates of **pyrite** replacing **pyrrhotite** in a and b). c) **Sphalerite** aggregate interspersed with subrounded **quartz** grains adjacent to disseminated **pyrrhotite–sphalerite–galena** in **quartz-altered** mudstone. d) Disseminated **pyrrhotite–sphalerite** in heavily **quartz-altered** mudstone. e) **Pyrrhotite–sphalerite** vein cutting and infiltrating S_0/S_1 foliation in host mudstone. f) **Pyrrhotite–sphalerite–galena** replacement of **epidote-altered** mudstone.

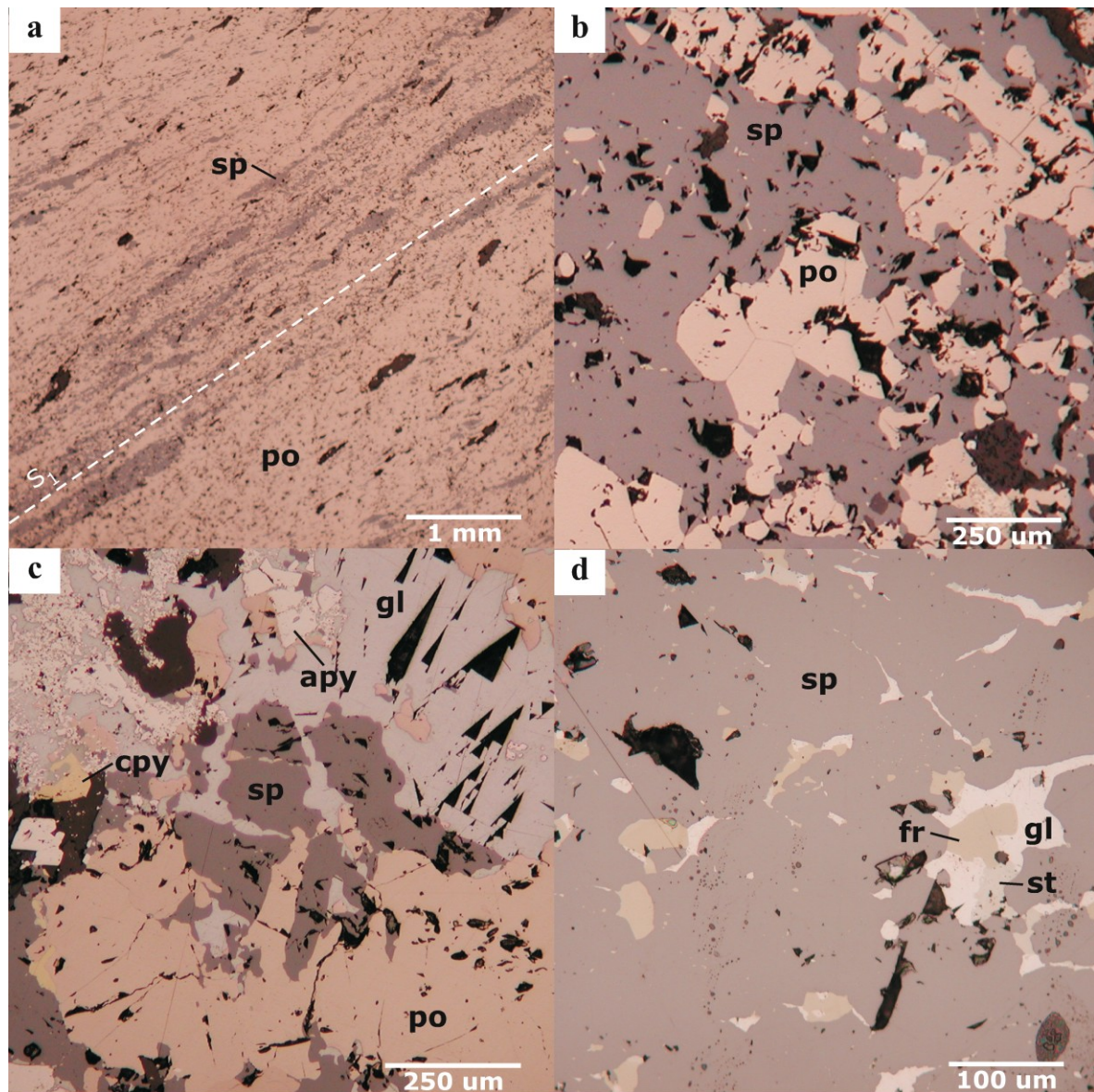


Figure 11. Photomicrographs of Nicholas-Denys sulphide textures in reflected light. a) Elongate **sphalerite** aggregates within massive anhedral **pyrrhotite** defining the S_1 ductile deformation fabric. b) Aggregates of polygonal **pyrrhotite** grains within massive anhedral **sphalerite**. c) **Pyrrhotite** and **sphalerite** forming irregular aggregates with embayed margins within coarse-grained, cubic **galena** with disseminated euhedral grains of **arsenopyrite** and subrounded fine-grained aggregates of **chalcopyrite**. d) **Galena–freibergite–stannite** inclusions in massive **sphalerite**.

locally. Coarse, cubic galena aggregates locally occur as the main sulphide phase (Fig. 11c), but more commonly occur with stannite and freibergite in interstices of massive pyrrhotite and sphalerite (Fig. 11d). Arsenopyrite occurs as fractured, euhedral grains (Fig. 11c). Traces of chalcopyrite occur as irregular aggregates within massive pyrrhotite–sphalerite–galena (Fig. 11c), more commonly at the boundaries between pyrrhotite and sphalerite or pyrrhotite and galena.

Electron microprobe analyses for thirteen samples of five Nicholas-Denys sulphides are presented in Table 4. Silver at Nicholas-Denys is largely hosted by freibergite $(\text{Ag}_{3.21}\text{Cu}_{6.77}\text{Fe}_{1.82}\text{Zn}_{0.20})(\text{Sb}_{3.98}\text{Sn}_{0.01}\text{As}_{0.01})\text{S}_{13}$ and galena with 0.026–0.479 wt% Ag. Almost all sulphide analyses report gold values below the lower detection limit of 0.01 wt%, with the exception of two galena analyses of 0.26 wt% Au and 0.06 wt% Au, suggesting gold distribution is non uniform among sulphide species, and may be principally bound in galena.

To summarize the paragenetic sequence for alteration and sulphide minerals at Nicholas Denys, the conformable relationship of banded sulphides to the ENE–WSW bedding-parallel S_1 foliation (Fig. 10a), in addition to the presence of foliated quartz grains in the proximal alteration zone (Figs. 8d and 8e), indicate that mineralization and hydrothermal alteration occurred prior to Devonian ENE–WSW RBM shearing (Fig. 12). Three generations of late alteration cut S_1 in the hydrothermally altered mudstone (Figs. 8a, 8d and 9): quartz (+/-chlorite, pyrite) veins are cut by epidote (+/-quartz, chlorite, calcite) veins, which in turn are cut by calcite (+/- quartz, pyrite) veins. The occurrence of pyrrhotite–sphalerite–galena as (1) veins cross-cutting the bedding-parallel S_1 foliation (Fig. 10e) and (2) replacement of epidote-altered mudstone beds (Fig. 10f) suggests sulphide remobilization occurred slightly after epidote alteration. Two types of breccias are observed: (1) epidote-altered mudstone breccia in a sulphide matrix (Fig. 9c) and (2) mudstone breccia in a calcite matrix. This suggests brecciation may have been contemporaneous with sulphide remobilization and calcite alteration, or post-dates calcite alteration.

Table 4. Electron microprobe analyses of sulphides.

Table 4.1 Major and trace elements in arsenopyrite.

| Sample No. | 6374-5 | 6373-1 | 6373-2 | 6055-4 | 6058-5 | 6053-1 | 6053-2 | 6040-4 | 6039-2 |
|------------|---------|---------|---------|---------|---------|---------|---------|---------|---------|
| Wt% | | | | | | | | | |
| Sb | 0.024 | 0.131 | 0.09 | 0.063 | 0.019 | 0.018 | 0.054 | 0.245 | 0.015 |
| Sn | BDL | BDL | BDL | BDL | BDL | 0.003 | 0.005 | BDL | BDL |
| Ag | BDL | BDL | BDL | BDL | BDL | BDL | 0.002 | BDL | 0.004 |
| Au | BDL |
| Pb | BDL | BDL | 0.037 | BDL | BDL | BDL | BDL | BDL | BDL |
| Fe | 35 | 35 | 35 | 35 | 35 | 35 | 35 | 35 | 35 |
| S | 22 | 22 | 22 | 22 | 22 | 22 | 22 | 22 | 22 |
| As | 43 | 43 | 43 | 43 | 43 | 43 | 43 | 43 | 43 |
| Total | 100.024 | 100.131 | 100.127 | 100.063 | 100.019 | 100.021 | 100.061 | 100.245 | 100.019 |
| At% | | | | | | | | | |
| Sb | 0.011 | 0.057 | 0.039 | 0.027 | 0.008 | 0.008 | 0.023 | 0.107 | 0.007 |
| Sn | BDL | BDL | BDL | BDL | BDL | 0.001 | 0.002 | BDL | BDL |
| Ag | BDL | BDL | BDL | BDL | BDL | BDL | 0.001 | BDL | 0.002 |
| Au | BDL |
| Pb | BDL | BDL | 0.009 | BDL | BDL | BDL | BDL | BDL | BDL |
| Fe | 33.211 | 33.196 | 33.199 | 33.206 | 33.212 | 33.212 | 33.206 | 33.179 | 33.212 |
| S | 36.364 | 36.347 | 36.35 | 36.358 | 36.365 | 36.365 | 36.359 | 36.329 | 36.365 |
| As | 30.414 | 30.4 | 30.403 | 30.409 | 30.415 | 30.415 | 30.409 | 30.385 | 30.415 |

Table 4.2 Major and trace elements in galena.

| Sample No. | 6370-4 | 6370-5 | 6374-1 | 6055-2 | 6059-1 | 6058-3 | 6053-4 | 6040-5 | 6039-5 | 6039-7 |
|------------|---------|---------|---------|--------|---------|---------|---------|---------|---------|---------|
| Wt% | | | | | | | | | | |
| Sb | 0.214 | 0.11 | 0.409 | 0.265 | 0.04 | 0.056 | 0.308 | 0.312 | 0.194 | 0.511 |
| Sn | 0.031 | 0.043 | 0.099 | 0.021 | 0.047 | 0.012 | 0.051 | 0.036 | 0.047 | 0.035 |
| Ag | 0.162 | 0.083 | 0.337 | 0.213 | 0.321 | 0.026 | 0.24 | 0.234 | 0.142 | 0.479 |
| Bi | BDL | BDL | BDL | BDL | BDL | BDL | BDL | BDL | BDL | BDL |
| As | BDL | BDL | 0.011 | 0.001 | BDL | 0.001 | 0.005 | BDL | 0.006 | BDL |
| Pb | 86.6 | 86.6 | 86.6 | 86.6 | 86.6 | 86.6 | 86.6 | 86.6 | 86.6 | 86.6 |
| S | 13.4 | 13.4 | 13.4 | 13.4 | 13.4 | 13.4 | 13.4 | 13.4 | 13.4 | 13.4 |
| Total | 100.407 | 100.236 | 100.856 | 100.5 | 100.408 | 100.095 | 100.604 | 100.582 | 100.389 | 101.025 |
| At% | | | | | | | | | | |
| Sb | 0.209 | 0.108 | 0.398 | 0.259 | 0.039 | 0.055 | 0.301 | 0.305 | 0.19 | 0.497 |
| Sn | 0.031 | 0.043 | 0.098 | 0.021 | 0.047 | 0.012 | 0.051 | 0.036 | 0.047 | 0.035 |
| Ag | 0.179 | 0.092 | 0.37 | 0.235 | 0.354 | 0.029 | 0.265 | 0.258 | 0.157 | 0.525 |
| Bi | BDL | BDL | BDL | BDL | BDL | BDL | BDL | BDL | BDL | BDL |
| As | BDL | BDL | 0.017 | 0.002 | BDL | 0.002 | 0.009 | BDL | 0.01 | BDL |
| Pb | 49.79 | 49.878 | 49.557 | 49.741 | 49.779 | 49.95 | 49.687 | 49.7 | 49.798 | 49.471 |
| S | 49.791 | 49.879 | 49.558 | 49.742 | 49.78 | 49.952 | 49.688 | 49.702 | 49.799 | 49.472 |

Table 4.3 Major and trace elements in pyrrhotite.

| Sample No. | 6370-2 | 6370-3 | 6049-1 | 6055-1 | 6059-3 | 6058-2 | 6058-4 | 6053-5 | 6040-1 |
|------------|---------|--------|---------|--------|--------|---------|---------|---------|---------|
| Wt% | | | | | | | | | |
| Sb | BDL | BDL | 0.018 | 0.099 | 0.582 | BDL | BDL | 0.652 | 0.002 |
| Sn | BDL | BDL | BDL | 0.004 | 0.007 | BDL | BDL | 0.003 | BDL |
| Ag | BDL | BDL | 0.001 | 0.016 | 0.127 | BDL | 0.005 | 0.103 | BDL |
| Au | BDL | BDL | BDL | BDL | BDL | BDL | BDL | BDL | BDL |
| As | BDL | 0.007 | 0.006 | 0.01 | 0.004 | 0.013 | BDL | 0.011 | 0.004 |
| Ni | 0.034 | 0.013 | 0.004 | 0.011 | BDL | BDL | 0.007 | 0.015 | BDL |
| Fe | 65.5 | 65.5 | 65.5 | 65.5 | 65.5 | 65.5 | 65.5 | 65.5 | 65.5 |
| S | 34.5 | 34.5 | 34.5 | 34.5 | 34.5 | 34.5 | 34.5 | 34.5 | 34.5 |
| Total | 100.034 | 100.02 | 100.029 | 100.14 | 100.72 | 100.013 | 100.012 | 100.784 | 100.006 |
| At% | | | | | | | | | |
| Sb | BDL | BDL | 0.007 | 0.036 | 0.212 | BDL | BDL | 0.238 | 0.001 |
| Sn | BDL | BDL | BDL | 0.002 | 0.003 | BDL | BDL | 0.001 | BDL |
| Ag | BDL | BDL | BDL | 0.006 | 0.052 | BDL | 0.002 | 0.042 | BDL |
| Au | BDL | BDL | BDL | BDL | BDL | BDL | BDL | BDL | BDL |
| As | BDL | 0.004 | 0.003 | 0.006 | 0.002 | 0.008 | BDL | 0.006 | 0.002 |
| Ni | 0.026 | 0.01 | 0.003 | 0.009 | BDL | BDL | 0.006 | 0.011 | BDL |
| Fe | 52.137 | 52.144 | 52.144 | 52.12 | 52.011 | 52.147 | 52.147 | 51.995 | 52.149 |
| S | 47.837 | 47.843 | 47.843 | 47.821 | 47.721 | 47.845 | 47.846 | 47.706 | 47.848 |

Table 4.3 continued

| Sample No. | 6040-3 | 6039-1 | 6039-4 |
|------------|---------|---------|---------|
| Wt% | | | |
| Sb | BDL | BDL | BDL |
| Sn | BDL | 0.017 | BDL |
| Ag | BDL | BDL | BDL |
| Au | BDL | BDL | BDL |
| As | 0.002 | BDL | 0.005 |
| Ni | BDL | 0.012 | BDL |
| Fe | 65.5 | 65.5 | 65.5 |
| S | 34.5 | 34.5 | 34.5 |
| Total | 100.002 | 100.029 | 100.005 |
| At% | | | |
| Sb | BDL | BDL | BDL |
| Sn | BDL | 0.006 | BDL |
| Ag | BDL | BDL | BDL |
| Au | BDL | BDL | BDL |
| As | 0.001 | BDL | 0.003 |
| Ni | BDL | 0.009 | BDL |
| Fe | 52.15 | 52.143 | 52.149 |
| S | 47.849 | 47.842 | 47.848 |

Table 4.4 Major and trace elements in sphalerite.

| Sample No. | 6370-1 | 6374-2 | 6373-3 | 6373-4 | 6049-2 | 6047-1 | 6043-1 | 6055-3 | 6059-2 |
|------------|--------|--------|--------|--------|--------|--------|--------|--------|--------|
| Wt% | | | | | | | | | |
| Sn | BDL | 0.002 | BDL | BDL | 0.002 | 0.001 | 0.002 | 0.058 | BDL |
| Ag | BDL | BDL | 0.007 | BDL | BDL | BDL | BDL | 0.079 | 0.025 |
| Pb | BDL | 0.056 | BDL |
| As | 0.005 | BDL | 0.010 | 0.018 | 0.008 | BDL | BDL | BDL | 0.003 |
| Fe | 13.3 | 13.3 | 13.3 | 13.3 | 13.3 | 13.3 | 13.3 | 13.3 | 13.3 |
| S | 30.3 | 30.3 | 30.3 | 30.3 | 30.3 | 30.3 | 30.3 | 30.3 | 30.3 |
| Zn | 54.2 | 54.2 | 54.2 | 54.2 | 54.2 | 54.2 | 54.2 | 54.2 | 54.2 |
| Mn | 1.9 | 1.9 | 1.9 | 1.9 | 1.9 | 1.9 | 1.9 | 1.9 | 1.9 |
| Total | 99.705 | 99.702 | 99.717 | 99.718 | 99.710 | 99.701 | 99.702 | 99.893 | 99.728 |
| At% | | | | | | | | | |
| Sn | BDL | 0.001 | BDL | BDL | 0.001 | BDL | 0.001 | 0.024 | BDL |
| Ag | BDL | BDL | 0.003 | BDL | BDL | BDL | BDL | 0.036 | 0.011 |
| Pb | BDL | 0.013 | BDL |
| As | 0.003 | BDL | 0.007 | 0.012 | 0.005 | BDL | BDL | BDL | 0.002 |
| Fe | 11.635 | 11.635 | 11.634 | 11.634 | 11.634 | 11.635 | 11.635 | 11.627 | 11.634 |
| S | 46.172 | 46.174 | 46.169 | 46.168 | 46.171 | 46.174 | 46.173 | 46.140 | 46.168 |
| Zn | 40.500 | 40.501 | 40.498 | 40.497 | 40.499 | 40.501 | 40.501 | 40.472 | 40.496 |
| Mn | 1.69 | 1.69 | 1.69 | 1.69 | 1.69 | 1.69 | 1.69 | 1.69 | 1.69 |

Table 4.4 continued

| Sample No. | 6058-1 | 6053-3 | 6040-2 | 6040-7 | 6039-3 |
|------------|--------|--------|--------|--------|--------|
| Wt% | | | | | |
| Sn | BDL | BDL | BDL | 0.001 | 0.007 |
| Ag | BDL | 0.006 | BDL | BDL | BDL |
| Pb | BDL | BDL | BDL | BDL | BDL |
| As | 0.003 | BDL | BDL | 0.012 | BDL |
| Fe | 13.3 | 13.3 | 13.3 | 13.3 | 13.3 |
| S | 30.3 | 30.3 | 30.3 | 30.3 | 30.3 |
| Zn | 54.2 | 54.2 | 54.2 | 54.2 | 54.2 |
| Mn | 1.9 | 1.9 | 1.9 | 1.9 | 1.9 |
| Total | 99.703 | 99.706 | 99.700 | 99.713 | 99.707 |
| At% | | | | | |
| Sn | BDL | BDL | BDL | BDL | 0.003 |
| Ag | BDL | 0.003 | BDL | BDL | BDL |
| Pb | BDL | BDL | BDL | BDL | BDL |
| As | 0.002 | BDL | BDL | 0.008 | BDL |
| Fe | 11.635 | 11.635 | 11.635 | 11.634 | 11.635 |
| S | 46.173 | 46.172 | 46.174 | 46.170 | 46.172 |
| Zn | 40.501 | 40.500 | 40.501 | 40.498 | 40.500 |
| Mn | 1.69 | 1.69 | 1.69 | 1.69 | 1.69 |

Table 4.5 Major and trace elements in freibergite.

| <i>Sample No.</i> | 6040-6 | 6039-6 | 6374-3 |
|-------------------|--------|--------|--------|
| Wt% | | | |
| S | 22.508 | 22.707 | 22.492 |
| Pb | BDL | BDL | BDL |
| Ag | 19.163 | 18.391 | 18.620 |
| Sn | 0.074 | 0.063 | 0.140 |
| Sb | 26.176 | 26.331 | 26.167 |
| Co | 0.016 | BDL | 0.001 |
| Ni | BDL | BDL | 0.002 |
| Au | BDL | BDL | BDL |
| Fe | 5.780 | 5.499 | 5.257 |
| Cu | 22.929 | 23.944 | 23.005 |
| Zn | 0.864 | 1.032 | 1.109 |
| As | 0.058 | 0.092 | BDL |
| Total | 97.568 | 98.059 | 96.793 |
| At% | | | |
| S | 44.603 | 44.603 | 44.870 |
| Pb | BDL | BDL | BDL |
| Ag | 11.288 | 10.739 | 11.042 |
| Sn | 0.040 | 0.033 | 0.075 |
| Sb | 13.661 | 13.621 | 13.747 |
| Co | 0.017 | BDL | 0.001 |
| Ni | BDL | BDL | 0.002 |
| Au | BDL | BDL | BDL |
| Fe | 6.576 | 6.202 | 6.021 |
| Cu | 22.927 | 23.731 | 23.157 |
| Zn | 0.840 | 0.994 | 1.085 |
| As | 0.049 | 0.077 | BDL |

Table 4.6 Major and trace elements in stannite.

| Sample No. | 6374-4 |
|------------|--------|
| Wt% | |
| S | 29.339 |
| Pb | BDL |
| Ag | 0.084 |
| Sn | 25.525 |
| Sb | 0.066 |
| Co | BDL |
| Ni | BDL |
| Au | BDL |
| Fe | 11.413 |
| Cu | 29.073 |
| Zn | 2.791 |
| As | 0.025 |
| Total | 98.316 |
| At% | |
| S | 49.830 |
| Pb | BDL |
| Ag | 0.042 |
| Sn | 11.710 |
| Sb | 0.029 |
| Co | BDL |
| Ni | BDL |
| Au | BDL |
| Fe | 11.129 |
| Cu | 24.915 |
| Zn | 2.325 |
| As | 0.018 |

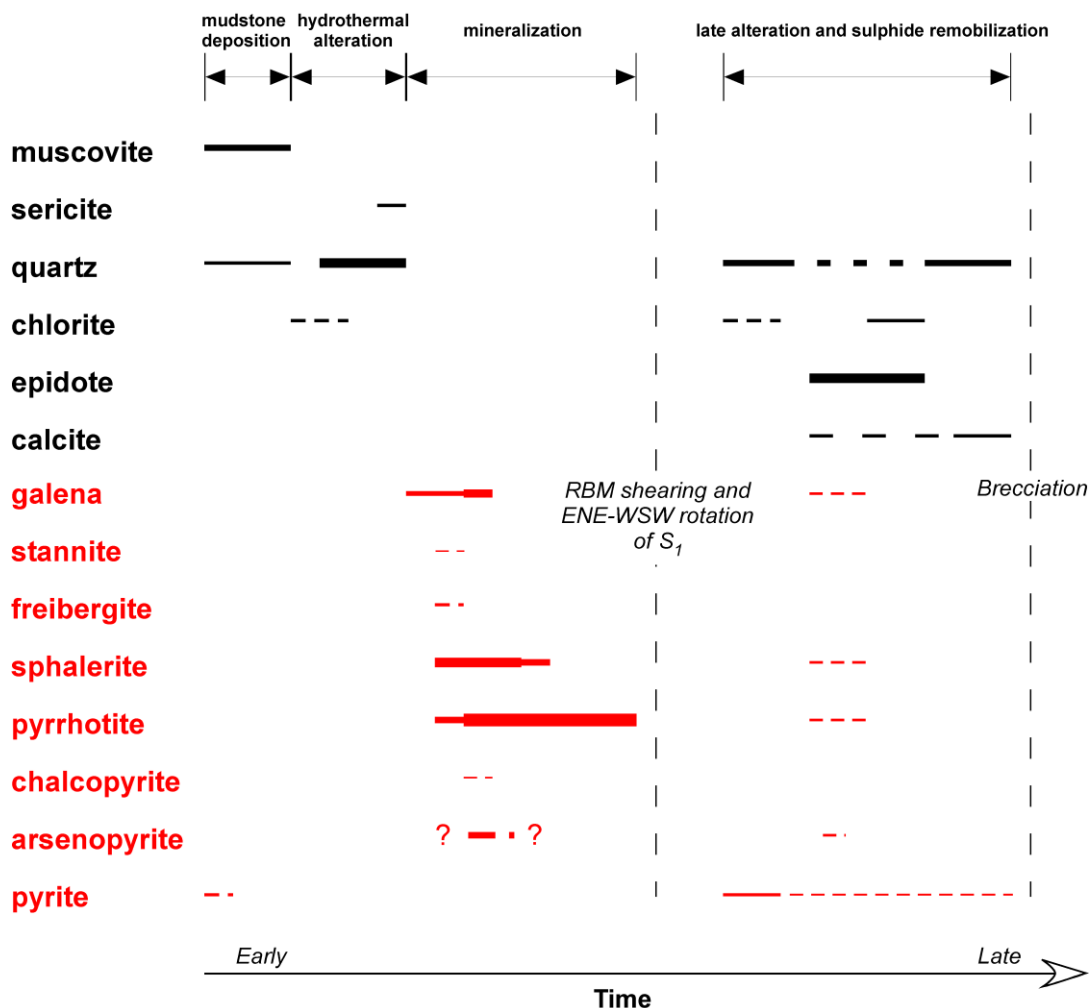


Figure 12. Paragenetic sequence for the Nicholas-Denys deposit.

2.4.4 Sulphur isotopes

The sulphur isotope composition of 62 mineral separates of pyrrhotite, sphalerite, galena, pyrite and arsenopyrite from Nicholas-Denys massive sulphides was measured (Table 5). $\delta^{34}\text{S}$ values of Nicholas-Denys sulphides have a narrow range (+0.9 to +4.8‰), with a mean value of +2.9‰ \pm 0.7‰. Differences between $\delta^{34}\text{S}_{\text{sphalerite}}$ and $\delta^{34}\text{S}_{\text{galena}}$ and between $\delta^{34}\text{S}_{\text{pyrrhotite}}$ and $\delta^{34}\text{S}_{\text{galena}}$ using the fractionation of Li and Liu (2006) yield one temperature estimate of 320°C, three estimates between 550°C and 675°C and one estimate of 943°C (Table 5). The scattered and geologically unreasonable temperature estimates (> 550°C) suggest isotopic disequilibrium prevailed for the Nicholas-Denys pyrrhotite–sphalerite–galena sulphide assemblage (Ohmoto and Goldhaber 1997). At isotopic disequilibrium, $\delta^{34}\text{S}_{\text{sphalerite}} \approx \delta^{34}\text{S}_{\text{galena}} \approx \delta^{34}\text{S}_{\text{H}_2\text{S}}$ (Ohmoto 1986), and the inferred $\delta^{34}\text{S}_{\text{H}_2\text{S}}$ for Nicholas-Denys would be about +2.8‰.

Table 5. Sulphur isotope compositions and temperature estimates for sulphides of the Fournier and Chaleurs groups.

| | Sample No. | $\delta^{34}\text{S}$ (‰) _{CDT} | | | | | T(°C) _{sp-ga} | T(°C) _{po-ga} |
|-------------------|------------|--|----------|------|------|------|------------------------|------------------------|
| | | Po | Sp | Gn | Apy | Py | | |
| Belledune mélange | 461657 | | | | | 25.3 | | |
| Turgeon | 451756 | | | | | 7.0 | | |
| | 451756 | | | | | 6.9 | | |
| Nicholas-Denys | 451708 | 3.2 | | 1.9 | | | | 554 |
| | 451676 | 3.1 | 2.7 | | | | | |
| | 451616 | 2.7 | | | | 2.4 | | |
| | 451630 | 3.6 | 1.4 | | 3.9 | | | |
| | 451625 | 3.1 | 3.1 | 2.1 | 3.5 | 3.2 | 587 | 670 |
| | 451622 | 3.9 | | | | 3.5 | | |
| | 451663 | 3.5 | 3.8 | | 3.6 | 3.4 | | |
| | 451665 | 3.2 | 3.1; 2.8 | | | 2.7 | | |
| | 451641 | 2.8 | | | | | | |
| | 451674 | 2.7 | 2.8 | | 3.1 | | | |
| | 451731 | | 1.8 | | | 2.9 | | |
| | 451675 | | 3.2 | | | 2.7 | | |
| | 451679 | | 4.3 | 2.2 | | 4.8 | 320 | |
| | 451613 | | 3.2 | | | 2.8 | | |
| | 451619 | | 2.3 | | | | | |
| | 451632 | | 3.1 | | | 3.1 | | |
| | 451732 | | 1.7 | 3.6 | 3.1 | | invalid | |
| | 451685 | | 3.4 | | | 0.9 | | |
| | 451644 | | 2.4 | | 2.7 | 2.3 | | |
| | 451648 | | 3.1 | 2.6 | | 3.3 | 943 | |
| | 451703 | | 1.3 | | | 2.0 | | |
| | 451856 | | 3.6 | 3.5 | | 3.4 | > 2 000°C | |
| | 451601 | | | | | 3.6 | | |
| | 451717 | | | 1.2 | | | | |
| | 451724 | 2.5 | | | | 2.3 | | |
| | 451727 | 2.8 | | | | | | |
| | 451753 | | 2.5 | | | 0.9 | | |
| Nigadoo | 451755 | | 2.0 | | 1.4 | | | |
| Cullinan | 451658 | | 2.1 | -3.2 | -0.8 | 0.1 | | |

The sulphur isotope composition of Nicholas-Denys sulphides is different from that of siliciclastic-felsic VMS deposits hosted by the Tetagouche Group of the BMC, which have $\delta^{34}\text{S}$ values ranging from +10 to +20‰, (Fig.13; Tupper 1960; Goodfellow and Peter 1996; Walker et al. 2006). The sulphur isotope composition for siliciclastic-felsic VMS deposits hosted by the California Lake Group is intermediate between Tetagouche Group VMS deposits and the Nicholas-Denys deposit, ranging from +3 to +11‰ (Tupper 1960; Walker et al. 2006). The sulphur isotope composition of

the mafic rock-hosted VMS Turgeon deposit in the Fournier Group is $\sim +7\text{‰}$ (Table 5). The Nigadoo and Cullinan veins hosted by Silurian rocks of the Chaleurs Group and Devonian Nigadoo intrusive have $\delta^{34}\text{S}$ values ranging from -3 to $+2\text{‰}$ (Table 5), lower than those of the Nicholas-Denys deposit.

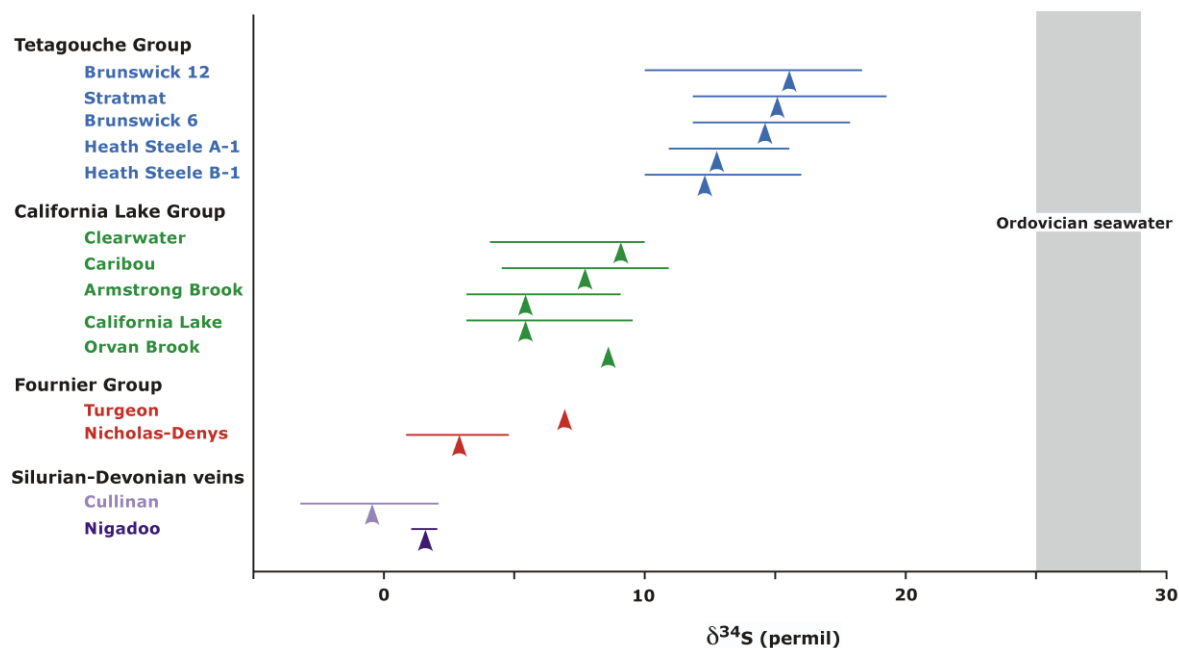


Figure 13. Bar plots of sulphur isotope compositions for sulphides from siliciclastic-felsic VMS deposits of the Tetagouche and California Lake Groups (Tupper 1960; Goodfellow and Peter 1996; Walker et al. 2006), from the Turgeon mafic rock-hosted VMS and Nicholas-Denys deposits of the Fournier Group, and for the Silurian-Devonian rock-hosted polymetallic Cullinan and Nigadoo veins. Range of sulphur isotope composition for Ordovician seawater sulphates (grey rectangle) based on diagenetic pyrite from the Belledune mélange of the Fournier Group and barite from the BMC (Goodfellow and Peter 1996), and on estimated global evaporite composition (Claypool et al. 1980). Line extremities indicate maximum and minimum values and arrow indicates mean value.

2.4.5 Lead isotopes

The lead isotope data for nine galena samples from the Nicholas-Denys deposit yield homogeneous values for $^{206}\text{Pb}/^{204}\text{Pb}$ (18.10–18.16), $^{207}\text{Pb}/^{204}\text{Pb}$ (15.54–15.59) and $^{208}\text{Pb}/^{204}\text{Pb}$ (38.00–38.11) (Table 6). The Nicholas-Denys galena lead isotope ratios plot between the Orogene and Mantle lead evolution curves (Zartman and Doe 1981), forming a linear array with a slope of 0.31 (Fig. 14). The lead isotope composition of Nicholas-Denys galena is less radiogenic than that of (1) BMC siliciclastic-felsic VMS deposits of the Middle Tetagouche Group, (2) the mafic-volcanic Turgeon VMS deposit of the Middle Ordovician Fournier Group and (3) the Cullinan and Nigadoo veins in

Silurian rocks of the Chaleurs Group and the Devonian Nigadoo porphyry (McCutcheon et al. 1993; R. Thorpe, personal communication to G. Beaudoin).

Table 6. Lead isotope ratios for galenas of the Fournier and Chaleurs groups.

| | Sample no. | $^{206}\text{Pb}/^{204}\text{Pb}$ | $^{207}\text{Pb}/^{204}\text{Pb}$ | $^{208}\text{Pb}/^{204}\text{Pb}$ |
|----------------|------------|-----------------------------------|-----------------------------------|-----------------------------------|
| Nicholas-Denys | 451625 | 18.11 | 15.55 | 38.05 |
| | 451856 | 18.10 | 15.57 | 38.08 |
| | 451679 | 18.10 | 15.57 | 38.10 |
| | 451632 | 18.12 | 15.58 | 38.11 |
| | 451708 | 18.11 | 15.56 | 38.05 |
| | 451749 | 18.10 | 15.54 | 38.00 |
| | 451732 | 18.12 | 15.57 | 38.10 |
| | 451630 | 18.12 | 15.57 | 38.08 |
| | 451648 | 18.11 | 15.56 | 38.09 |
| | 189274 | 18.11 | 15.56 | 38.07 |
| | 183975 | 18.10 | 15.56 | 38.09 |
| | 190397 | 18.11 | 15.57 | 38.13 |
| | 189284 | 18.11 | 15.57 | 38.08 |
| | 135487 | 18.06 | 15.55 | 38.08 |
| Nigadoo | 451751 | 18.16 | 15.59 | 38.06 |
| | 1 | 18.14 | 15.56 | 38.01 |
| | 2 | 18.14 | 15.56 | 38.01 |
| Cullinan | 451658 | 18.16 | 15.59 | 38.12 |

2.5 Discussion

Determination of the timing of mineralization at Nicholas-Denys is hindered by deformation affecting the deposit. Most VMS deposits of the BMC have experienced deformation related to Silurian subduction and collision (van Staal et al. 2003), demonstrating that mineralization predates closure of the backarc basin. Moreover, preservation of bedded sulphide textures at most VMS deposits of the BMC indicates their syngenetic nature (Goodfellow and McCutcheon 2003). Nicholas-Denys sulphide lenses and alteration zones are conformable relative to bedding (Fig. 5), but no bedded sulphides are preserved. The proximity of the Nicholas-Denys deposit to the RBM shear zone (Figs. 1 and 2) has resulted in substantial late Devonian shearing of sulphides (Figs. 3, 10a and 11a) that has obliterated primary geological features of the deposit. Macroscopic features of the Nicholas-Denys deposit, such as clockwise rotation of the S_1 foliation to an ENE–WSW orientation and the ENE–WSW orientation of sulphide lenses (Figs. 2 and 3), are consistent with ENE–WSW RBM deformation, and constrain the timing of mineralization at Nicholas-Denys to pre-Devonian deformation during the Acadian orogeny.

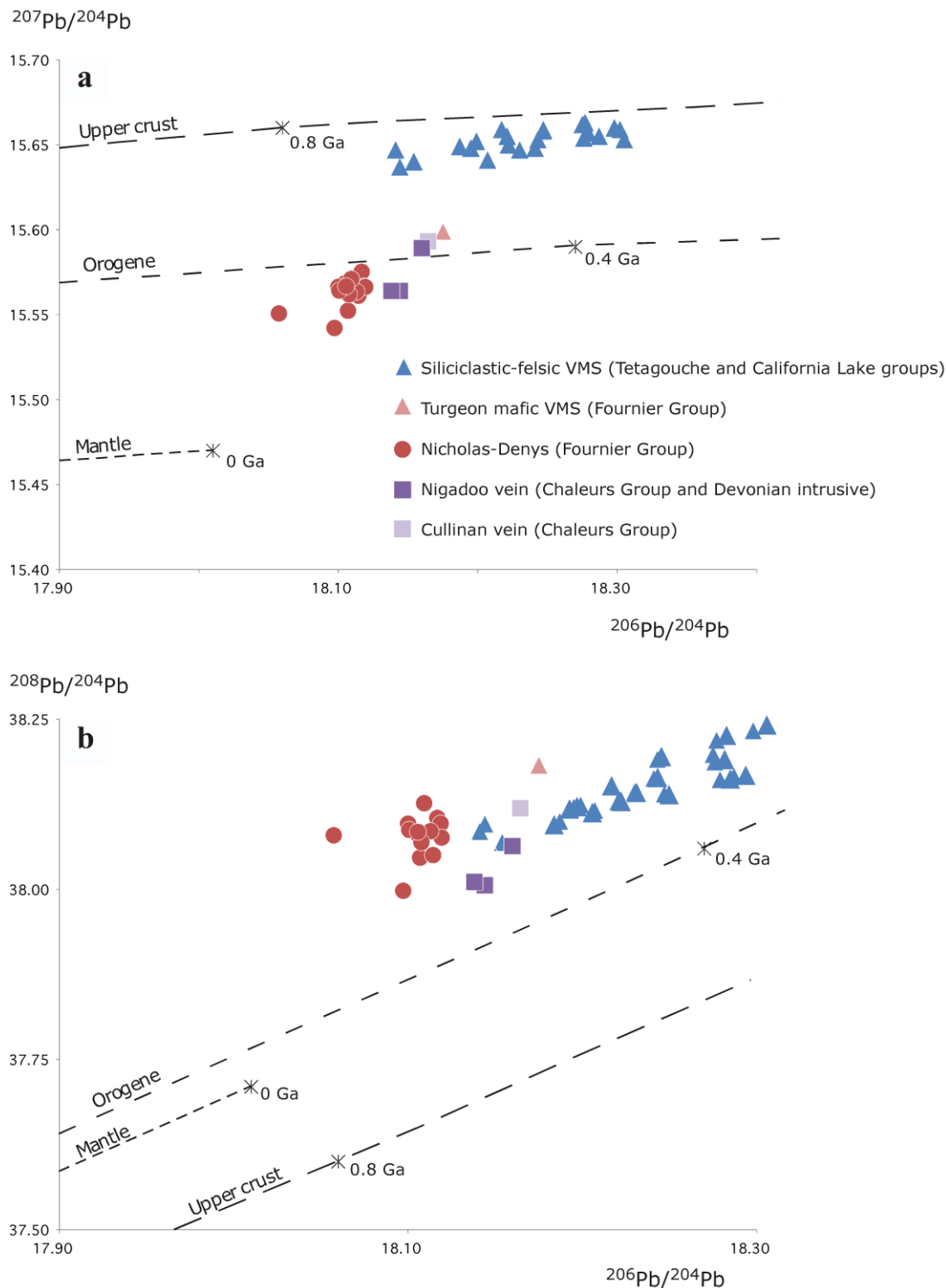


Figure 14. Lead isotope ratio plots for the siliciclastic-felsic VMS deposits of the Tetagouche and California Lake Groups, for the Turgeon mafic rock-hosted VMS (McCutcheon et al. 1993; R. Thorpe, personal communication to G. Beaudoin) and Nicholas-Denys deposits of the Fournier Group and for Silurian-Devonian rock-hosted polymetallic Nigadoo and Cullinan veins. a) $^{207}\text{Pb}/^{204}\text{Pb}$ vs $^{206}\text{Pb}/^{204}\text{Pb}$ diagram. b) $^{208}\text{Pb}/^{204}\text{Pb}$ vs $^{206}\text{Pb}/^{204}\text{Pb}$ diagram. Lead evolution curves for the Upper Crust, Orogene and Mantle reservoirs from Zartman and Doe (1981).

2.5.1 Provenance of sediments

Unaltered Millstream Formation sandstone and mudstone samples from the Nicholas-Denys deposit were plotted in the tectonic setting discrimination diagrams of Bhatia and Crook (1986), which use elements thought to remain immobile during hydrothermal alteration. Based on Ti/Zr and La/Sc ratios, Millstream Formation sandstone samples plot in the active continental margin field whereas the higher Ti/Zr ratios in mudstone samples places them near the oceanic island arc field (Fig. 15).

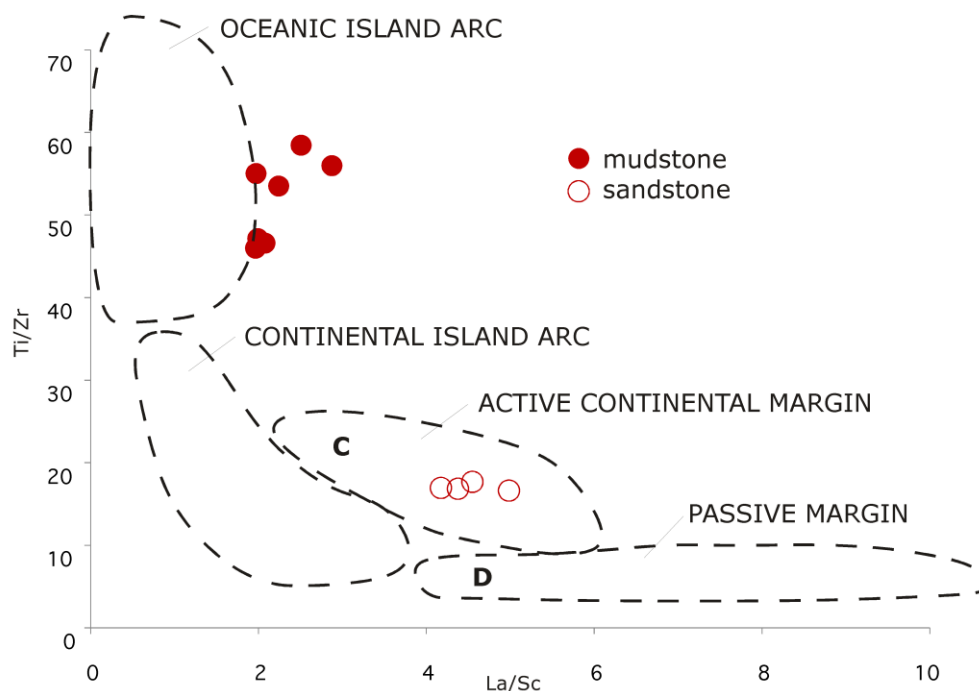


Figure 15. Sedimentary rock tectonic setting discriminant plot for unaltered Millstream Formation samples from the Nicholas-Denys deposit. Fields are from Bhatia and Crook (1986).

The Zr/TiO₂ versus Ni diagram is useful for differentiating between sedimentary rocks derived from igneous and sedimentary sources, with Ni content indicating the degree of fractionation of the igneous source (Rogers et al. 2003). Mudstone samples straddle the boundary between the sedimentary and igneous fields, suggesting mixing of sedimentary rock detrital material with a relatively mafic (high Ni content) igneous sediment source, whereas lower Ni values and higher Zr/TiO₂ ratio in sandstone samples suggest a dominantly sedimentary rock source (Fig. 16a). This is consistent with the Cr/Nb versus Ni/Nb diagram, in which values for mudstone and sandstone samples suggest mixing between intermediate island arc and typical N-MORB signatures, with a more pronounced N-MORB affinity for mudstone samples (Fig. 16b).

The binary distribution of mudstone and sandstone samples in diagrams of Figures 15 and 16 indicates two different sediment sources. The sharp primary contact between the sandstone bed and adjacent mudstone in drill core (Fig. 4c) suggests an abrupt change in sedimentation regime. Load casts in mudstone suggest rapid burial of muds by sand, before mudstone dewatering and compaction took place (Boggs 2001). The inferred continental margin tectonic setting from Figure 15, geochemical similarity with samples of the Miramichi Group in sediment provenance diagrams (Fig. 16), textural immaturity (Fig. 6b) and abrupt change in sedimentation suggest that the Nicholas-Denys sandstone unit is a gravity-driven deposit triggered by a slope instability along the Ganderian continental margin, or a fault-scarp derived turbiditic deposit from a nearby uplifted basement block.

Litho-geochemical compositions of Nicholas-Denys mudstone samples suggest a combination of sedimentary- and igneous-derived material. The Ganderian continental margin and remnant volcanic arc are considered regional sediment sources for the BMC (Rogers et al. 2003), and would have contributed sedimentary and igneous detritus during sedimentation of mudstone at Nicholas-Denys. The mafic igneous sediment source suggested by high Ni content in Nicholas-Denys mudstone samples is consistent with the interpretation that the Fournier Group is a remnant fragment of oceanic crust which provided a locally-derived igneous sediment source for the Millstream Formation mudstone. However, Rogers et al. (2003) noted that deep oceanic mafic volcanism associated with formation of an oceanic crust would not likely provide considerable detritus for sedimentation. van Staal et al. (2003) proposed that the obducted and eroded ophiolitic basement of an older, uplifted volcanic arc was a regional source of igneous mafic sediments, a source of sediments compatible with the oceanic island arc field characterizing Nicholas-Denys mudstone samples in Figure 15. The multiple sediment sources proposed for the Millstream Formation (remnant volcanic arc, Ganderian continental margin and obducted ophiolite) are consistent with the intermediate character of Nicholas-Denys mudstone and sandstone samples in Figure 16b, plotting between sediments derived from island arcs and sediments derived from midocean ridge basalts.

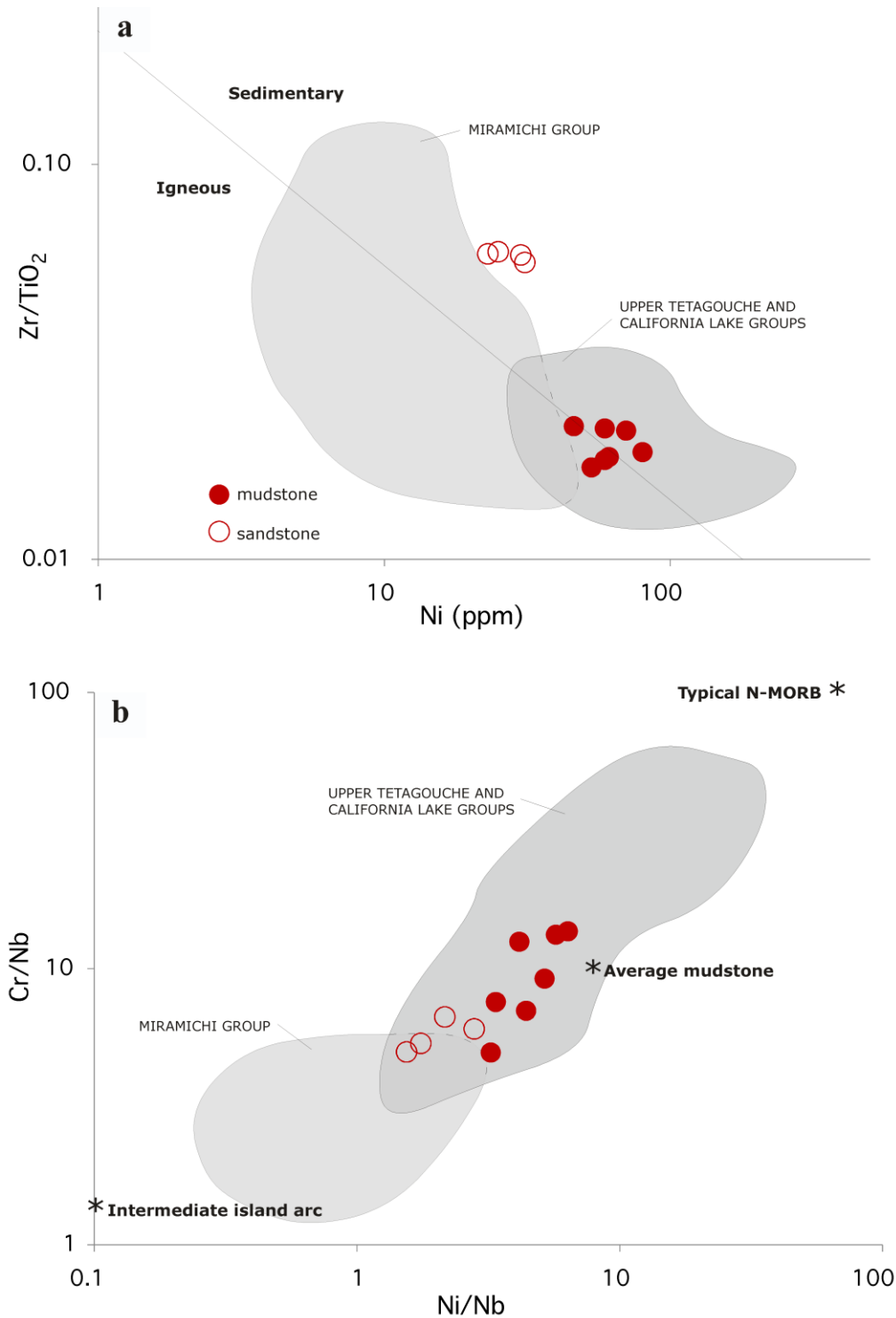


Figure 16. Sediment provenance discriminant plots for unaltered Millstream Formation samples from the Nicholas-Denys deposit. a) Zr/TiO₂ vs Ni plot distinguishes between igneous- and sedimentary-derived sediments, and Ni content indicates the degree of fractionation of igneous source material. b) Cr/Nb vs Ni/Nb plot distinguishes material eroded from midocean ridge basalts (typical N-MORB), mudstones and calc-alkaline island arcs (intermediate island arc). Plots are from Winchester et al. (1980) and Floyd et al. (1991) as cited in Rogers et al. (2003). Fields for the Miramichi, Upper Tetagouche and Upper California Lake Groups from Rogers et al. (2003).

2.5.2 Physiochemical properties of the ambient environment and mineralizing fluid

Several geochemical indices based on redox-sensitive major and trace elements have been used to determine paleoxygenation of the water column (Whitehead 1973; Quinby-Hunt and Wilde 1994; Jones and Manning 1994; Hoffman et al. 1998). Among the major elements, Fe and Mn are used to indicate bottomwater conditions as their solubility is affected by ambient pE and pH (Whitehead 1973). Millstream Formation unaltered mudstone samples from Nicholas-Denys have Mn and Fe contents ranging from 790 ppm to 3 930 ppm (mean = 1 962 ppm \pm 1 211 ppm) and from 4.46% to 9.38% (mean = 7.08% \pm 2.10%), respectively (Table 1). Quinby-Hunt and Wilde (1994) used solubilities of Mn and Fe to determine paleoxygenation levels and the prevailing oxidizing agent in the water column. In oxic bottomwater conditions where oxygen is the primary oxidizing agent, Quinby-Hunt and Wilde argued that low Mn and Fe solubilities would favour their fixation in sediment, yielding high Mn and Fe contents in mudstones. In anoxic bottomwater conditions with nitrate as the primary oxidizing agent, Mn solubility increases with decreasing pE , resulting in low Mn contents in the sediments. Fe remains bound in oxide minerals within the sediments, although high Fe solubility at very low pE values leads to decreasing Fe content in sediments. Although low Mn and high Fe concentrations may characterize nitrate-reducing conditions, low Mn and high Fe may also occur in anoxic conditions in which sulphate is the primary oxidizing agent, as Mn remains dissolved in the water column and reduced sulphur fixes Fe in the sediments. Unaltered Millstream Formation mudstone from the Nicholas-Denys deposit have high Mn contents compatible with deposition in oxygenated bottomwaters, whereas Fe contents are permissive of oxic as well as anoxic sulphate-reducing conditions (Fig. 17). However, Mn was shown to have been mobile during hydrothermal alteration, compared to the relatively immobile behaviour of Fe. Consequently, Mn may not be suited for determination of paleoxygenation levels, whereas Fe is considered a more reliable indicator.

Hoffman et al. (1998) coupled ichnofabric criteria with redox-sensitive trace element indices to discriminate between oxic (> 2.0 ml O_2/l H_2O), suboxic (0.5–2.0 ml O_2/l H_2O), dysoxic (0.2–0.5 ml O_2/l H_2O) and anoxic (< 0.2 ml O_2/l H_2O) conditions. Among these indices, the V/Cr and V/(V+Ni) ratios are particularly useful for anoxic and dysoxic conditions as low oxygen levels largely suppress benthic activity, rendering the use of ichnofabric criteria unsuitable. Vanadium binds to organic matter, and is considered a useful indicator of organic matter preservation (Brumsack 1986). Cr is associated with the detrital fraction of the mudstone, where it substitutes for Al in clays or occurs as chromite grains (Jones and Manning 1994). The V/Cr ratio is thus a measure of organic

matter versus detrital material in the mudstone, which in turn reflects bottomwater conditions as anoxic conditions favour the preservation of organic matter. The V/Cr ratios for Millstream Formation mudstone samples from the Nicholas-Denys deposit range from 0.96 to 2.02 (mean = 1.34 ± 0.45) indicating anoxic ($5 > V/Cr > 1.0$) to dysoxic conditions ($V/Cr < 1.0$) (Hoffman et al. 1998; Fig. 18). The mean V/Cr value is close to unity, suggesting an oxic-anoxic interface within the sediments (Jones and Manning 1994). Ni, another redox-sensitive element, is useful because it is preferentially incorporated into sulphides, in contrast to the detrital and organic affinities of Cr and V, respectively. The V/(V+Ni) ratios of Millstream Formation mudstone samples range from 0.60 to 0.84 (mean = 0.71 ± 0.09), plotting in the anoxic field ($0.9 > V/(V+Ni) > 0.6$), near the boundary with the dysoxic field ($V/(V+Ni) < 0.6$) (Hoffman et al. 1998; Fig. 18).

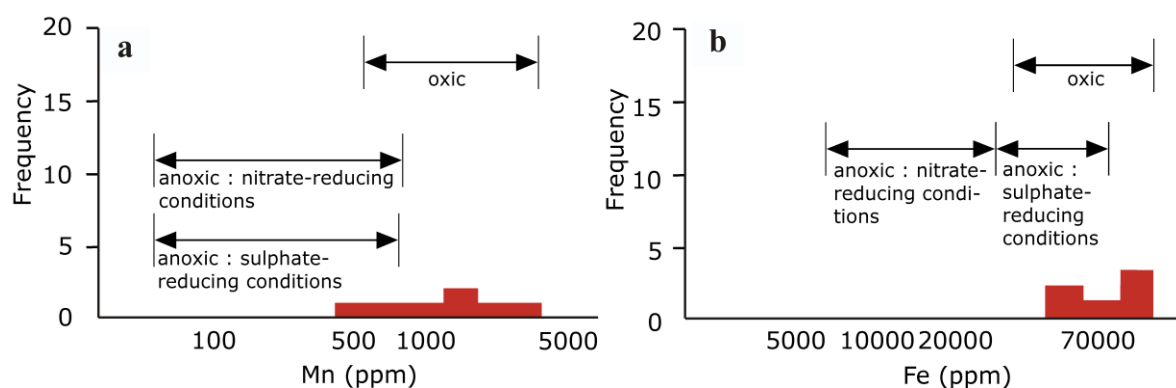


Figure 17. Fe- and Mn-based paleoenvironment discriminant diagrams for unaltered Millstream Formation mudstone samples from the Nicholas-Denys deposit. Fields from Quinby-Hunt and Wilde (1994). a) Mn content indicates oxic paleoconditions during sedimentation of mudstone. b) Fe content is permissive of both oxic and anoxic sulphate-reducing conditions.

Dysoxic-anoxic bottomwater oxygen levels are further supported by low total organic carbon (TOC) contents in the mudstone samples, ranging from below the detection limit (< 0.05) to 0.06 (Table 1), yielding high S/C ratios which are typical of anoxic conditions (Jones and Manning 1994). The high Fe content, absence of bioturbation and V/Cr, V/(V+Ni) and S/C geochemical indices thus indicate dysoxic to anoxic conditions, favourable for sulphate reduction. Whether sulphate-reduction occurred in the water column or in the sediments is unclear. In sufficiently oxic conditions under an open system, bacterial reduction occurs within the sediments due to diffusion of sulphate through the water-sediment interface (Goodfellow and Peter 1996). Ambient dysoxic conditions may potentially restrict the anaerobic bacteria to the sediments, and evidence that this happened are V/Cr ratios close to unity in host mudstone samples, which Jones and Manning (1994) interpret to indicate an oxic-anoxic boundary within the sediments.

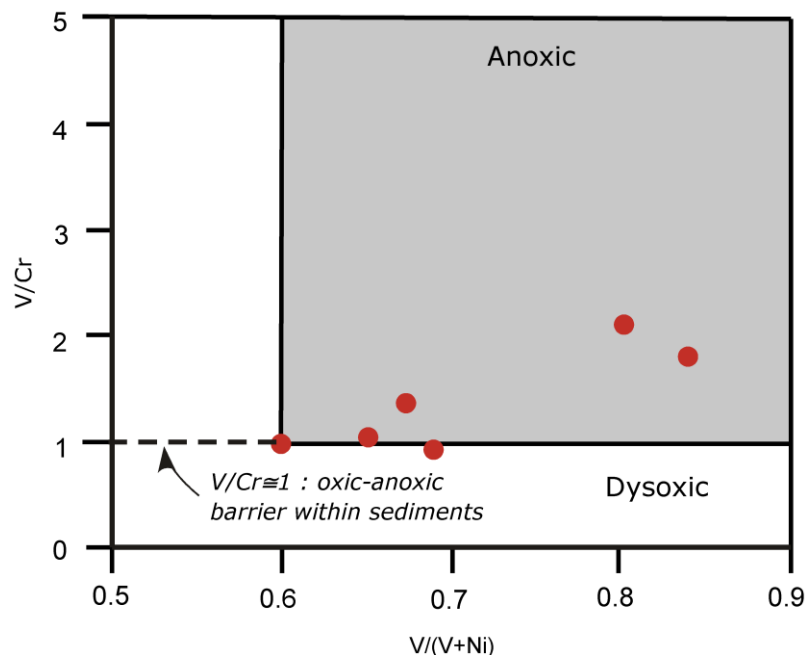


Figure 18. Redox conditions discriminant plot for unaltered Millstream Formation mudstone samples from the Nicholas-Denys deposit (modified after Moreno et al. 2008). Boundaries from Hoffman et al (1998). Samples plot in the anoxic field, near the boundary with the dysoxic field. V/Cr ratios close to unity for several samples suggest the oxic-anoxic barrier is within the sediments (Jones and Manning, 1994).

The mineralogy of the Nicholas-Denys deposit has implications for the redox potential of the mineralizing fluid. The dominance of pyrrhotite over pyrite in the sulphide assemblage suggests the Nicholas-Denys sulphides precipitated from a highly reduced mineralizing fluid where $m\text{H}_2\text{S} \gg m\text{SO}_4^{2-}$, an interpretation presented by Cooke et al. (2000) to account for the pyrrhotite-rich mineralization of the Sullivan SEDEX deposit of the Purcell basin (British Columbia, Canada). It was further stipulated that euxinic conditions ($m\text{H}_2\text{S} \gg m\text{SO}_4^{2-}$) may have prevailed during formation of the Sullivan deposit and prevented barite precipitation upon exhalation of the Ba-rich, reduced mineralizing fluid onto the seafloor. Likewise, the absence of barite at Nicholas-Denys despite significant Ba contents in hydrothermally altered Millstream Formation mudstone (224–800 ppm) (Table 1) suggests euxinic conditions may have prevailed in the backarc basin at the time of sulphide precipitation. The presence of stannite in the Nicholas-Denys sulphide assemblage also has implications for the physiochemical properties of the mineralizing fluid. Although tin is usually considered soluble at high temperatures ($> 300^\circ\text{C}$), Cooke et al. (2000) demonstrated that tin may be carried in solution along with Pb and Zn at temperatures as low as 250°C by a highly reduced ($-41 < \log f\text{O}_2 < -38$), acidic ($3 < \text{pH} < 6$) fluid within the pyrrhotite stability field. Likewise, the

coupled transport of Pb, Zn, Sn and Ba by a reduced, acidic mineralizing fluid is interpreted for the Nicholas-Denys deposit.

2.5.3 Source of sulphur

The sulphur isotope composition of Nicholas-Denys sulphides (0 to +5‰) is the lightest among deposits in the BMC. Although rocks of the BMC are considered more or less coeval, BMC sulphur isotope compositions are heaviest for sulphides of the Tetagouche Group (+10 to +20‰), followed by sulphides of the California Lake Group (+3 to +11‰), and lightest for sulphides of the Fournier Group (0 to +7‰) (Fig. 13). Outside the BMC, the polymetallic Nigadoo and Cullinan veins, hosted by younger Silurian-Devonian rocks, have lighter sulphur isotope compositions (-3 to +2‰) than Nicholas-Denys sulphides.

High $\delta^{34}\text{S}$ values reported for VMS deposits of the Tetagouche and California Lake groups are interpreted to result from bacterial reduction of seawater sulphate in an anoxic closed or partly closed basin, which yields progressively heavier sulphides as the ratio of reduced sulphide to sulphate increases (Goodfellow and Peter 1996). Ordovician seawater sulphates have an estimated sulphur isotope composition of +28‰ (Claypool et al. 1980). A fractionation factor of approximately 25‰ is required to form sulphides with the low $\delta^{34}\text{S}$ values near those of Nicholas-Denys, and is a reasonable value for bacterial sulphate reduction in a system open to sulphate (Ohmoto and Rye 1979). Conditions open to sulphate in which the rate of sulphate supply is greater than the rate of sulphate reduction is expected to yield sulphides with a narrow compositional range (Ohmoto 1986), such as those in the Nicholas-Denys deposit.

Slow rates of bacterial sulphate reduction in deep euxinic basins open to sulphate, such as the Black Sea, are known to yield sulphides with sulphur isotope compositions significantly lighter (up to 60‰) than seawater sulphates (Ohmoto and Rye, 1979). Furthermore, exhalation of the mineralizing fluid into H_2S -rich bottomwaters would lead to isotopic disequilibrium between different sulphide phases (Ohmoto and Goldhaber, 1997). The light sulphur isotope compositions of Nicholas-Denys sulphides relative to Ordovician seawater sulphates (Fig. 13) and isotopic disequilibrium between sulphide species are consistent with euxinia prevailing in the backarc basin. The lack of barite despite significant Ba content in altered host mudstone further supports ambient euxinic bottomwater conditions.

Slightly lighter sulphur isotope compositions reported for deposits of the California Lake Group (+3 to +11‰) than deposits in the Tetagouche Group (+10 to +20‰) have been interpreted to reflect the

transition from a continental to an oceanic crust marking the California Lake Group, and increased leaching of lighter, igneous-derived H_2S from mafic volcanic rocks (Goodfellow and Peter 1996; van Staal et al. 1991). Similarly, formation of oceanic crust characterizes the Fournier Group and abundant mafic volcanic rocks may have contributed lighter H_2S to sulphides of the Turgeon and Nicholas-Denys deposits. Particularly, Millstream Formation mudstone is underlain by synvolcanic gabbros of the Sormany Formation (Fig. 2), from which igneous-derived H_2S may have been leached and mixed with sulphur from bacterially reduced seawater sulphates to form Nicholas-Denys sulphides.

Low, homogeneous and non-equilibrium values of $\delta^{34}\text{S}$ for Nicholas-Denys sulphides are thus compatible with bacterial sulphate reduction in euxinic bottomwater conditions, with relatively light compositions compared to other BMC deposits reflecting (1) a change from a closed or partly closed system under anoxic conditions to an open system under dysoxic-anoxic conditions, likely a consequence of the transition from a continental rift to a backarc basin, and/or (2) incorporation of lighter, igneous-derived reduced sulphur from increased mafic volcanic activity accompanying formation of oceanic crust in the Fournier Group.

2.5.4 Source of lead

Galena from the Nicholas-Denys deposit plots between the Orogene and Mantle reservoir evolution curves of Zartman and Doe (1981) on a $^{207}\text{Pb}/^{204}\text{Pb}$ vs $^{206}\text{Pb}/^{204}\text{Pb}$ diagram (Fig. 14a), suggesting a mixed crustal-mantle source for lead in the deposit. Backarc basin sedimentary rocks of the Millstream Formation can be considered to approximate average crustal lead of the Orogene reservoir as provenance analysis suggests sediments were derived from a range of domains: (1) continental margin of Ganderia, (2) remnant volcanic arc and (3) obducted ophiolite. $^{207}\text{Pb}/^{204}\text{Pb}$ ratios below the Orogene curve for Nicholas-Denys galenas are thus suggestive of mixing between lead leached from the backarc basin sediments and a less radiogenic mantle source.

Mixing of crustal lead with mantle lead is documented for the Mount Bulga, Wiseman Creek and Calula Silurian deposits of the Lachlan Fold Belt, Australia (Carr et al. 1995), which form a steep, linear array similar to that of Nicholas-Denys galena samples (Fig. 14). Carr et al. (1995) proposed that underlying Ordovician shoshonites and basalts were the most likely sources of less radiogenic lead for the Lachlan deposits. Likewise, synvolcanic gabbros of the Middle Ordovician Sormany Formation underlie the sedimentary rocks of the Millstream Formation. The lead isotope

composition of the Nicholas-Denys sulphides is interpreted to reflect mixing of lead leached from the synvolcanic gabbros of the Sormany Formation (Mantle reservoir) with lead leached from the backarc basin sediments of the Millstream Formation (Orogene reservoir).

The lead isotope composition of siliciclastic-felsic VMS deposits of the Tetagouche and California Lake groups (McCutcheon et al. 1993; R. Thorpe, personal communication to G. Beaudoin) is more radiogenic than Nicholas-Denys and plot between the Orogene and Upper Crust curves (Fig. 14), suggesting that lead in BMC VMS deposits was leached from the rifted continental crust. The lead isotope composition of the mafic rock-hosted VMS Turgeon deposit is less radiogenic than slightly older Tetagouche- and California-Lake hosted VMS deposits, and is more radiogenic than the Nicholas-Denys deposit. The less radiogenic lead isotope composition of Nicholas-Denys sulphides compared to older BMC VMS deposits is best interpreted as an increasing mantle component from (1) progressive formation of oceanic crust during deposition of the Fournier Group and/or (2) increased sediment input from nearby obducted ophiolite.

Outside the BMC, the Nigadoo veins, hosted by Silurian sedimentary rocks of the Chaleurs Group and the Devonian Nigadoo intrusive, have lead isotope ratios plotting above and below the Orogene curve, whereas the Cullinan vein, hosted by Silurian sedimentary rocks of the Chaleurs Group, plots above the Orogene curve (Fig. 14). The more radiogenic lead isotope composition of the undeformed Nigadoo and Cullinan veins compared to the Nicholas-Denys deposit is consistent with the post-Devonian deformation timing of vein mineralization, compared to the older, pre-Devonian deformation timing of Nicholas-Denys mineralization.

2.5.5 Implications for genetic classification

Physiochemical conditions and sediment provenance interpretations suggest that (1) anoxic bottomwaters coupled with (2) a system closed or partly closed to sulphate in a (3) continental backarc rift prevailing during deposition of the Tetagouche and California Lake Groups shifted to (1) anoxic-dysoxic bottomwaters coupled with (2) a system open to sulphate in a (3) sedimented backarc basin floored by oceanic crust during deposition of the Millstream Formation of the Fournier Group (van Staal et al. 1991; Goodfellow and Peter 1996). This paleoenvironment transition is mirrored by a change in conditions of sulphide precipitation, as sulphur isotope compositions of VMS deposits hosted by the Tetagouche, California Lake and Fournier groups become progressively lighter. The absence of felsic and mafic volcanic rocks, abundance of fine-

grained sedimentary rocks and younger stratigraphic age for the Millstream Formation relative to BMC VMS deposits are features consistent with a post-felsic volcanism setting, such that magmatism had significantly waned in the backarc and sedimentation predominated. This likely led to different mineralization conditions for the Nicholas-Denys deposit than those which prevailed for the Tetagouche and California Lake VMS deposits that are genetically associated with episodes of felsic volcanism. The sedimented backarc rift basin setting for the BMC constitutes a favourable environment for the formation of both VMS and SEDEX mineralization (Goodfellow and Lydon 2007).

2.5.5.1 SEDEX mineralization

SEDEX deposits typically occur within fine-grained marine sedimentary rocks overlying coarse-grained sedimentary and volcanic rocks in a continental rift basin, and are commonly spatially associated with synsedimentary faults (Goodfellow and Lydon 2007). Synsedimentary faults are commonly recognized by an abrupt facies change from fine-grained deep marine sediments to coarse-grained turbiditic flows (Leach et al. 2005). The sharp contact between the texturally immature sandstone and adjacent mudstone in the Millstream Formation near the Nicholas-Denys deposit (Fig. 4c) suggests the presence of such a synsedimentary fault, which may have acted as a pathway for mineralizing fluids.

Hydrothermal alteration in SEDEX deposits is generally less well documented than in VMS deposits due to the impermeable and less reactive nature of fine-grained sediments, such that feeder pipes and footwall alteration are commonly subtle or absent (Goodfellow and Lydon 2007). Geochemical halos and silicate alteration are most commonly reported, and Tl and Mn are typically enriched within the mineralized horizon and considered significant vectors to SEDEX alteration (Leach et al. 2005). At Nicholas-Denys, Tl and Mn display significant enrichments of 375% and 325%, respectively, in the proximal, mineralized alteration facies (Fig. 8f), compared to typical enrichment of 20% and 60%, respectively in the intermediate and distal facies. Fine-grained, wall rock silicification observed in the proximal hydrothermal alteration facies at Nicholas-Denys (Figs. 8d et 8e) is reported at several SEDEX deposits (Tom, Jason, Vangorda, Rammelsberg, Century, Red Dog) and is generally interpreted to precede or overlap the mineralization event (Broadbent et al. 1998; Leach et al. 2005; Slack et al. 2004).

The Pb–Zn–Ag sulphide assemblage of SEDEX deposits typically consists of massive sphalerite and galena, with a mean $Zn/(Zn+Pb)$ ratio of 0.7, as well as sulfosalts as the main silver-bearing minerals (Leach et al. 2005). The Nicholas-Denys deposit has a mean $Zn/(Zn+Pb)$ ratio of 0.67, and galena and the sulfosalt freibergite host the majority of silver for the deposit. The pyrrhotite-rich mineralization of Nicholas-Denys is a feature that has also been reported at the Mt. Isa (Australia) and Sullivan SEDEX deposits (Leach et al. 2005; Lydon 2004).

The sedimented backarc rift tectonic setting, fine-grained marine sedimentary host rock sequence, bedding-parallel Pb-Zn-Ag sulphide lenses and Si, Tl and Mn geochemical enrichments lead to a SEDEX classification for the Nicholas-Denys deposit. The occurrence of pyrrhotite and stannite and absence of barite in the Nicholas-Denys mineral assemblage, although uncommon features of SEDEX deposits, are consistent with a reduced ($-41 < \log fO_2 < -38$), acidic ($3 < pH < 6$), moderate- to high-temperature ($> 250^\circ C$) mineralizing fluid discharged into a euxinic environment.

2.5.5.2 Comparison of the Nicholas-Denys deposit to similar deposits

A few BMC deposits have similar features to the Nicholas-Denys deposit and affinity to SEDEX mineralization, such as the Canoe Landing Lake and Orvan Brook deposits (Jambor 1979; Goodfellow and McCutcheon 2003; Walker et al. 2006). These deposits are characterized by fine-grained sedimentary host rocks, low Cu grade, absence of a sulphide stringer zone, and sheet-like, unzoned sulphide lenses, and are generally regarded as distal-type VMS deposits within the classification scheme of Goodfellow (2007). However, the Canoe Landing Lake and Orvan Brook deposits differ from the Nicholas-Denys deposit by the presence of volcanic rocks in their stratigraphic footwall, a pyrite-sphalerite-galena sulphide assemblage, and heavier sulphur isotope compositions, such that they are considered siliciclastic-felsic VMS deposits rather than SEDEX deposits.

The Draa Sfar deposit in the Jebilet Massif of western Morocco (Belkabir et al. 2008; Marcoux et al. 2008; Moreno et al. 2008) has many features in common with the Nicholas-Denys deposit. Its genetic classification has been the subject of much debate, and suggestions range from syngenetic (Belkabir et al. 2008; Bernard et al. 1988; Marcoux et al. 2008) to epigenetic (Essaifi and Hibti 2008). The Draa Sfar deposit is thought to have formed in a volcano-sedimentary rift basin within anoxic sediments in an oxic-suboxic water column. Sulphides have experienced several phases of deformation, dominated by shearing. The occurrence of boudinaged, subvertical sulphide lenses

spatially associated with shear zones at Draa Sfar mirror the structural features of the Nicholas-Denys deposit (Figs. 3 and 4). Sulphide lenses occur in a thick shale sequence, and pyrrhotite dominates the sulphide assemblage, with abundant sphalerite, and accessory galena and chalcopyrite, yet rare colbaltite, Bi-bearing minerals and electrum reported at Draa Sfar are not present at Nicholas-Denys. As with Nicholas-Denys sulphides, no bedded sulphides are observed at the Draa Sfar deposit, and the effects of deformation are heterogeneous with banded sulphides occurring next to granoblastic textures (Moreno et al. 2008). Hydrothermal alteration is markedly different at the Draa Sfar deposit than at the Nicholas-Denys deposit; at Draa Sfar, alteration consists of strong, proximal, footwall chloritization and distal sericitization. Rhyodacite and associated volcanoclastic facies in the footwall of Draa Sfar are cut by a sulphide stringer zone underlying massive sulphides. The alteration mineralogy, zonation pattern and presence of volcanic rocks have favoured the classification of Draa Sfar as a siliciclastic-felsic VMS deposit (Belkadir et al. 2008).

The Nicholas-Denys deposit demonstrates certain similarities with the Sullivan SEDEX deposit of the Purcell basin in British Columbia, such as a pyrrhotite-rich mineralization and the presence of a tin-bearing mineral in the sulphide assemblage. These common features suggest similar physiochemical properties of the mineralizing fluid, however massive sulphide textures and hydrothermal alteration are markedly different for the two deposits. The Sullivan deposit has well-preserved bedded sulphides, a tourmaline pipe and muscovite-altered sediments in its footwall and a chlorite–albite–pyrite hangingwall alteration assemblage (Leach et al. 2005). These characteristics are not consistent with the sheared, brecciated and recrystallized Nicholas-Denys sulphides, or with the chlorite–quartz and quartz–sericite hydrothermal alteration zones.

2.6 Conclusion

The Nicholas-Denys deposit shares characteristics with both distal-type VMS deposits and SEDEX deposits. Several authors have discussed the continuum of characteristics between these two types of mineralization (Leach et al. 2005; Goodfellow and Lydon 2007; Franklin et al. 2005). The affinity of the Nicholas-Denys deposit to SEDEX mineralization and its close spatial association to VMS deposits in older units of the BMC emphasizes the potential of sedimented backarc rift basins to host both types of syngenetic mineralization. The Nicholas-Denys deposit is interpreted to reflect SEDEX mineralization in the late stages of backarc rifting, when sedimentation had become predominant.

Sediments of the Millstream Formation infilling the backarc basin originated from various sources (continental margin of Ganderia, remnant volcanic arc and obducted ophiolite). Sediments were deposited in a dysoxic to anoxic water column favourable to sulphate-reduction. Bacterial reduction of seawater sulphates provided reduced sulphur for Nicholas-Denys sulphides, although dysoxic to anoxic conditions may have restricted the sulphate-reducing bacteria to the underlying sediments. Opening of the continental rift to a backarc basin potentially favoured bacterial sulphate reduction under conditions open to sulphate, whereas generation of oceanic crust marking the Fournier Group may have contributed lighter reduced sulphur to Nicholas-Denys sulphides. Lead for the Nicholas-Denys deposit was leached from backarc basin sediments and underlying synvolcanic gabbros.

Many features of the Nicholas-Denys deposit are compatible with a SEDEX classification: (1) a sedimented back-arc rift tectonic setting, (2) fine-grained marine sedimentary host rock lithology, (3) Pb–Zn–Ag sulphide lenses conformable to bedding, (4) an asymmetric alteration halo lacking a sulphide stringer zone, (5) dominant quartz hydrothermal alteration, and (6) significant Tl and Mn geochemical enrichments in the mineralized horizon. Certain particularities of the Nicholas-Denys deposit such as the abundance of pyrrhotite, the occurrence of stannite and absence of barite are compatible with SEDEX deposits that are precipitated from a reduced, acidic mineralizing fluid into H₂S-rich bottomwater conditions.

Chapitre 3 - Conclusion

Le mudstone de la Formation Millstream d'âge Ordovicien moyen à tardif qui encaisse les sulfures de Nicholas-Denys a été déposé dans un contexte postdatant le volcanisme felsique dans le bassin d'arrière-arc du CMB, soit dans un environnement où la sédimentation était devenue prédominante. Les sédiments proviennent de plusieurs sources : (1) l'arc volcanique en supra-subduction, (2) la marge passive continentale de Ganderia et (3) un ophiolite exhumé. Un lit de grès immature intercalé dans le mudstone présente une source différente de sédiments par rapport au mudstone, soit une provenance de marge passive, évoquant l'interprétation du grès comme une coulée de débris du talus continental. D'autre part, un tel changement soudain de faciès signale peut-être la présence d'une faille dans le socle et la chute de débris d'un bloc soulevé à proximité.

La géochimie du mudstone révèle des conditions anoxiques à dysoxiques dans la colonne d'eau ordovicienne, propice à la réduction des sulfates. La composition isotopique du soufre des sulfures de Nicholas-Denys indique que le soufre réduit provient de la réduction bactérienne des sulfates de l'eau de mer dans un système ouvert aux sulfates, compatible avec les conditions réductrices de la colonne d'eau, avec une contribution de soufre réduit des roches volcaniques mafiques sous-jacentes.

La composition isotopique du plomb à Nicholas-Denys indique que le plomb a été lessivé des sédiments du bassin d'arrière-arc et des roches volcaniques mafiques sous-jacentes. La pyrrhotite comme sulfure de fer prédominant, la présence de stannite et l'absence de barite malgré de fortes concentrations en barium indique un transport couplé de Pb, Zn, Sn et Ba, un critère compatible avec un fluide minéralisateur réduit (faible pH et faible fugacité de l'oxygène), dans la zone de stabilité de la pyrrhotite.

La déformation du gîte de Nicholas-Denys par une faille dévonienne de décrochement dextre d'orientation ENE masque plusieurs caractéristiques primaires du gîte. Des sulfures lités sont préservés dans la majorité des SMV du camp minier de Bathurst, et les effets de la déformation sont principalement liés à la fermeture du bassin d'arrière-arc durant le Silurien précoce. D'autre part, les sulfures de Nicholas-Denys ne sont pas lités, et démontrent plutôt des textures de déformation ductile liées au décrochement dextre dévonien, ainsi que des textures de recristallization, de bréchification et de remobilization possiblement liées à des événements de déformation d'âge

dévonien ou plus jeune. La faille de décrochement dextre se manifeste également au niveau macroscopique par le développement de zones de cisaillement d'orientation ENE aux contacts des lentilles de sulfures avec les épontes, et par l'étirement et le boudinement des lentilles de sulfures dans une direction ENE. La cartographie des lentilles ainsi que les textures des sulfures indiquent donc que la minéralisation à Nicholas-Denys prédate le décrochement dextre d'âge Dévonien.

Plusieurs caractéristiques du gîte de Nicholas-Denys sont compatibles avec une minéralisation SEDEX : (1) un contexte géodynamique de bassin d'arrière-arc sédimenté, (2) des lentilles de sulfures à Pb–Zn–Ag concordantes au litage, (3) un encaissant de roches sédimentaires finement grenues, (4) une altération asymétrique, concordante et discrète, caractérisée par l'abondance du quartz et l'enrichissement des éléments Tl et Mn dans l'horizon minéralisé, et (5) l'absence d'un stockwerk. La présence de la pyrrhotite a rarement été signalée dans les gîtes SMV, à l'exception des gîtes marocains des Jébilet dont Draa Sfar. Le gîte de Draa Sfar démontre plusieurs similitudes au gîte de Nicholas-Denys, tels l'absence de sulfures lités, des textures de déformation ductile et de recristallisation des sulfures, un encaissant sédimentaire et un environnement réducteur. Par contre, la présence de roches volcaniques felsiques dans le mur stratigraphique du gisement ainsi qu'une forte altération en chlorite et séricite ont favorisé l'interprétation des sulfures de Draa Sfar comme un gîte SMV de type silicoclastique-felsique.

Le gîte de Nicholas-Denys partage quelques caractéristiques avec les gîtes SMV de Canoe Landing Lake et Orvan Brook dans le camp minier de Bathurst. Ces gîtes sont caractérisés par un encaissant de shale noir, une faible teneur en cuivre et l'absence d'un stockwerk, et sont interprétés comme des gîtes de type SMV distaux dans le camp minier de Bathurst. Ce rapprochement entre les gîtes SMV distaux du camp minier de Bathurst et le gîte de Nicholas-Denys illustre la continuité entre les attributs des gîtes SMV et des gîtes SEDEX. Les gîtes du camp minier de Bathurst étaient auparavant considérés comme des hybrides entre les SMV et les SEDEX, quoique la classification récente de Franklin et al (2005) favorise une classification SMV du sous-type silicoclastique-felsique.

L'étude du gîte de Nicholas-Denys a d'importantes implications pour l'évolution du contexte géodynamique et des conditions oxydo-réductrices dans le bassin d'arrière-arc. Les sulfures de Nicholas-Denys sont encaissés par les roches les plus jeunes du camp minier de Bathurst, et sont interprétés comme reflétant la transition d'un environnement propice aux SMV à un environnement propice aux SEDEX durant l'Ordovicien moyen à tardif.

Bibliographie

- Belkabir, A., H. L. Gibson, E. Marcoux, D. Lentz, and S. Rziqi (2008), Geology and wall rock alteration at the Hercynian Draa Sfar Zn-Pb-Cu massive sulphide deposit, Morocco, *Ore Geology Reviews*, 33(3-4), 280-306.
- Bernard, A. J., O. W. Maier, and A. Mellal (1988), Aperçu sur les amas sulfurés massifs des hercynides Marocaines, *Mineralium Deposita*, 23(2), 104-114.
- Bhatia, M. R., and K. A. W. Crook (1986), Trace element characteristics of graywackes and tectonic setting discrimination of sedimentary basins, *Contributions to Mineralogy and Petrology*, 92(2), 181-193.
- Boggs, S. (Ed.) (2001), *Principles of Sedimentology and Stratigraphy*, 726 pp., Prentice Hall.
- Broadbent, G. C., R. E. Myers, and J. V. Wright (1998), Geology and origin of shale-hosted Zn-Pb-Ag mineralization at the Century Deposit, Northwest Queensland, Australia, *Economic Geology*, 93(8), 1264-1294.
- Brumsack, H. J. (1986), The inorganic geochemistry of Cretaceous black shales (DSDP 41) in comparison to modern upwelling sediments from the Gulf of California, in *North Atlantic Palaeoceanography*, edited by Summerhayes and N. Shackelton, Geological Society of London, Special Publication 21, 447-462.
- Carr, G. R., J. A. Dean, D. W. Suppel, and P. S. Heithersay (1995), Precise lead isotope fingerprinting of hydrothermal activity associated with Ordovician to Carboniferous metallogenic events in the Lachlan fold belt of New South Wales, *Economic Geology*, 90(6), 1467-1505.
- Claypool, G. E., W. T. Holser, I. R. Kaplan, H. Sakai, and I. Zak (1980), The age curves of sulfur and oxygen isotopes in marine sulfate and their mutual interpretation, *Chemical Geology*, 28, 199-260.
- Cooke, D. R., S. W. Bull, R. R. Large, and P. J. McGoldrick (2000), The importance of oxidized brines for the formation of Australian proterozoic stratiform sediment-hosted Pb-Zn (sedex) deposits, *Economic Geology*, 95(1), 1-17.
- Davies, J. L., W. M. Tupper, D. Bachinski, R. W. Boyle, and R. Martin (1969), Geology and mineral deposits of the Nigadoo River-Millstream River area, Gloucester County, New Brunswick. Geological Survey of Canada, Paper 67-49, 70pp.
- Dimitrov, I., and S. R. McCutcheon (2007), Stratigraphic and Structural Constraints on Limestone Exploration: A Case Study from Northern New Brunswick, Canada, *Exploration and Mining Geology*, 16(1-2), 25-36.
- Dimitrov, I., S. R. McCutcheon, and P. F. Williams (2003), Progress report: structural investigations in the vicinity of the Rocky Brook-Millstream Fault, Gloucester and Restigouche counties, northern New Brunswick, in *Current Research 2002*, edited by B. M. W. Carroll, New Brunswick Department of Natural Resources; Minerals, Policy and Planning Division, Mineral Resource Report 2003-4, 59-71.
- Dimitrov, I., S. R. McCutcheon, and P. F. Williams (2004), Stratigraphic and structural observations

- in Silurian rocks between Pointe Rochette and the Southeast Upsalquitch River, northern New Brunswick: A progress report, in *Geological Investigations in New Brunswick for 2003*, edited by G. L. Martin, New Brunswick Department of Natural Resources; Minerals, Policy and Planning Division, Mineral Resource Report 2004-4, 41-74.
- Essaifi, A., and M. Hibti (2008), The hydrothermal system of Central Jebilet (Variscan Belt, Morocco): A genetic association between bimodal plutonism and massive sulphide deposits, *Journal of African Earth Sciences*, 50(2-4), 188-203.
- Floyd, P. A., R. Shail, B. E. Leveridge, and W. Franke (1991), Geochemistry and provenance of Rhenohercynian synorogenic sandstones: implications for tectonic environment discrimination, *Geological Society of London, Special Publication 57*, 173-188.
- Franklin, J. M., H. L. Gibson, I. R. Jonasson, and A. G. Galley (2005), Volcanogenic massive sulfide deposits, *Economic Geology 100th Anniversary Volume*, 523-560.
- Goodfellow, W. D. (1987), Anoxic stratified oceans as a source of sulfur in sediment-hosted Stratiform Zn-Pb Deposits (Selwyn Basin, Yukon, Canada), *Chemical Geology*, 65(3-4), 359-382.
- Goodfellow, W. D. (2007), Metallogeny of the Bathurst Mining Camp, northern New Brunswick, in *Mineral Deposits of Canada: A Synthesis of Major Deposit-Types, District Metallogeny, the Evolution of Geological Provinces, and Exploration Methods*, edited by W. D. Goodfellow, Geological Association of Canada, Mineral Deposits Division, Special Publication No. 5, 449-469.
- Goodfellow, W. D., and J. M. Peter (1996), Sulphur isotope composition of the Brunswick No 12 massive sulphide deposit, Bathurst Mining Camp, New Brunswick: Implications for ambient environment, sulphur source, and ore genesis, *Canadian Journal of Earth Sciences*, 33(2), 231-251.
- Goodfellow, W. D., and J. M. Peter (1999), Sulphur isotope composition of the Brunswick No. 12 massive sulphide deposit, Bathurst Mining Camp, New Brunswick: implications for ambient environment, sulphur source, and ore genesis - Reply, *Canadian Journal of Earth Sciences*, 36(1), 127-134.
- Goodfellow, W. D., and S. R. McCutcheon (2003), Geologic and genetic attributes of volcanic sediment-hosted massive sulfide deposits of the Bathurst Mining Camp, northern New Brunswick - a synthesis, *Economic Geology, Monograph 11*, 245-301.
- Goodfellow, W. D., and J. W. Lydon (2007), Sedimentary exhalative (SEDEX) deposits, in *Mineral Deposits of Canada: A Synthesis of Major Deposit Types, District Metallogeny, the Evolution of Geological Provinces, and Exploration Methods*, edited by W. D. Goodfellow, Geological Association of Canada, Mineral Deposits Division, Special Publication No. 5, 163-183.
- Goodfellow, W. D., J. M. Peter, J. A. Winchester, and C. R. van Staal (2003), Ambient marine environment and sediment provenance during formation of massive sulfide deposits in the Bathurst Mining Camp: Importance of reduced bottom waters to sulfide precipitation and preservation, *Economic Geology, Monograph 11*, 129-156.
- Grant, J. A. (1986), The isocon diagram; a simple solution to Gresens' equation for metasomatic alteration, *Economic Geology*, 81(8), 1976-1982.
- Hoffman, D. L., T. J. Algeo, J. B. Maynard, M. M. Joachimski, J. C. Hower, and J. Jaminski (1998), Regional and stratigraphic variation in bottomwater anoxia in offshore core shales of Upper Pennsylvanian cyclothems from the eastern midcontinent shelf (Kansas), U.S.A., in *Shales and*

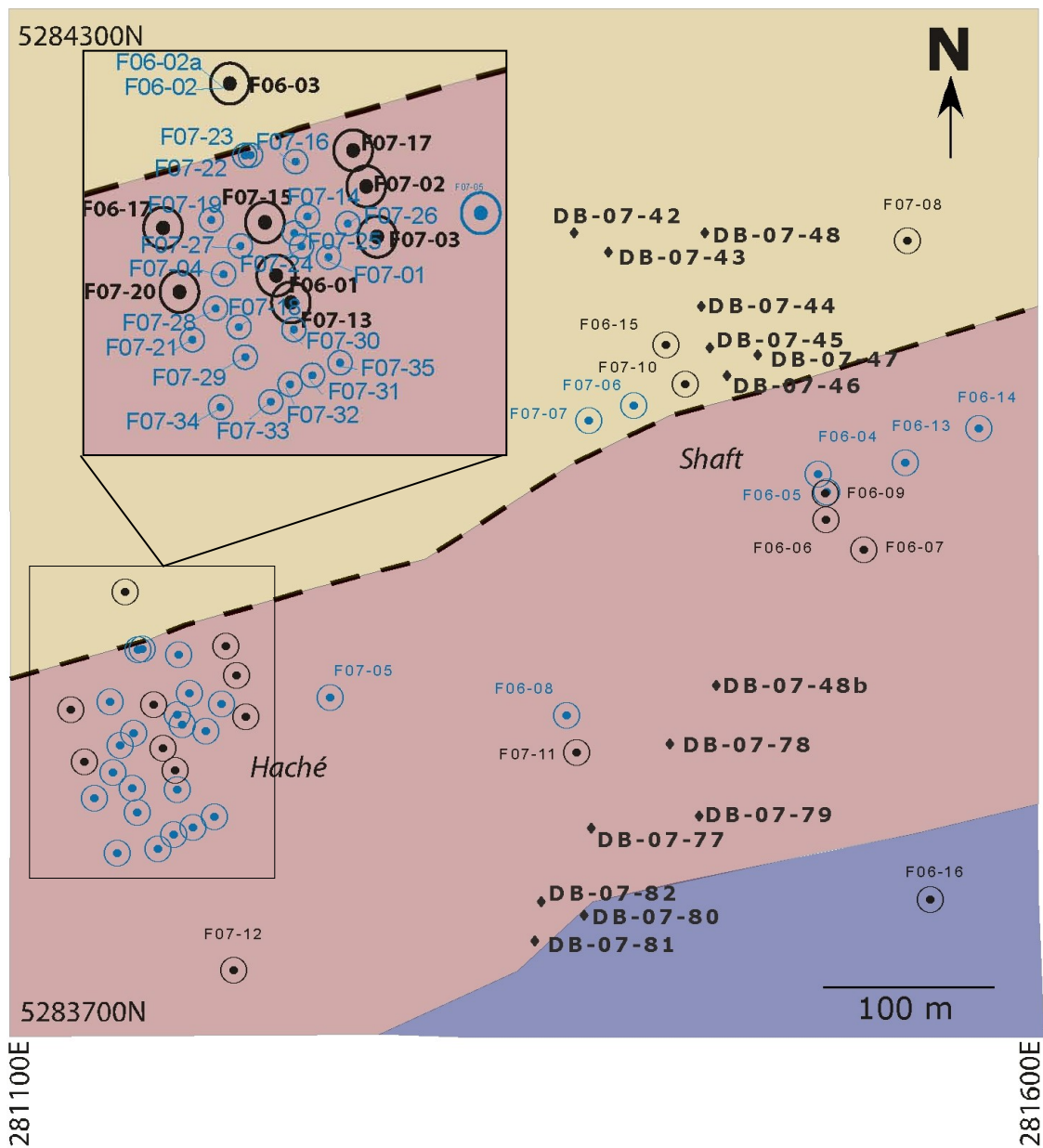
- Mudstones I, edited by J. Schieber, W. Zimmerle and P. Sethi, E. Schweizerbart'sche Verlagsbuchhandlung, Stuttgart, 243-269.
- Jambor, J. L. (1979), Mineralogical evaluation of proximal-distal features in New Brunswick massive-sulfide deposits, *Canadian Mineralogist*, 17(3), 649-664.
- Jones, B., and D. A. C. Manning (1994), Comparison of geochemical indices used for the interpretation of palaeoredox conditions in ancient mudstones, *Chemical Geology*, 111, 111-129.
- Leach, D. L., D. F. Sangster, K. D. Kelley, R. R. Large, G. Garven, C. R. Allen, J. Gutzmer, and S. Walters (2005), Sediment-hosted lead-zinc deposits: A global perspective, *Economic Geology 100th Anniversary Volume*, 561-607.
- Lentz, D. R. (1996), Recent advances in lithogeochemical exploration for massive-sulphide deposits in volcano-sedimentary environments: petrogenetic, chemostratigraphic, and alteration aspects with examples from the Bathurst camp, New Brunswick, in *Current Research 1995*, edited by B. M. W. Carroll, New Brunswick Department of Natural Resources and Energy, Minerals and Energy Division, Mineral Resource Report 96-1, 73-119.
- Lentz, D. R., and W. D. Goodfellow (1996), Intense silicification of footwall sedimentary rocks in the stockwork alteration zone beneath the Brunswick No. 12 massive sulphide deposit, Bathurst, New Brunswick, *Canadian Journal of Earth Sciences*, 33, 284-302.
- Li, Y., and J. Liu (2006), Calculation of sulfur isotope fractionation in sulfides, *Geochimica Cosmochimica Acta*, 70(7), 1789-1795.
- Lydon, J. W. (2004), Geology of the Belt-Purcell basin and the Sullivan deposit, in *Sediment-hosted Lead-Zinc Sulphide Deposits*, edited by M. Deb and W. D. Goodfellow, 367 pp., Narosa Publishing House, New Delhi.
- Marcoux, E., A. Belkadir, H. L. Gibson, D. Lentz, and G. Ruffet (2008), Draa Sfar, Morocco: A Viséan (331 Ma) pyrrhotite-rich, polymetallic volcanogenic massive sulphide deposit in a Hercynian sediment-dominant terrane, *Ore Geology Reviews*, 33(3-4), 307-328.
- McCutcheon, S. R., J. P. Langton, C. R. van Staal, and D. R. Lentz (1993), Stratigraphy, tectonic setting and massive-sulphide deposits of the Bathurst Mining Camp, in *Guidebook to the Metallogeny of the Bathurst Camp*, edited by S. R. McCutcheon and D. R. Lentz, Trip no. 4, 3rd Annual Field Conference, Bathurst, New Brunswick, 1993, 1-39.
- Meyer, C. (1985), Ore Metals through Geologic History, *Science*, 227(4693), 1421-1428.
- Moreno, C., R. Saez, F. Gonzalez, G. Almodovar, M. Toscano, G. Playford, A. Alansari, S. Rziqi, and A. Bajddi (2008), Age and depositional environment of the Draa Sfar massive sulfide deposit, Morocco, *Mineralium Deposita*, 43(8), 891-911.
- New Brunswick Department of Natural Resources, Mineral Occurrence Database.
- Ohmoto, H. (1986), Stable Isotope Geochemistry of Ore-Deposits, *Reviews in Mineralogy and Geochemistry*, 16, 491-559.
- Ohmoto, H., and R. O. Rye (1979), Isotopes of sulfur and carbon, in *Geochemistry of hydrothermal ore deposits*, edited by H. L. Barnes, John Wiley, New York, 509-565.
- Ohmoto, H., and M. B. Goldhaber (1997), Sulfur and carbon isotopes, in *Geochemistry of*

- hydrothermal ore deposits, edited by H. L. Barnes, John Wiley & Sons, New York, 519-611.
- Quinby-Hunt, M. S., and P. Wilde (1994), Thermodynamic zonation in the black shale facies based on iron-manganese-vanadium content, *Chemical Geology*, 113(3-4), 297-317.
- Rogers, N., and C. R. van Staal (1997), Comparing the Bathurst Mining Camp to the Japan Sea and Okinawa trough: Ancient, recent and active arc-arcs [abs], Geological Association of Canada-Mineralogical Association of Canada, Annual Meeting, Ottawa, Ontario, 1997, Abstract Volume, A-127.
- Rogers, N., and C. R. van Staal, J. A. Winchester, L. R. Fyffe (2003), Provenance and chemical stratigraphy of the sedimentary rocks of the Miramichi, Tetagouche, California Lake, and Fournier Groups, Northern New Brunswick, *Economic Geology*, Monograph 11, 111-128.
- Slack, J. F., K. D. Kelley, V. M. Anderson, J. L. Clark, and R. A. Ayuso (2004), Multistage hydrothermal silicification and Fe-Ti-As-Sb-Ge-REE enrichment in the Red Dog Zn-Pb-Ag District, Northern Alaska: geochemistry, origin, and exploration applications, *Economic Geology*, 99(7), 1481-1508.
- Solomon, M. (1999), Sulphur isotope composition of the Brunswick No. 12 massive sulphide deposit, Bathurst Mining Camp, New Brunswick: implications for ambient environment, sulphur source, and ore genesis - Discussion, *Canadian Journal of Earth Sciences*, 36(1), 121-125.
- Thurlow, J. G. (1993), 1992 Geological and diamond drilling report on the Turgeon prospect, Belledune project, northern New Brunswick, Phelps Dodge Corporation of Canada Ltd.
- Tremblay, A., and B. Dubé (1991), Structural relationships between some gold occurrences and fault zones in the Bathurst area, northern New Brunswick, in *Current Research, Part D, Geological Survey of Canada, Paper 91-1D*, 89-100.
- Tupper, W. M. (1960), Sulfur isotopes and the origin of sulfide deposits of the Bathurst-Newcastle area of northern New Brunswick, *Economic Geology*, 55, 1676-1707.
- Turcotte, B., and C. Pelletier (2008), Technical report on the mineral resource estimates for the Hachey zone, Puma Exploration.
- van Staal, C. R. (1987), Tectonic setting of the Tetagouche Group in northern New Brunswick: implications for plate tectonic models of the northern Appalachians, *Canadian Journal of Earth Sciences*, 24, 1329-1351.
- van Staal, C. R. (1994), Brunswick subduction complex in the Canadian Appalachians: Record of the Late Ordovician to Late Silurian collision between Laurentia and the Gander margin of Avalon, *Tectonics*, 13(4), 946-962.
- van Staal, C. R. (2007), Pre-Carboniferous metallogeny of the Canadian Appalachians, in *Mineral resources of Canada: A Synthesis of Major Deposit-Types, District Metallogeny, the Evolution of Geological Provinces, and Exploration Methods*, edited by W. D. Goodfellow, Geological Association of Canada, Mineral Deposits Division, Special Publication No. 5, 793-818.
- van Staal, C. R., and L. R. Fyffe (1991), Dunnage and Gander Zones, New Brunswick: Canadian Appalachian Region, *Geoscience Report*, 91-2, 39pp.
- van Staal, C. R., L. R. Fyffe, J. P. Langton, and S. R. McCutcheon (1992), The Ordovician Tetagouche Group, Bathurst Camp, northern New Brunswick, Canada; history, tectonic setting and distribution of massive-sulfide deposits, *Exploration and Mining Geology*, 1(2), 93-103.

- van Staal, C. R., and J. A. de Roo (1995), Mid-Paleozoic tectonic evolution of the Appalachian Central Mobile belt in northern New Brunswick, Canada: Collision, extensional collapse and dextral transpression, in *Current Perspectives in the Appalachian-Caledonian Orogen*, edited by J. P. Hibbard, C. R. van Staal and P. A. Cawood, Geological Association of Canada, Special Paper 41, 367-389.
- van Staal, C. R., J. A. Winchester, and J. H. Bédard (1991), Geochemical variations in Middle Ordovician volcanic rocks of the northern Miramichi Highlands and their tectonic significance, *Canadian Journal of Earth Sciences*, 28(7), 1031-1049.
- van Staal, C. R., R. A. Wilson, N. Rogers, L. R. Fyffe, J. P. Langton, S. R. McCutcheon, V. McNicoll, and C. E. Ravenhurst (2003), Geology and tectonic history of the Bathurst supergroup, Bathurst Mining Camp, and its relationships to coeval rocks in southwestern New Brunswick and adjacent Maine - a synthesis, *Economic Geology*, Monograph 11, 37-60.
- Walker, J. A., S. Gower, and S. R. McCutcheon (1991), Antinouri-Nicolas project, Gloucester and Restigouche counties, New Brunswick, New Brunswick Department of Natural Resources and Energy Information Circular 91-2, 87-100.
- Walker, J. A., D. R. Lentz, and S. H. McClenaghan (2006), The Orvan Brook volcanogenic massive sulfide deposit: anatomy of a highly attenuated massive sulfide system, Bathurst Mining Camp, New Brunswick, *Exploration and Mining Geology*, 15(3-4), 155-176.
- Whitehead, R. E. (1973), Environment of stratiform sulphide deposition; variation in Mn:Fe ratio in host rocks at Heath Steele Mine, New Brunswick, Canada, *Mineralium Deposita*, 8(2), 148-160.
- Winchester, J. A., R. G. Park, and J. G. Holland (1980), The geochemistry of Lewisian semipelitic schists from the Gairloch district, Wester Ross, *Scottish Journal of Geology*, 16, 165-179.
- Zartman, R. E., and B. R. Doe (1981), Plumbotectonics-the model, *Tectonophysics*, 75(1-2), 135-162.

ANNEXE A

Localisation des forages et des affleurements



| <u>Forage</u> | <u>x</u> | <u>y</u> | <u>Direction</u> | <u>Angle</u> | <u>Profondeur (m)</u> |
|---------------|----------|----------|------------------|--------------|-----------------------|
| F06-01 | 281093 | 5283868 | 160 | 45 | 72 |
| F06-02 | 281071 | 5283958 | 145 | 70 | 246 |
| F06-02A | 281071 | 5283958 | 145 | 66 | 390 |
| F06-03 | 281071 | 5283958 | 150 | 55 | 228 |
| F06-04 | 281475 | 5284027 | 340 | 45 | 42 |
| F06-05 | 281479 | 5284016 | 340 | 61 | 70 |
| F06-06 | 281487 | 5284004 | 340 | 70 | 123 |
| F06-07 | 281501 | 5283982 | 340 | 70 | 189 |
| F06-08 | 281328 | 5283886 | 340 | 45 | 132 |
| F06-09 | 281479 | 5284016 | 340 | 64 | 220 |
| F06-10 | 278827 | 5283227 | 160 | 45 | 81 |
| F06-11 | 278825 | 5283230 | 160 | 45 | 41 |
| F06-12 | 278821 | 5283234 | 135 | 45 | 62 |
| F06-13 | 281525 | 5284032 | 340 | 45 | 48 |
| F06-14 | 281568 | 5284053 | 340 | 48 | 51 |
| F06-15 | 281386 | 5284102 | 160 | 55 | 181 |
| F06-16 | 281540 | 5283779 | 340 | 55 | 519 |
| F06-17 | 281039 | 5283891 | 160 | 45 | 129 |
| F07-01 | 281118 | 5283877 | 160 | 45 | 69 |
| F07-02 | 281136 | 5283910 | 160 | 45 | 51 |
| F07-03 | 281141 | 5283887 | 160 | 45 | 162 |
| F07-04 | 281068 | 5283869 | 160 | 45 | 171 |
| F07-05 | 281190 | 5283897 | 160 | 45 | 159 |
| F07-06 | 281367 | 5284067 | 160 | 45 | 149 |
| F07-07 | 281341 | 5284058 | 160 | 55 | 225 |
| F07-08 | 281526 | 5284163 | 160 | 45 | 246 |
| F07-10 | 281397 | 5284079 | 160 | 45 | 279 |
| F07-11 | 281334 | 5283865 | 340 | 60 | 249 |
| F07-12 | 281134 | 5283738 | 340 | 65 | 399 |
| F07-13 | 281100 | 5283855 | 160 | 45 | 106 |
| F07-14 | 281108 | 5283899 | 160 | 45 | 162 |
| F07-15 | 281087 | 5283896 | 160 | 45 | 159 |
| F07-16 | 281102 | 5283922 | 160 | 45 | 129 |
| F07-17 | 281130 | 5283926 | 160 | 45 | 138 |
| F07-18 | 281075 | 5283844 | 160 | 45 | 99 |
| F07-19 | 281062 | 5283894 | 160 | 45 | 153 |
| F07-20 | 281047 | 5283860 | 160 | 45 | 123 |
| F07-21 | 281053 | 5283838 | 160 | 45 | 96 |

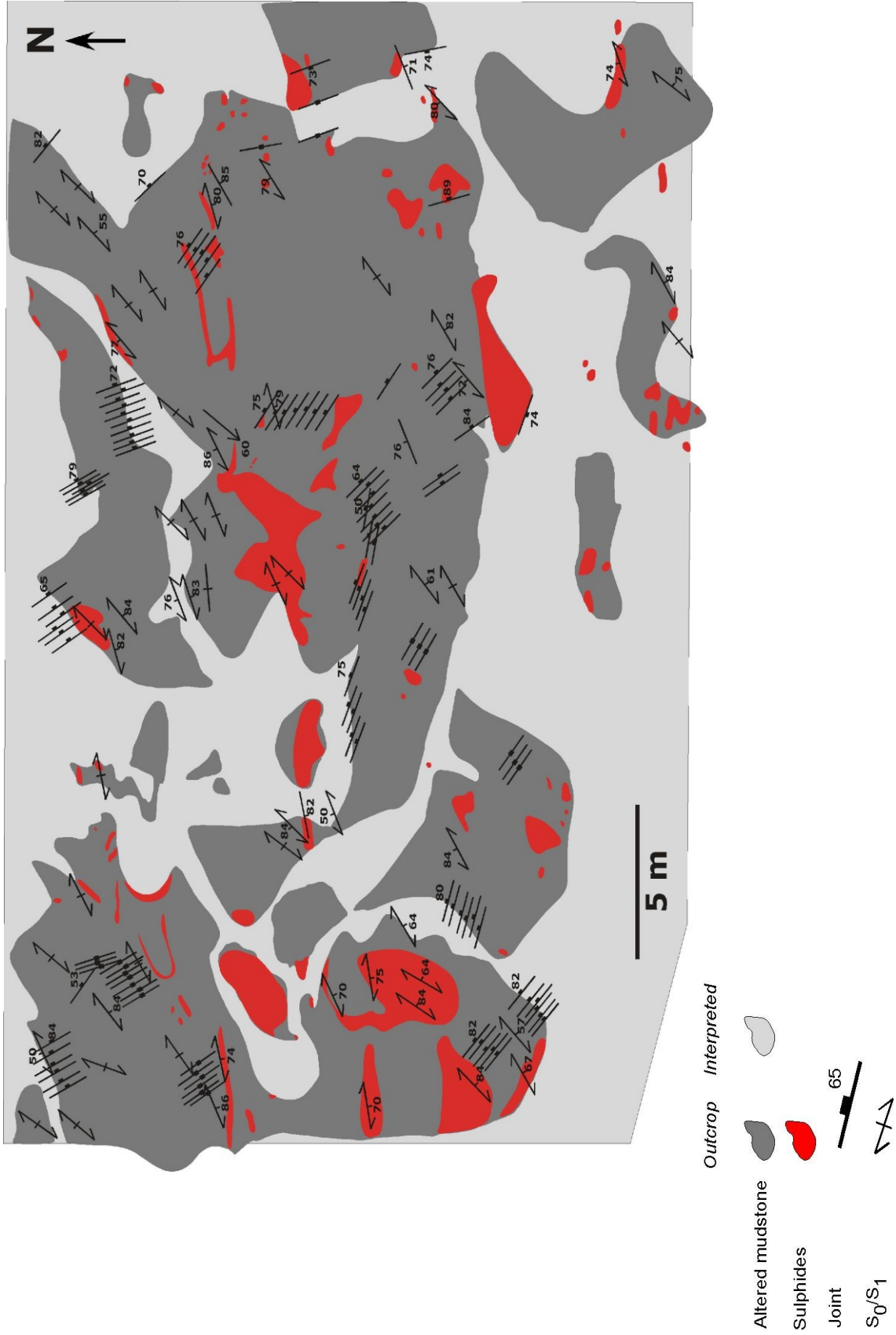
Forage en gras : forage étudié

Forage en police normale : autre forage

| <u>x</u> | <u>y</u> | <u>Affleurement</u> | <u>Formation</u> |
|----------|----------|---------------------|------------------------------|
| 281858 | 5285125 | DB-07-39 | Simpson Field |
| 282857 | 5285307 | DB-07-40 | La Vieille |
| 283029 | 5285388 | DB-07-41 | Simpsons Field ou La Vieille |
| 281330 | 5284173 | DB-07-42 | Simpsons Field |
| 281350 | 5284162 | DB-07-43 | Simpsons Field |
| 281404 | 5284130 | DB-07-44 | Simpsons Field |
| 281409 | 5284106 | DB-07-45 | Simpsons Field |
| 281419 | 5284090 | DB-07-46 | Simpsons Field |
| 281437 | 5284102 | DB-07-47 | Simpsons Field |
| 281406 | 5284173 | DB-07-48 | Simpsons Field |
| 284228 | 5284588 | DB-07-71 | Millstream ou Sormany |
| 284069 | 5284561 | DB-07-72 | Millstream ou Sormany |
| 283912 | 5283935 | DB-07-73 | Millstream |
| 283862 | 5284027 | DB-07-74 | Gabbro siluro-dévonien |
| 283657 | 5284645 | DB-07-75 | Millstream (Pine Tree) |
| 283793 | 5284595 | DB-07-76 | Millstream (Pine Tree) |
| 281340 | 5283826 | DB-07-77 | Millstream (Shaft-Haché) |
| 281386 | 5283875 | DB-07-78 | Millstream (Shaft-Haché) |
| 281403 | 5283833 | DB-07-79 | Millstream (Shaft-Haché) |
| 281336 | 5283775 | DB-07-80 | Gabbro siluro-dévonien |
| 281307 | 5283760 | DB-07-81 | Millstream (Shaft-Haché) |
| 281311 | 5283783 | DB-07-82 | Millstream (Shaft-Haché) |
| 286112 | 5285210 | DB-07-83 | Millstream? |
| 278892 | 5282980 | DB-07-84 | Millstream (Henry) |
| 278893 | 5283062 | DB-07-85 | Millstream (Henry) |

ANNEXE B

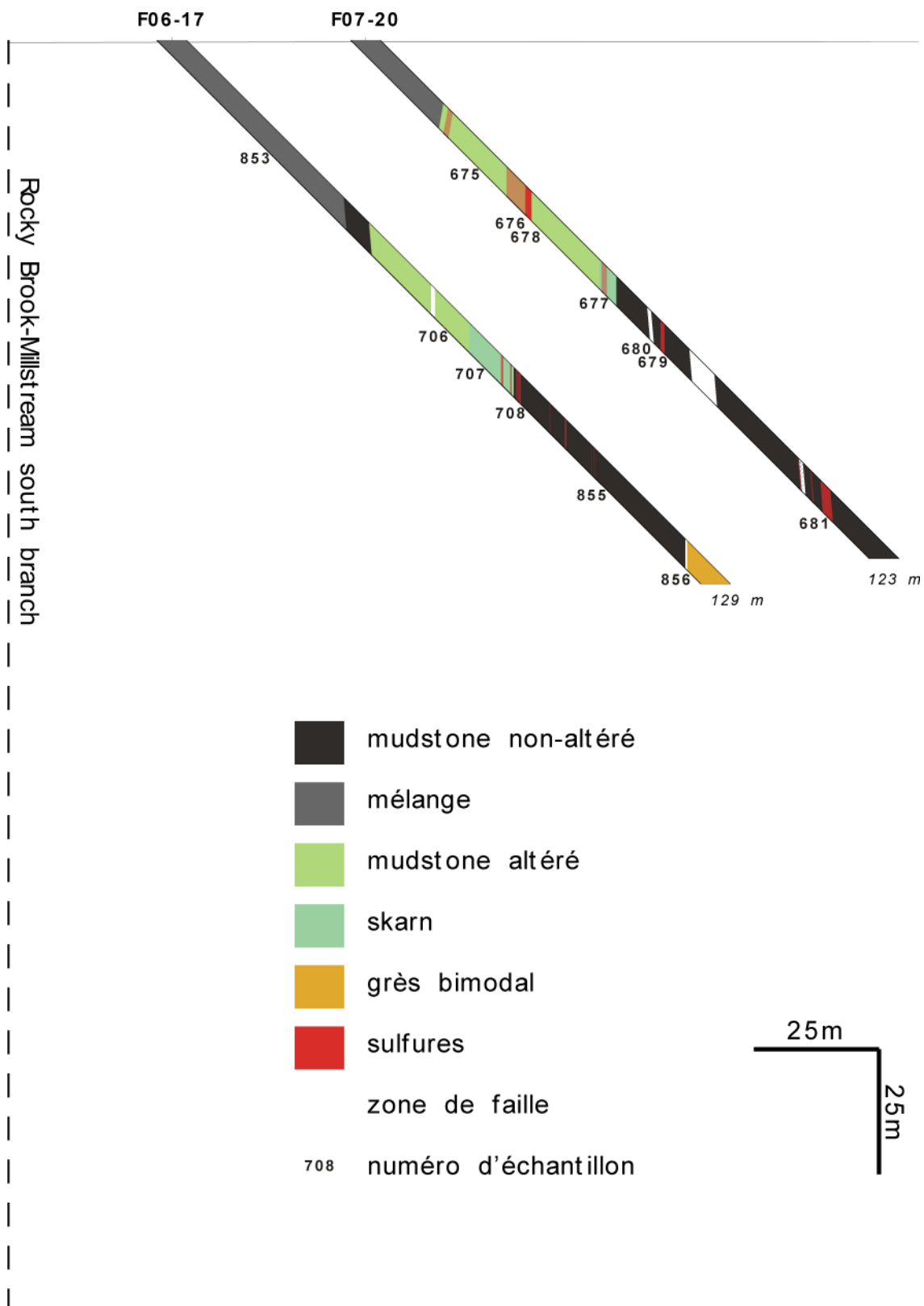
Cartographie de l'indice Shaft



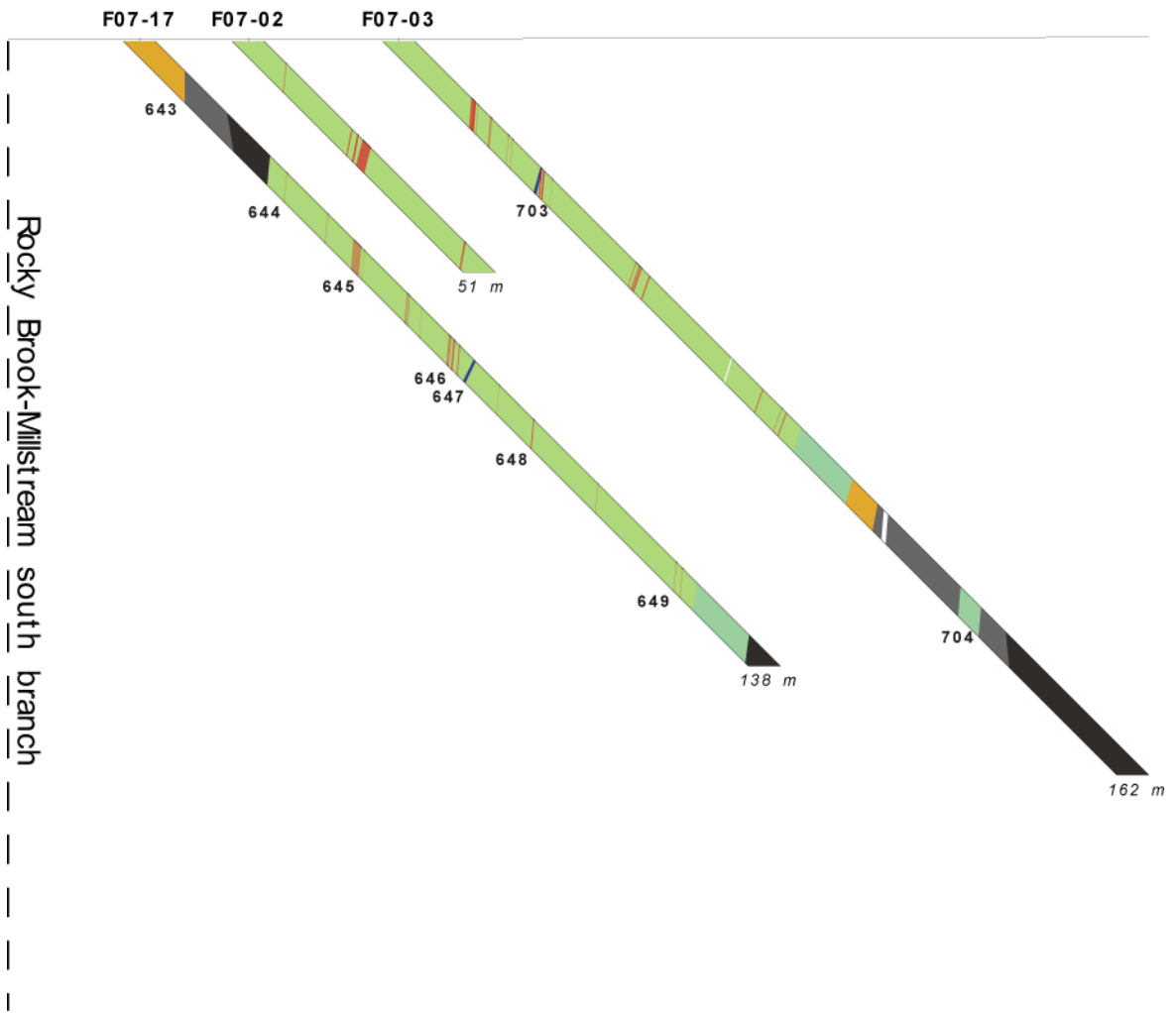
ANNEXE C

Sections de forages

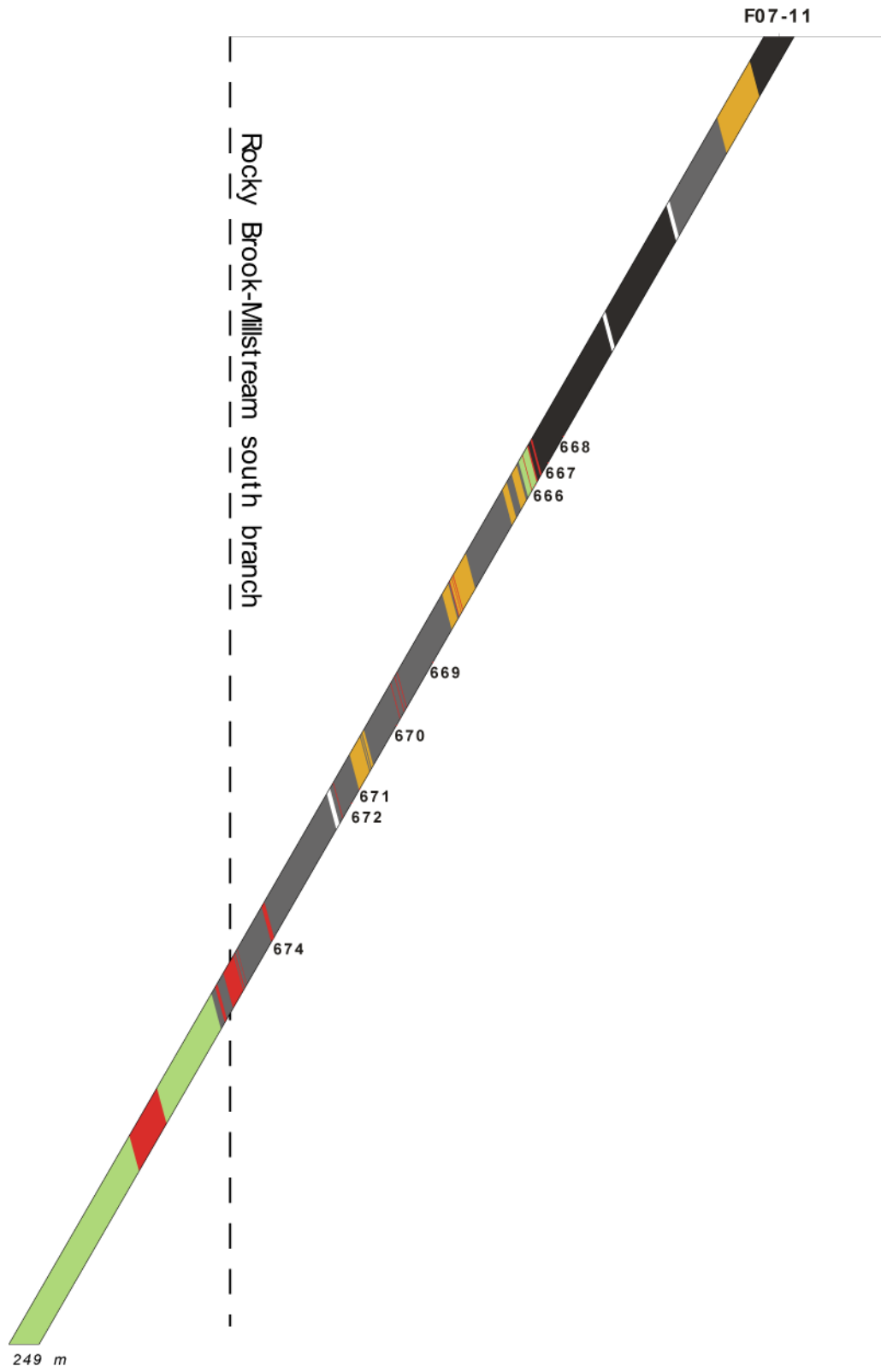
Haché - 50 ouest



Haché - 50 est



Haché - 225 est / Shaft - 185 ouest



ANNEXE D

Liste des échantillons

| <u>Échantillon</u> | <u>Forage</u> | <u>Lentille</u> | <u>De</u> | <u>À</u> | <u>Lithologie</u> | <u>Sulfures</u> |
|--------------------|---------------|-----------------|-----------|----------|-------------------|-----------------|
| 451601 | F07-15 | Haché | 9.36 | 9.51 | mudstone | |
| 451602 | F07-15 | Haché | 9.0 | 9.15 | mudstone f-alt | |
| 451603 | F07-15 | Haché | 10.42 | 10.46 | mudstone | |
| 451604 | F07-15 | Haché | 14.13 | 14.32 | mélange m-alt | |
| 451605 | F07-15 | Haché | 15.7 | 15.9 | mélange | |
| 451606 | F07-15 | Haché | 21.0 | 21.22 | mélange m-alt | |
| 451607 | F07-15 | Haché | 22.17 | 22.32 | mélange | |
| 451608 | F07-15 | Haché | 24.65 | 25.45 | mudstone f-alt | |
| 451609 | F07-15 | Haché | 26.48 | 26.68 | mudstone f-alt | |
| 451610 | F07-15 | Haché | 27.8 | 28.28 | mudstone f-alt | |
| 451611 | F07-15 | Haché | 35.0 | 35.25 | mélange alt | |
| 451612 | F07-15 | Haché | 35.25 | 35.45 | mélange alt | SSM |
| 451613 | F07-15 | Haché | 37.3 | 37.6 | skarn | SD |
| 451614 | F07-15 | Haché | 37.9 | 38.2 | skarn | SD |
| 451615 | F07-15 | Haché | 39.85 | 39.97 | mudstone t-alt | SD |
| 451616 | F07-15 | Haché | 41.15 | 41.55 | mudstone m-alt | SD |
| 451617 | F07-15 | Haché | 49.75 | 49.85 | mudstone m-alt | SD |
| 451618 | F07-15 | Haché | 51.45 | 51.75 | mélange | SD |
| 451619 | F07-15 | Haché | 58.7 | 58.95 | mudstone t-alt | |
| 451620 | F07-15 | Haché | 62.18 | 62.27 | mélange alt | SD |
| 451621 | F07-15 | Haché | 63.1 | 63.2 | mélange alt | SSM |
| 451622 | F07-15 | Haché | 66.9 | 67.1 | mélange alt | SSM |
| 451623 | F07-15 | Haché | 68.0 | 68.1 | mudstone f-alt | SD |
| 451624 | F07-15 | Haché | 68.65 | 68.75 | mudstone f-alt | SD |
| 451625 | F07-15 | Haché | 71.3 | 71.48 | mélange alt | SSM |
| 451626 | F07-15 | Haché | 71.8 | 71.9 | mélange | SSM |
| 451627 | F07-15 | Haché | 72.14 | 72.28 | sulfures | SM |
| 451628 | F07-15 | Haché | 74.1 | 74.2 | mudstone | SSM |
| 451629 | F07-15 | Haché | 78.0 | 78.1 | mudstone | SD |
| 451630 | F07-15 | Haché | 78.4 | 78.5 | mudstone | SSM |
| 451631 | F07-15 | Haché | 79.1 | 79.2 | mélange | SSM |
| 451632 | F07-15 | Haché | 94.55 | 94.75 | mélange alt à | SSM |
| 451634 | F07-15 | Haché | 127.1 | 127.25 | mudstone t-alt | |
| 451635 | F07-15 | Haché | 133.37 | 133.45 | mudstone alt | |
| 451636 | F07-15 | Haché | 139.4 | 139.55 | mélange | |
| 451637 | F07-15 | Haché | 141.3 | 141.4 | mélange | |
| 451638 | F07-15 | Haché | 140.65 | 140.75 | mudstone alt | |
| 451639 | F07-15 | Haché | 144.4 | 144.5 | grès | |
| 451640 | F07-15 | Haché | 145.7 | 145.8 | grès | SD |
| 451641 | F07-15 | Haché | 152.25 | 152.4 | grès | SSM |
| 451643 | F07-17 | Haché | 12.55 | 12.65 | grès | |
| 451644 | F07-17 | Haché | 35.3 | 35.4 | mélange alt | SSM |
| 451645 | F07-17 | Haché | 51.7 | 51.8 | mudstone alt | SSM |
| 451646 | F07-17 | Haché | 72.55 | 72.65 | sulfures | SM |
| 451647 | F07-17 | Haché | 75.4 | 75.5 | cendres (?) | |
| 451648 | F07-17 | Haché | 89.9 | 90.0 | sulfures | SM |

| | | | | | | |
|--------|--------|-------|--------|--------|-------------------------|-----|
| 451649 | F07-17 | Haché | 121.2 | 121.4 | mudstone alt | SSM |
| 451650 | F07-10 | Shaft | 8.00 | 8.05 | grès | SD |
| 451651 | F07-10 | Shaft | 21.8 | 21.9 | mélange | |
| 451652 | F07-10 | Shaft | 57.1 | 57.2 | mudstone alt | SSM |
| 451653 | F07-10 | Shaft | 78.45 | 78.6 | mélange alt | SSM |
| 451654 | F07-10 | Shaft | 138.7 | 138.8 | grès | |
| 451655 | F07-10 | Shaft | 206.5 | 206.6 | mudstone | |
| 451656 | F07-10 | Shaft | 220.0 | 220.1 | siltstone alt | SD |
| 451657 | | | | | mélange de Belledune | |
| 451658 | | | | | Cullinan | |
| 451659 | F07-10 | Shaft | 224.7 | 224.8 | mudstone | SD |
| 451660 | F07-10 | Shaft | 233.1 | 233.2 | grès et mudstone | |
| 451661 | F07-10 | Shaft | 244.45 | 244.55 | grès alt | |
| 451662 | F07-10 | Shaft | 95.7 | 95.8 | mélange alt | SSM |
| 451663 | F07-13 | Haché | 33.4 | 33.5 | mélange alt | SSM |
| 451664 | F07-13 | Haché | 41.85 | 41.90 | mudstone alt | SSM |
| 451665 | F07-13 | Haché | 58.4 | 58.5 | skarn | SSM |
| 451666 | F07-11 | Haché | 85.4 | 85.5 | mudstone t-alt | |
| 451667 | F07-11 | Haché | 81.1 | 81.2 | mudstone | |
| 451668 | F07-11 | Haché | 76.1 | 76.2 | mudstone (fluorite?) | |
| 451669 | F07-11 | Haché | 119.1 | 119.2 | mudstone alt silicifié | |
| 451670 | F07-11 | Haché | 131.1 | 131.2 | mudstone | SD |
| 451671 | F07-11 | Haché | 143.2 | 143.3 | mudstone | |
| 451672 | F07-11 | Haché | 145.9 | 146.0 | mudstone | SSM |
| 451674 | F07-11 | Haché | 171.7 | 171.9 | mélange alt | SSM |
| 451675 | F07-20 | Haché | 29.4 | 29.5 | mélange alt à skarn | SSM |
| 451676 | F07-20 | Haché | 42.2 | 42.3 | mélange alt | SM |
| 451677 | F07-20 | Haché | 60.1 | 60.2 | skarn | SD |
| 451678 | F07-20 | Haché | 42.5 | 42.6 | sulfures | SM |
| 451679 | F07-20 | Haché | 73.9 | 74.0 | mudstone | SSM |
| 451680 | F07-20 | Haché | 72.4 | 72.5 | mudstone | |
| 451681 | F07-20 | Haché | 112.2 | 112.3 | mudstone | SSM |
| 451682 | F07-12 | Haché | 20.7 | 20.8 | mélange alt | |
| 451683 | F07-12 | Haché | 109.95 | 110.05 | mudstone | |
| 451684 | F07-12 | Haché | 144.1 | 144.2 | mudstone | SSM |
| 451685 | F07-12 | Haché | 179.7 | 179.8 | grès | SD |
| 451696 | | | | | Zarina | |
| 451701 | F07-12 | Haché | 198.3 | 198.4 | cornéenne | |
| 451702 | F07-12 | Haché | 382.7 | 382.8 | mud t-alt | |
| 451703 | F07-03 | Haché | 35.0 | 35.1 | skarn | SSM |
| 451704 | F07-03 | Haché | 129.9 | 130.0 | mud t-alt | SD |
| 451705 | F07-03 | Haché | 132.1 | 132.2 | mudstone t-alt | SD |
| 451706 | F06-17 | Haché | 67.95 | 68.05 | mélange alt à skarn | |
| 451707 | F06-17 | Haché | 76.9 | 77.0 | skarn | |
| 451708 | F06-17 | Haché | 86.1 | 86.2 | mélange alt | SSM |
| 451709 | F06-07 | Shaft | 50.2 | 50.3 | skarn | |
| 451710 | F06-07 | Shaft | 62.8 | 62.9 | mélange silicifié | |
| 451711 | F06-07 | Shaft | 66.1 | 66.2 | mélange | SSM |
| 451712 | F06-07 | Shaft | 111.85 | 111.9 | skarn | SD |

| | | | | | | |
|--------|--------|-------|--------|--------|-----------------------|-----|
| 451713 | F06-07 | Shaft | 121.2 | 121.3 | skarn à mud alt | SSM |
| 451714 | F06-07 | Shaft | 169.5 | 169.6 | mélange alt | SSM |
| 451715 | F06-07 | Shaft | 177.05 | 177.15 | mélange bréchiq | SSM |
| 451716 | F06-06 | Shaft | 72.4 | 72.5 | mélange alt | SSM |
| 451717 | F06-06 | Shaft | 119.5 | 119.6 | skarn | SSM |
| 451718 | F06-15 | Shaft | 18.3 | 18.4 | siltstone t-alt | |
| 451719 | F06-15 | Shaft | 55.6 | 55.7 | mélange | |
| 451720 | F06-15 | Shaft | 92.1 | 92.2 | mudstone | |
| 451721 | F06-15 | Shaft | 121.0 | 121.1 | mélange alt | |
| 451722 | F06-15 | Shaft | 142.6 | 142.7 | mudstone | SM |
| 451723 | F06-15 | Shaft | 147.3 | 147.4 | mudstone | SM |
| 451724 | F06-15 | Shaft | 148.35 | 148.5 | mudstone | SM |
| 451725 | F06-15 | Shaft | 170.5 | 170.6 | cornéenne (?) | |
| 451726 | F07-08 | Shaft | 46.9 | 47.0 | gabbro | SD |
| 451727 | F07-08 | Shaft | 130.3 | 130.4 | skarn | SSM |
| 451728 | F07-08 | Shaft | 174.15 | 174.23 | mudstone | SSM |
| 451729 | F07-08 | Shaft | 239.6 | 239.7 | grès | SD |
| 451730 | F06-01 | Haché | 36.9 | 37.0 | mélange alt | SD |
| 451731 | F06-01 | Haché | 46.5 | 46.6 | sulfures | SM |
| 451732 | F06-01 | Haché | 46.7 | 46.8 | mudstone | SSM |
| 451733 | F06-16 | Shaft | 22.2 | 22.3 | mudstone | SD |
| 451734 | F06-16 | Shaft | 36.2 | 36.3 | mudstone | |
| 451735 | F06-16 | Shaft | 53.2 | 53.3 | gabbro | |
| 451736 | F06-16 | Shaft | 105.6 | 105.7 | mélange bréchiq | |
| 451737 | F06-16 | Shaft | 136.4 | 136.45 | mélange alt silicifié | |
| 451738 | F06-16 | Shaft | 288.0 | 288.05 | gabbro (?) | |
| 451739 | F06-16 | Shaft | 354.0 | 354.1 | grès | |
| 451740 | F06-16 | Shaft | 368.35 | 368.5 | mudstone | SD |
| 451741 | F06-16 | Shaft | 401.95 | 402.05 | skarn | SD |
| 451742 | F06-16 | Shaft | 409.65 | 409.8 | skarn | SSM |
| 451743 | F06-16 | Shaft | 516.0 | 516.1 | mudstone f-alt | |
| 451744 | F06-09 | Shaft | 65.9 | 66.9 | grès ou intrusif | |
| 451745 | F06-03 | Haché | 32.65 | 32.75 | cornéenne | SD |
| 451746 | F06-03 | Haché | 30.6 | 30.7 | skarn | SD |
| 451747 | F06-03 | Haché | 59.9 | 60.0 | mudstone alt | SD |
| 451748 | F06-03 | Haché | 108.0 | 108.2 | mudstone | SD |
| 451749 | F06-03 | Haché | 145.1 | 145.2 | mélange alt | SSM |
| 451750 | F06-12 | Henry | 50.4 | 50.5 | mélange | SSM |
| 451751 | | | | | Nigadoo | |
| 451752 | | | | | Millstream Iron | |
| 451753 | F08-28 | Haché | 343.4 | 363.4 | mudstone altéré | |
| 451754 | F08-68 | Haché | 91.6 | 91.7 | sulfures | SM |
| 451755 | | | | | Nigadoo | |
| 451756 | | | | | Turgeon | |
| 422853 | F06-17 | Haché | 25.6 | 25.7 | mélange f-alt | |
| 422855 | F06-17 | Haché | 105.6 | 105.7 | mudstone | |
| 422856 | F06-17 | Haché | 125.6 | 125.7 | grès | SD |
| 422857 | F07-13 | Haché | 88.8 | 88.9 | mélange | |

Abbéviations

f-alt : faiblement altéré

m-alt : moyennement altéré

t-alt : fortement altéré

SM : sulfures massifs

SSM : sulfures semi-massifs

SD : sulfures dissiminés

ANNEXE E

Analyses isotopiques du soufre

| <u>No. échantillon</u> | <u>Indice</u> | <u>Minéral</u> | <u>Delta 34S cdt</u> | <u>%S</u> |
|------------------------|----------------|-------------------|----------------------|--------------|
| 451708-1 | Haché | pyrrhotite | 3,2 | 26,78 |
| 451676-1 | Haché | pyrrhotite | 3,08 | 29,2 |
| 451616-1 | Haché | pyrrhotite | 2,72 | 26,55 |
| 451630-3 | Haché | pyrrhotite | 3,6 | 27,79 |
| 451625-3 | Haché | pyrrhotite | 3,1 | 24,05 |
| 451622-2 | Haché | pyrrhotite | 3,91 | 34,27 |
| 451663-2 | Haché | pyrrhotite | 3,53 | 25,48 |
| 451663-2 QCDuplicate | | | 3,71 | 24,46 |
| 451665-1 | Haché | pyrrhotite | 3,23 | 15,97 |
| 451641 | Haché | pyrrhotite | 2,79 | 15,63 |
| 451674-1 | Haché | pyrrhotite | 2,66 | 31,54 |
| <i>N751-2c</i> | <i>Nigadoo</i> | <i>pyrrhotite</i> | <i>9,47</i> | <i>40,35</i> |
| 451731-1 | Haché | sphalérite | 1,76 | 31,83 |
| 451676-2 | Haché | sphalérite | 2,66 | 30,11 |
| 451675-1 | Haché | sphalérite | 3,24 | 22,29 |
| 451679-3 | Haché | sphalérite | 4,31 | 28,82 |
| 451613-1 | Haché | sphalérite | 3,21 | 48,84 |
| 451619-1 | Haché | sphalérite | 2,25 | 16,45 |
| 451619-1 QCDuplicate | | | 2,34 | 15,65 |
| 451630-2 | Haché | sphalérite | 1,37 | 31,64 |
| 451625-4 | Haché | sphalérite | 3,07 | 28,61 |
| 451632-1 | Haché | sphalérite | 3,13 | 32,89 |
| 451732-2 | Haché | sphalérite | 1,68 | 27,96 |
| 451663-3 | Haché | sphalérite | 3,76 | 32,89 |
| 451665-2 | Haché | sphalérite | 3,06 | 32,37 |
| 451665-4 | Haché | sphalérite | 2,83 | 28,92 |
| 451685-2 | Haché | sphalérite | 3,38 | 33,63 |
| 451644-2 | Haché | sphalérite | 2,38 | 22,52 |
| 451648-1 | Haché | sphalérite | 3,07 | 28,24 |
| 451648-1 QCDuplicate | | | 2,96 | 27,06 |
| 451703-2 | Haché | sphalérite | 1,31 | 25,96 |
| 451674-3 | Haché | sphalérite | 2,84 | 30,11 |
| 451856-3 | Haché | sphalérite | 3,59 | 32,07 |
| 451708-2 | Haché | galène | 1,94 | 14,49 |
| 451856-2 | Haché | galène | 3,51 | 23,3 |
| 451679-1 | Haché | galène | 2,24 | 15,5 |
| 451625-1 | Haché | galène | 2,11 | 19,54 |
| 451732-3 | Haché | galène | 3,57 | 15,8 |
| 451648-3 | Haché | galène | 2,63 | 18 |
| 451856-1 | Haché | pyrite | 3,42 | 52,41 |
| 451731-2 | Haché | pyrite | 2,94 | 48,99 |
| 451675-2 | Haché | pyrite | 2,71 | 47,99 |
| 451679-2 | Haché | pyrite | 4,79 | 51,8 |
| 451601 | Haché | pyrite | 3,58 | 47,07 |
| 451616-2 | Haché | pyrite | 2,36 | 42,66 |
| 451613-2 | Haché | pyrite | 2,83 | 46,57 |

| | | | | |
|----------------------|---------|--------------|------|-------|
| 451622-1 | Haché | pyrite | 3,51 | 49,02 |
| 451632-2 | Haché | pyrite | 3,07 | 50,29 |
| 451663-4 | Haché | pyrite | 3,43 | 53,85 |
| 451663-4 QCDuplicate | | | 3,43 | 52,91 |
| 451665-3 | Haché | pyrite | 2,74 | 52,19 |
| 451685-1 | Haché | pyrite | 0,85 | 44,1 |
| 451644-3 | Haché | pyrite | 2,33 | 39,16 |
| 451648-2 | Haché | pyrite | 3,27 | 42,87 |
| 451703-1 | Haché | pyrite | 2,01 | 44,22 |
| 451625-5 | Haché | pyrite | 3,24 | 49,65 |
| 451630-1 | Haché | arsénopyrite | 3,91 | 22,06 |
| 451625-2 | Haché | arsénopyrite | 3,48 | 27,5 |
| 451732-1 | Haché | arsénopyrite | 3,12 | 23,22 |
| 451732-1 QCDuplicate | | | 3,1 | 22,97 |
| 451663-1 | Haché | arsénopyrite | 3,56 | 26,9 |
| 451644-1 | Haché | arsénopyrite | 2,74 | 23,37 |
| 451674-2 | Haché | arsénopyrite | 3,12 | 13,25 |
| 451717-1 | Shaft | galène | 1,22 | 12,99 |
| 451724-1 | Shaft | pyrrhotite | 2,45 | 23,05 |
| 451724-2 | Shaft | pyrite | 2,28 | 47,32 |
| 451727-1 | Shaft | pyrrhotite | 2,8 | 36,37 |
| 451753-1 | Haché | sphalérite | 2,47 | 28,2 |
| 451753-1 QCDuplicate | | | 2,64 | 30,22 |
| N755-1 | Nigadoo | sphalérite | 2 | 30,97 |
| N755-2 | Nigadoo | arsénopyrite | 1,36 | 23,1 |
| T756-1 | Turgeon | pyrite | 6,99 | 54,34 |
| T756-2 | Turgeon | pyrite | 6,87 | 47,88 |

ANNEXE F
Lithogéochimie

| Unit Symbol | SiO2 | Al2O3 | Fe2O3(T) | MnO | MgO | CaO | Na2O | K2O | TiO2 | P2O5 | LOI | Total |
|-----------------|-------|-------|----------|-------|-------|-------|------|------|-------|------|-------|-------|
| Detection Limit | % | % | % | % | % | % | % | % | % | % | % | % |
| 451667 | 0.01 | 0.01 | 0.01 | 0.001 | 0.01 | 0.01 | 0.01 | 0.01 | 0.001 | 0.01 | | 0.01 |
| 422857 | 66 | 15,41 | 4,46 | 0,079 | 2,19 | 1,6 | 0,1 | 4,86 | 0,588 | 0,12 | 5,31 | 100,7 |
| 422855 | 56,54 | 19,48 | 8,32 | 0,16 | 2,97 | 0,4 | 0,8 | 4,52 | 0,76 | 0,1 | 4,64 | 98,68 |
| 451670 | 57,84 | 17,44 | 9,38 | 0,393 | 3,5 | 0,78 | 0,12 | 4,11 | 0,985 | 0,12 | 5,33 | 100 |
| 451748 | 57,84 | 15,1 | 8,74 | 0,29 | 2,35 | 2,46 | 0,16 | 4,17 | 0,75 | 0,1 | 6,87 | 98,83 |
| 422858 | 53,81 | 22,1 | 6,63 | 0,051 | 2,5 | 0,34 | 1,36 | 4,95 | 0,851 | 0,11 | 5,8 | 98,49 |
| 422851 | 66,22 | 13,98 | 4,71 | 0,102 | 3,2 | 4,38 | 0,82 | 2,28 | 0,598 | 0,1 | 3,01 | 99,4 |
| 451608 | 65,51 | 11,24 | 6,87 | 0,153 | 5,07 | 0,76 | 0,05 | 2,68 | 0,494 | 0,06 | 6,03 | 98,92 |
| 451730 | 61,62 | 12,79 | 5,69 | 0,231 | 5,98 | 5,33 | 0,62 | 2,78 | 0,57 | 0,12 | 3,06 | 98,78 |
| 422853 | 60,85 | 14,61 | 4,79 | 0,16 | 3,64 | 4,58 | 1,17 | 4,05 | 0,614 | 0,16 | 4,26 | 98,89 |
| 451747 | 61,93 | 17,96 | 5,1 | 0,095 | 3,57 | 1,38 | 0,55 | 4,69 | 0,748 | 0,23 | 4,69 | 100,9 |
| 451746 | 60,89 | 15,2 | 4,47 | 0,206 | 3,91 | 5,36 | 0,8 | 4,34 | 0,678 | 0,13 | 2,59 | 98,58 |
| 451745 | 43,29 | 14,92 | 11,03 | 0,313 | 6,82 | 6,05 | 0,18 | 6,2 | 0,578 | 0,09 | 10,11 | 99,58 |
| 422861 | 57,33 | 14,19 | 8,68 | 0,17 | 5,33 | 3,43 | 1,46 | 2,97 | 0,675 | 0,12 | 5,18 | 99,52 |
| 451613 | 59,31 | 11,97 | 6,32 | 0,211 | 7,3 | 8,13 | 0,96 | 1,88 | 0,473 | 0,16 | 2,17 | 98,89 |
| 451707 | 46,27 | 6,14 | 12,82 | 0,839 | 12,16 | 12,68 | 0,68 | 0,6 | 0,293 | 0,11 | 7,1 | 99,7 |
| 451703 | 48,82 | 6,64 | 7,82 | 0,847 | 10,49 | 16,47 | 1,87 | 0,28 | 0,274 | 0,06 | 5,2 | 98,77 |
| 451683 | 67,46 | 7,15 | 6,54 | 0,399 | 4,53 | 3,88 | 0,62 | 3,35 | 0,271 | 0,07 | 5,93 | 100,2 |
| 451640 | 43,35 | 10,57 | 18,61 | 0,404 | 10,74 | 8,96 | 0,56 | 1,57 | 0,387 | 0,06 | 4,7 | 99,93 |
| 451639 | 73,77 | 11,83 | 4,14 | 0,116 | 1,31 | 1,81 | 2,18 | 2,59 | 0,792 | 0,14 | 1,68 | 100,4 |
| 422860 | 74 | 12,12 | 4,68 | 0,042 | 1,26 | 0,25 | 2,09 | 2,31 | 0,903 | 0,14 | 2,34 | 100,1 |
| 451856 | 73,98 | 12,74 | 3,37 | 0,103 | 1,21 | 0,4 | 0,23 | 4,1 | 0,701 | 0,15 | 3,08 | 100,1 |
| 451647 | 72,75 | 12,37 | 4,52 | 0,081 | 1,18 | 0,58 | 1,16 | 3,07 | 0,773 | 0,11 | 3,24 | 99,84 |
| | 37,42 | 17,46 | 17,38 | 0,509 | 8,16 | 1,31 | 0,09 | 5 | 2,659 | 0,61 | 9,46 | 100,1 |

| <i>Unit Symbol Detection Limit</i> | Au ppb | Ag ppm | As ppm | Ba ppm | Be ppm | Bi ppm | Br ppm | Cd ppm | Co ppm | Cr ppm | Cs ppm | Cu ppm | Ga ppm | Ge ppm | Hf ppm |
|--|-----------|-----------|-----------|-----------|-----------|-----------|-----------|-----------|-----------|-----------|-----------|-----------|-----------|-----------|-----------|
| 451667 | 12 | 1 | 58 | 583 | 3 | <0.1 | <0.5 | 1.4 | 29 | 105 | 8 | 50 | 26 | 1.8 | 2.3 |
| 422857 | <1 | 0.5 | 20 | 603 | 3 | 0.3 | <0.5 | 0.5 | 25.6 | 119 | 5.9 | 43 | 27 | 2.3 | 3 |
| 422855 | <1 | 0.6 | 30 | 563 | 2 | 0.3 | <0.5 | 0.6 | 27.9 | 93.9 | 5.6 | 52 | 26 | 2.4 | 4.1 |
| 451670 | 8 | 7.7 | 223 | 800 | 3 | 1.9 | <0.5 | 25.2 | 41.7 | 112 | 6.2 | 101 | 23 | 2 | 3.6 |
| 451748 | <1 | <0.5 | 33 | 817 | 3 | 0.4 | 1.8 | 0.8 | 33.4 | 186 | 6.5 | 51 | 31 | 1.9 | 4.3 |
| 422858 | <1 | <0.5 | 5 | 224 | 3 | <0.1 | 1.8 | <0.5 | 9.5 | 139 | 7 | 18 | 19 | 1.6 | 2.9 |
| 422851 | <1 | 3.3 | 42 | 261 | 3 | <0.1 | 1.7 | 1.1 | 17.2 | 127 | 7.9 | 95 | 18 | 1.4 | 2.3 |
| 451608 | 9 | <0.5 | 30 | 772 | 2 | 0.1 | <0.5 | <0.5 | 12.6 | 119 | 5.2 | 39 | 18 | 2.6 | 2.9 |
| 451730 | 18 | 2.4 | 186 | 673 | 3 | 0.1 | 1.4 | 5.5 | 15.9 | 151 | 4.8 | 87 | 20 | 1.6 | 2.7 |
| 422853 | <1 | 0.6 | 27 | 796 | 2 | 0.4 | 1 | <0.5 | 21.7 | 146 | 6.9 | 44 | 25 | 1.9 | 3.7 |
| 451747 | 219 | <0.5 | 2460 | 636 | 3 | 0.4 | <0.5 | 0.6 | 29.4 | 144 | 7.4 | 48 | 21 | 2 | 2.8 |
| 451746 | 22 | 0.8 | 2310 | 975 | 1 | 0.9 | <0.5 | <0.5 | 15.9 | 47.6 | 0.8 | 2 | 25 | 2 | 5.1 |
| 451745 | <1 | <0.5 | 379 | 476 | 2 | 0.3 | <0.5 | <0.5 | 15.8 | 93.6 | 3.4 | 24 | 23 | 1.8 | 4.6 |
| 422861 | <1 | <0.5 | 18 | 423 | 2 | <0.1 | <0.5 | 0.8 | 14.3 | 84.6 | 6.1 | 13 | 17 | 1.8 | 2.4 |
| 451613 | 20 | 4.1 | 3 | 155 | 2 | 1 | <0.5 | 187 | 11.6 | 50.3 | 1.7 | 155 | 16 | 2.1 | 2 |
| 451707 | <1 | 0.5 | 1 | 43 | 2 | 0.2 | <0.5 | 4.3 | 2.2 | 70.2 | 5.7 | 2 | 13 | 3.1 | 1.6 |
| 451703 | 34 | 5.4 | 20 | 332 | 2 | 0.1 | <0.5 | 448 | 11.3 | 46.8 | 1.2 | 46 | 25 | <0.5 | 1.2 |
| 451683 | <1 | 2.5 | 61 | 115 | 1 | 0.7 | <0.5 | 2 | 64.8 | 320 | 5.9 | 327 | 14 | 3.1 | 0.7 |
| 451640 | 25 | <0.5 | 7 | 339 | 1 | <0.1 | <0.5 | <0.5 | 9.4 | 76.8 | 5.5 | 14 | 17 | 1.6 | 9.6 |
| 451639 | <1 | <0.5 | 4 | 285 | 1 | 0.1 | <0.5 | <0.5 | 9.2 | 74.4 | 2.7 | 14 | 16 | 1.5 | 10.9 |
| 422860 | <1 | <0.5 | 9 | 517 | 2 | <0.1 | <0.5 | <0.5 | 9.4 | 67.2 | 6.6 | 18 | 17 | 1.4 | 8.2 |
| 451856 | <1 | 1.2 | 70 | 545 | 2 | 0.2 | <0.5 | 5.6 | 12.1 | 93 | 3.8 | 45 | 18 | 1.7 | 9.5 |
| 451647 | 25 | 2.6 | 238 | 209 | 8 | <0.1 | <0.5 | 0.9 | 13.1 | 148 | 13.3 | 38 | 34 | 1.9 | 4.8 |

| Unit Symbol | Hg | In | Ir | Mo | Nb | Ni | Pb | Rb | S | Sb | Sc | Se | Sn | Sr | Ta | Th |
|-----------------|-----|-------|-----|-----|------|-----|------|-----|-------|------|------|-------|-----|-----|-------|------|
| Detection Limit | ppm | ppm | ppb | ppm | ppm | ppm | ppm | ppm | % | ppm | ppm | ppm | ppm | ppm | ppm | ppm |
| 451667 | < 1 | 0.1 | 1 | 2 | 0.2 | 1 | 5 | 2 | 0.001 | 0.1 | 0.01 | 0.5 | 1 | 2 | 0.1 | 0.05 |
| 422857 | < 1 | < 0.1 | < 1 | 29 | 11.4 | 59 | 45 | 195 | 0.917 | 7.8 | 14.3 | < 0.5 | 6 | 45 | 0.6 | 10.4 |
| 422855 | < 1 | < 0.1 | < 1 | < 2 | 15.7 | 53 | 23 | 158 | 0.376 | 4.7 | 19.9 | < 0.5 | 3 | 51 | 1.1 | 14.5 |
| 451670 | < 1 | < 0.1 | < 1 | < 2 | 18.9 | 61 | 12 | 136 | 0.954 | 5.5 | 20.3 | < 0.5 | 8 | 30 | 1.4 | 14.7 |
| 451748 | < 1 | 0.2 | < 1 | < 2 | 15.9 | 70 | 2690 | 145 | 2.33 | 10.8 | 20.6 | < 0.5 | 11 | 31 | 1.2 | 13.5 |
| 422858 | < 1 | < 0.1 | < 1 | 6 | 14 | 80 | 28 | 184 | 1.16 | 1 | 25 | < 0.5 | 3 | 90 | 1 | 16.2 |
| 422851 | < 1 | < 0.1 | < 1 | 12 | 11.1 | 46 | 14 | 105 | 0.309 | 4.2 | 16.6 | < 0.5 | 2 | 145 | 0.7 | 10.8 |
| 451608 | < 1 | < 0.1 | < 1 | 8 | 9.3 | 59 | 99 | 110 | 1.28 | 27.6 | 14.3 | < 0.5 | 17 | 25 | 0.6 | 8.65 |
| 451730 | < 1 | < 0.1 | < 1 | 6 | 10.6 | 36 | 21 | 94 | 0.423 | 5.1 | 14.3 | < 0.5 | 14 | 157 | 0.7 | 10.8 |
| 422853 | < 1 | < 0.1 | < 1 | 6 | 11 | 53 | 231 | 114 | 1.24 | 7.8 | 17.1 | < 0.5 | 23 | 186 | 0.7 | 11 |
| 451747 | < 1 | < 0.1 | < 1 | 4 | 11.8 | 51 | 5 | 160 | 0.471 | 2.1 | 18.6 | < 0.5 | 4 | 109 | 0.9 | 13.6 |
| 451746 | < 1 | < 0.1 | < 1 | 8 | 11.7 | 62 | 27 | 136 | 0.831 | 6 | 16.1 | < 0.5 | 8 | 176 | 0.8 | 11.6 |
| 451745 | < 1 | < 0.1 | < 1 | 4 | 11.3 | 10 | 12 | 137 | 2.62 | 24.8 | 12.1 | < 0.5 | 10 | 104 | 0.7 | 7.4 |
| 422861 | < 1 | < 0.1 | < 1 | < 2 | 11.5 | 33 | 8 | 108 | 1.95 | 3.1 | 15.7 | < 0.5 | 4 | 137 | 0.8 | 8.88 |
| 451613 | < 1 | 1.2 | < 1 | 4 | 4.6 | 82 | 403 | 16 | 0.104 | 3.2 | 11.8 | < 0.5 | 4 | 183 | 0.5 | 7.95 |
| 451707 | < 1 | 0.2 | < 1 | 3 | 4.6 | 16 | 262 | 11 | 3.7 | 5.6 | 4.87 | < 0.5 | 50 | 139 | 0.3 | 4.15 |
| 451703 | < 1 | 2.1 | < 1 | 10 | 4 | 19 | 144 | 117 | 0.035 | 2.2 | 7.98 | < 0.5 | 29 | 110 | 0.3 | 4.63 |
| 451683 | < 1 | 0.2 | < 1 | < 2 | 0.3 | 345 | 60 | 74 | 3.23 | 15.5 | 7.02 | < 0.5 | 33 | 48 | 0.3 | 2.9 |
| 451640 | < 1 | < 0.1 | < 1 | < 2 | 14.3 | 25 | 12 | 89 | 3.21 | 16 | 33.8 | < 0.5 | 23 | 234 | < 0.1 | 0.42 |
| 451639 | < 1 | < 0.1 | < 1 | < 2 | 14.9 | 23 | 7 | 71 | 0.179 | 3.1 | 6.18 | < 0.5 | 4 | 119 | 0.8 | 9.38 |
| 422860 | < 1 | < 0.1 | < 1 | < 2 | 11.1 | 31 | 19 | 133 | 0.041 | 1.1 | 7.68 | < 0.5 | 2 | 28 | 0.9 | 10.4 |
| 451856 | < 1 | < 0.1 | < 1 | < 2 | 13.9 | 30 | 325 | 98 | 0.068 | 2.2 | 7.32 | < 0.5 | 3 | 29 | 0.7 | 10.4 |
| 451647 | < 1 | < 0.1 | < 1 | 44 | 29 | 55 | 11 | 185 | 0.48 | 5 | 8.58 | < 0.5 | 5 | 39 | 0.9 | 11 |
| | | | | | | | | | 5.67 | 59 | 20 | < 0.5 | 6 | 48 | 2 | 1.89 |

| Unit Symbol | U | V | W | Y | Zn | Zr | La | Ce | Pr | Nd | Sm | Eu | Gd | Tb |
|-----------------|------|-----|-----|-----|-------|-----|------|------|------|------|------|-------|------|------|
| Detection Limit | ppm | ppm | ppm | ppm | ppm | ppm | ppm | ppm | ppm | ppm | ppm | ppm | ppm | ppm |
| 451667 | 0,05 | 5 | 1 | 1 | 1 | 1 | 0,05 | 0,1 | 0,02 | 0,05 | 0,01 | 0,005 | 0,02 | 0,01 |
| 422857 | 6,92 | 109 | 5 | 13 | 498 | 105 | 41,1 | 76,5 | 9,25 | 28,9 | 5,04 | 1,2 | 3,91 | 0,59 |
| 422855 | 2,35 | 116 | <1 | 26 | 114 | 130 | 49,9 | 96,5 | 11,8 | 38,3 | 7,34 | 1,53 | 5,83 | 0,9 |
| 451670 | 2,64 | 122 | 2 | 30 | 99 | 179 | 40 | 85,2 | 9,98 | 33,4 | 6,67 | 1,06 | 5,81 | 0,98 |
| 451748 | 2,1 | 107 | 3 | 26 | 1380 | 159 | 41 | 87,6 | 10,2 | 34,2 | 6,98 | 1,37 | 5,79 | 0,94 |
| 422858 | 6,31 | 125 | <1 | 25 | 93 | 159 | 56 | 104 | 13 | 39 | 6,78 | 1,48 | 5,43 | 0,87 |
| 422851 | 11,3 | 244 | <1 | 19 | 63 | 130 | 32,6 | 62,5 | 7,69 | 25,4 | 4,89 | 1,2 | 4,23 | 0,69 |
| 451608 | 7,3 | 256 | 2 | 23 | 109 | 106 | 29,7 | 54,8 | 6,88 | 22,1 | 4,13 | 0,907 | 3,61 | 0,65 |
| 451730 | 7,29 | 224 | <1 | 25 | 81 | 130 | 35,1 | 69,8 | 8,57 | 28 | 5,67 | 1,53 | 4,93 | 0,81 |
| 422853 | 6,17 | 201 | 4 | 20 | 385 | 123 | 35,4 | 67,8 | 8,33 | 27,5 | 5,19 | 1,24 | 4,27 | 0,67 |
| 451747 | 5,2 | 168 | <1 | 22 | 51 | 138 | 47,8 | 89,5 | 11,4 | 36,4 | 6,62 | 1,26 | 5,28 | 0,81 |
| 451746 | 8,39 | 215 | 4 | 21 | 54 | 129 | 36,9 | 69,9 | 8,61 | 28 | 5,31 | 1,29 | 4,46 | 0,7 |
| 451745 | 2,79 | 150 | <1 | 21 | 97 | 234 | 23,6 | 55,7 | 7,1 | 24,1 | 4,64 | 1,3 | 4,05 | 0,64 |
| 422861 | 2,92 | 140 | 2 | 26 | 86 | 223 | 29,9 | 61,8 | 7,68 | 26,6 | 5,48 | 1,19 | 5,18 | 0,84 |
| 451613 | 2,07 | 87 | <1 | 17 | 126 | 107 | 25 | 50 | 6,23 | 20,6 | 4,1 | 0,851 | 3,6 | 0,57 |
| 451707 | 4,18 | 79 | <1 | 14 | 13600 | 75 | 15,7 | 30,2 | 3,94 | 13,2 | 2,66 | 1,18 | 2,55 | 0,43 |
| 451703 | 3,2 | 135 | <1 | 9 | 351 | 79 | 17,2 | 32,7 | 4,07 | 13,7 | 2,52 | 0,788 | 2,08 | 0,33 |
| 451683 | 2,2 | 111 | <1 | 12 | 34300 | 56 | 9,55 | 18,6 | 2,34 | 8,3 | 1,9 | 0,752 | 1,9 | 0,34 |
| 451640 | 0,33 | 146 | <1 | 20 | 200 | 18 | 2,45 | 5,1 | 0,74 | 3,99 | 1,31 | 0,583 | 2,13 | 0,44 |
| 451639 | 1,76 | 60 | <1 | 20 | 41 | 476 | 30,8 | 66,3 | 7,95 | 27,1 | 5,27 | 1,12 | 4,42 | 0,71 |
| 422860 | 1,89 | 64 | <1 | 26 | 68 | 536 | 33,6 | 71,3 | 8,71 | 29,8 | 5,92 | 1,37 | 5,23 | 0,87 |
| 451856 | 1,89 | 57 | <1 | 20 | 63 | 396 | 33,3 | 70,3 | 8,61 | 28,5 | 5,8 | 1,25 | 4,98 | 0,78 |
| 451647 | 2,12 | 63 | <1 | 17 | 374 | 456 | 35,8 | 75,1 | 9,02 | 30,1 | 5,65 | 1,35 | 4,44 | 0,69 |
| | 2,98 | 297 | 16 | 30 | 179 | 212 | 14,2 | 34 | 4,99 | 21,8 | 5,83 | 1,33 | 6,16 | 0,97 |

| <i>Unit Symbol</i> | Dy | Ho | Er | Tl | Tm | Yb | Lu | Mass | C-Organ |
|------------------------|------|------|------|------|-------|------|-------|-------|---------|
| <i>Detection Limit</i> | ppm | ppm | ppm | ppm | ppm | ppm | ppm | g | % |
| 451667 | 0,02 | 0,01 | 0,01 | 0,05 | 0,005 | 0,01 | 0,002 | 1,158 | 0,05 |
| 422857 | 3,08 | 0,57 | 1,65 | 2,08 | 0,241 | 1,5 | 0,221 | 1,135 | < 0,05 |
| 422855 | 4,98 | 0,96 | 2,81 | 1,19 | 0,411 | 2,59 | 0,376 | 1,239 | 0,05 |
| 451670 | 5,85 | 1,17 | 3,45 | 1,19 | 0,518 | 3,33 | 0,481 | 1,323 | 0,06 |
| 451748 | 5,3 | 1,03 | 3,01 | 1,53 | 0,446 | 2,79 | 0,395 | 1,074 | < 0,05 |
| 422858 | 4,82 | 0,93 | 2,72 | 1,06 | 0,394 | 2,47 | 0,363 | 1,237 | < 0,05 |
| 422851 | 3,9 | 0,77 | 2,29 | 1,11 | 0,354 | 2,36 | 0,361 | 1,104 | < 0,05 |
| 451608 | 4,05 | 0,86 | 2,57 | 1,16 | 0,401 | 2,56 | 0,379 | 1,517 | < 0,05 |
| 451730 | 4,64 | 0,9 | 2,62 | 1,19 | 0,382 | 2,4 | 0,339 | 1,344 | < 0,05 |
| 422853 | 3,71 | 0,72 | 2,15 | 0,9 | 0,319 | 2,03 | 0,306 | 1,348 | < 0,05 |
| 451747 | 4,3 | 0,82 | 2,34 | 0,74 | 0,348 | 2,22 | 0,334 | 1,379 | < 0,05 |
| 451746 | 4,01 | 0,8 | 2,41 | 1,3 | 0,363 | 2,27 | 0,322 | 1,482 | < 0,05 |
| 451745 | 3,6 | 0,71 | 2,17 | 1,91 | 0,337 | 2,16 | 0,318 | 1,518 | < 0,05 |
| 422861 | 4,91 | 0,98 | 2,86 | 1,55 | 0,425 | 2,67 | 0,385 | 1,492 | < 0,05 |
| 451613 | 3,25 | 0,64 | 1,83 | 0,58 | 0,263 | 1,62 | 0,24 | 1,732 | < 0,05 |
| 451707 | 2,45 | 0,5 | 1,44 | 0,09 | 0,209 | 1,3 | 0,196 | 1,659 | < 0,05 |
| 451703 | 1,9 | 0,37 | 1,08 | 0,09 | 0,161 | 1,11 | 0,294 | 1,502 | 0,09 |
| 451683 | 2,06 | 0,42 | 1,19 | 1,74 | 0,168 | 1,01 | 0,14 | 1,639 | < 0,05 |
| 451640 | 3,1 | 0,69 | 2,13 | 0,94 | 0,327 | 2,16 | 0,375 | 1,268 | < 0,05 |
| 451639 | 4,04 | 0,79 | 2,34 | 0,83 | 0,348 | 2,21 | 0,337 | 1,47 | < 0,05 |
| 422860 | 4,97 | 0,95 | 2,73 | 0,58 | 0,395 | 2,48 | 0,373 | 1,328 | < 0,05 |
| 451856 | 4,32 | 0,81 | 2,34 | 1 | 0,34 | 2,14 | 0,308 | 1,384 | < 0,05 |
| 451647 | 3,91 | 0,75 | 2,22 | 0,87 | 0,331 | 2,15 | 0,329 | 1,43 | < 0,05 |
| | 5,47 | 1,08 | 3,15 | 4,29 | 0,465 | 3,03 | 0,471 | | < 0,05 |

ANNEXE G

**Calculs de changement de masse et de concentration
selon la méthode de Gresen**

| Éléments immobiles modifiés | | | | | |
|-----------------------------|-------------------|---------------|---------------------|-------------------------------|-----------------------------|
| | <u>Non altéré</u> | <u>Distal</u> | <u>Intermediate</u> | <u>Proximal unmineralized</u> | <u>Proximal mineralized</u> |
| | 451855 | 451748 | 451608 | 451730 | 451703 |
| Pr | 9,98 | 13 | 8,57 | 8,33 | 2,34 |
| 2Sm | 13,34 | 13,56 | 11,34 | 10,38 | 3,8 |
| 3Gd | 17,43 | 16,29 | 14,79 | 12,81 | 5,7 |
| 10Tb | 9,8 | 8,7 | 8,1 | 6,7 | 3,4 |
| Zr/4 | 44,75 | 39,75 | 32,5 | 30,75 | 14 |
| 20TiO2 | 19,7 | 17,02 | 11,4 | 12,28 | 5,42 |
| 3Dy | 17,55 | 14,46 | 13,92 | 11,13 | 6,18 |
| 20Ho | 23,4 | 18,6 | 18 | 14,4 | 8,4 |
| 10Er | 34,5 | 27,2 | 26,2 | 21,5 | 11,9 |
| 75Tm | 38,85 | 29,55 | 28,65 | 23,925 | 12,6 |
| 10Yb | 33,3 | 24,7 | 24 | 20,3 | 10,1 |
| 75Lu | 36,075 | 27,225 | 25,425 | 22,95 | 10,5 |
| Nb | 18,9 | 14 | 10,6 | 11 | 4 |
| 10Ta | 14 | 10 | 7 | 7 | 3 |

| Éléments mobiles modifiés | | | | | |
|---------------------------|-------------------|---------------|---------------------|-------------------------------|-----------------------------|
| | <u>Non altéré</u> | <u>Distal</u> | <u>Intermediate</u> | <u>Proximal unmineralized</u> | <u>Proximal mineralized</u> |
| | 451855 | 451748 | 451608 | 451730 | 451703 |
| SiO2/2 | 28,92 | 26,905 | 30,81 | 30,425 | 33,73 |
| Al2O3 | 17,44 | 22,1 | 12,79 | 14,61 | 7,15 |
| 3Fe2O3(T) | 28,14 | 19,89 | 17,07 | 14,37 | 19,62 |
| 100MnO | 39,3 | 5,1 | 23,1 | 16 | 39,9 |
| 5MgO | 17,5 | 12,5 | 29,9 | 18,2 | 22,65 |
| 5CaO | 3,9 | 1,7 | 26,65 | 22,9 | 19,4 |
| 10Na2O | 1,2 | 13,6 | 6,2 | 11,7 | 6,2 |
| 10K2O | 41,1 | 49,5 | 27,8 | 40,5 | 33,5 |
| 100P2O5 | 12 | 11 | 12 | 16 | 7 |
| As/4 | 7,5 | 8,25 | 7,5 | 46,5 | 5 |
| Ba/20 | 28,15 | 40,85 | 38,6 | 33,65 | 16,6 |
| 10Be | 20 | 30 | 20 | 30 | 20 |
| Co | 27,9 | 33,4 | 12,6 | 15,9 | 11,3 |
| Cr/4 | 23,475 | 46,5 | 29,75 | 37,75 | 11,7 |
| Cs | 5,6 | 6,5 | 5,2 | 4,8 | 1,2 |
| Cu/2 | 26 | 25,5 | 19,5 | 43,5 | 23 |
| Ga | 26 | 31 | 18 | 20 | 25 |
| 10Hf | 41 | 43 | 29 | 27 | 12 |
| Ni/2 | 30,5 | 40 | 18 | 26,5 | 9,5 |
| Pb/5 | 2,4 | 5,6 | 4,2 | 46,2 | 28,8 |
| Rb/4 | 34 | 46 | 23,5 | 28,5 | 29,25 |
| 10S | 9,54 | 11,6 | 4,23 | 12,4 | 32,3 |
| Sb | 5,5 | 1 | 5,1 | 7,8 | 15,5 |
| Sc | 20,3 | 25 | 14,3 | 17,1 | 7,02 |
| Sn | 8 | 3 | 14 | 23 | 33 |
| Sr/4 | 7,5 | 22,5 | 39,25 | 46,5 | 12 |
| Th | 14,7 | 16,2 | 10,8 | 11 | 2,9 |

| | | | | | |
|---------|-------|-------|-------|-------|-------|
| U | 13,2 | 31,55 | 36,45 | 30,85 | 11 |
| V/5 | 24,4 | 25 | 44,8 | 40,2 | 22,2 |
| Y | 30 | 25 | 25 | 20 | 12 |
| Zn/1000 | 0,099 | 0,093 | 0,081 | 0,385 | 34,3 |
| La/2 | 20 | 28 | 17,55 | 17,7 | 4,775 |
| Ce/3 | 28,4 | 34,66 | 23,26 | 22,6 | 6,2 |
| Nd | 33,4 | 39 | 28 | 27,5 | 8,3 |
| 10TI | 11,9 | 10,6 | 11,9 | 9 | 17,4 |

Formule de Gresen selon Grant, 1986: $(\Delta C_i / C_i^O) = (M^A / M^O) * (C_i^A / C_i^O) - 1$

C_i : concentration de l'élément i

C_i^O : concentration de l'élément i dans l'échantillon non altéré

C_i^A : concentration de l'élément i dans l'échantillon altéré

M^A : masse de l'échantillon altéré

M^O : masse de l'échantillon non altéré

On obtient M^O / M^A à partir de la pente de la ligne de régression formée par les éléments immobiles

Exemple de calcul pour le changement de concentration de SiO_2 de l'échantillon non altéré (451855) par rapport à l'échantillon altéré (451730):

$$M^O / M^A = 0,6433$$

$$M^A / M^O = 1 / 0,6433 = 1,55$$

$$C_{\text{SiO}_2}^O = 28,92$$

$$C_{\text{SiO}_2}^A = 30,425$$

Changement de concentration of SiO_2 ($\Delta C_{\text{SiO}_2} / C_{\text{SiO}_2}^O$) = $1,55 * (30,425 / 28,92) - 1 = 0,63$ (ou 63%)